Characterization and Interpretation of Feldspathic Chromite Assemblages (FCAs) in Four Ordinary Chondrites: An Electron Backscatter Diffraction (EBSD) Study

By

Kimberly Louisa Maccini

A thesis submitted in partial fulfillment of the
requirements for the degree of

Master of Science
In
Geology

Thesis Committee:
Alexander Ruzicka, Chair
Richard Hugo
Melinda Hutson

Portland State University
2021

Abstract

Feldspathic Chromite Assemblages (FCAs) are chemically distinctive assemblages rich in Na, Al, and Cr that are found in a variety of chondrites. They consist of concentrations of chromite associated mainly with feldspathic material, either feldspar or the glassy material known as maskelynite. Professor Alan Rubin (2003) has proposed that some FCAs formed by shock melting, but the origin of different types of feldspathic chromite assemblages are unclear and have not been studied with more modern techniques such as Electron Backscatter Electron Diffraction (EBSD).

Here EBSD was used to study FCAs in four metamorphosed ordinary chondrites of different shock stages, including Estacado (H6, S1), Spade (H6, S4), NWA 13533 (L6, S4), and Alfianello (L6, S5). EBSD results indicate that FCAs can be grouped into three different assemblages, including Coarse Clumped Chromite (CCC), Fine Clumped Chromite (FCC), and Chromite Poor (CP) assemblages. CCCs are compact assemblages that contain chromite crystals often larger than 5μm in diameter size with little physical distance between adjacent chromite grains. FCCs are compact assemblages that contain numerous chromite grains less than 5μm in diameter that have physical space between the chromite grains. CPs are assemblages that contains chromite congregated in one area but with less chromite grains than the FCC or CCC assemblages.

The four meteorites used in this study are a mix of high and low shock stage. Out of the three assemblage types, it was found that CCCs were present in both high and low shocked meteorites. FCCs were also found in both high and low shock meteorites, but had a noticeable absence in Spade. The two CP assemblages were present only in higher

shocked meteorites (Spade and NWA 13533). Quantitative characteristics (grain sizes of chromite, grain number density of chromite, grain lattice preferred orientation of chromite, and grain orientation spread (or GOS)) of these assemblages and their minerals do not appear to be different between high and low shock meteorites other than differences in the grain orientation spread. These GOS characteristics appear more related to the host meteorite. We postulate that the origins of the FCCs are an end product of exsolution of a previous grain, while the CCCs origins are more likely to be aggregates of pre-existing grains or grain-clumps that have been crystallized from a melt. The CPs found in this study do not particularly fit either model.

My findings support those of Rubin (2003) in terms of Estacado being annealed but support only some of the findings of Rubin and Jones (2003) for Spade, namely that Spade is a melt breccia with the plagioclase having been melted.

Acknowledgements

First and foremost, I would like to give a heart-felt thank you to Dr. Alexander Ruzicka, for putting up with my nonsense and constant connections made between meteorites and food. Your enthusiasm for meteoritics opened my eyes to a field of study I had not previously given much consideration to, and for that I will be endlessly grateful. Additionally, I would like to thank my committee members, Richard Hugo, and Melinda Hutson, for your guidance and assistance in crafting this thesis.

I would also like to thank my fellow graduate students, who were helpful and inspiring and held me up when I was down. My time at Portland State University will forever be a cherished memory that you all helped create.

A huge thanks you must also be given to Landon, who sat through so many demonstrations of my presentation, and listened to endless drafts of my thesis that I did not know I was speaking out loud. You are the rock that got me through it all and I can only hope to one day repay the love and encouragement you showed during this process.

Lastly, the largest thank you goes out to my parents and siblings. Dad, Mom, Jessica, Joey, and Mikey, your support during this journey kept me going, thank you, thank you, thank you for believing in me and my dreams.

Table Of Contents

List of Tables

List of Figures

List of Abbreviations & Symbols

Abbreviation	Definition
SEM	Scanning Electron Microscope
EBSD	Electron Backscatter Diffraction
EDS	Energy Dispersive Spectrometer (or Energy Dispersive Spectrometry)
OM	Optical Microscopy
FCA	Feldspathic Chromite Assemblage
FCC	Fine Clumped Chromite assemblage
CCC	Coarse Clumped Chromite assemblage
CP	Chromite Poor assemblage
d	Grain Size (equivalent diameter of a grain with the measured area, in units of microns)
LAM	EBSD Large Area Map
TM	EBSD Targeted Map
GOS	Grain Orientation Spread, an EBSD metric of the average misorientation within a grain, given in degrees
MOS	Maximum Orientation Spread, an EBSD metric of the maximum misorientation within a grain, given in degrees
GROD angle	Grain Reference Orientation Deviation angle, an EBSD metric of the misorientation of a given pixel within a grain from the average misorientation of the grain, in degrees
IPF	Inverse Pole Figure, an EBSD pole figure that displays the orientation of a grain (crystal direction or plane) relative to a sample x, y, z coordinate system; IPF orientations can also be displayed in maps using false color schemes
LPO	Lattice Preferred Orientation
LPO # $\Delta_{<100>}$	LPO strength for chromite, given as the difference between maximum MUD and minimum MUD values in a <100> pole figure plot for chromite, based on 15-degree half-width contouring
% d >5/>1	A measure of overall grain coarseness, given by the percentage of grains with d>5 relative to grains with d>1
n_g	number of grains
CRA	Crystal Rotation Axis plot, an EBSD plot showing misorientation rotation axis directions in a crystal reference frame
MUD	Multiples of Uniform Distribution, a measure of the deviation of a spatial distribution from a totally random spatial distribution in a pole figure or CRA plot, with MUD > 1 indicating an excess relative to a random spatial distribution (MUD = 1), and MUD < 1 indicating a deficit relative to a random spatial distribution

1) INTRODUCTION

Felspathic Chromite Assemblages (FCAs) are chemically distinctive assemblages rich in Na, Al, Si, and Cr (as well as other various elements) that are found in a variety of chondrites. Composed chiefly of Cr-spinel (chromite) and feldspathic material (plagioclase or feldspathic glass), they are widely present in ordinary chondrites, where they take on a variety of textural forms, both inside and outside of chondrules (Ramdohr, 1967; Bischoff and Keil, 1984; Krot and Ivanova, 1992; Krot and Rubin, 1993; Rubin, 2003, 2004). Previously called aggregate (or heap) chromite, pseudomorphous (or decomposition) chromite (among other types; Ramdohr, 1967, 1973), or chromite plagioclase assemblages (Rubin, 2003), they are here called feldspathic chromite assemblages (FCAs) instead, to acknowledge that feldspathic glass sometimes occurs instead of plagioclase (Ramdohr, 1967, 1973; Rubin, 2003). This feldspathic glass corresponds to the shock-produced material known as maskelynite (e.g., Chen and El Goresy, 2000; Rubin, 2003; Fritz et al., 2005). Rubin (2003) found FCAs in every equilibrated ordinary chondrite in which he looked, suggesting they could be important to understanding the thermal histories of these chondrites and their parent asteroids. It has been proposed that at least some FCAs formed at high temperatures (Ramdohr, 1967, 1973) by shock melting (Krot and Rubin, 1993; Rubin, 2003), but whether all textural varieties formed by shock melting, and how their compositions, mineralogies, and textural variety were established, has not been adequately explained in detail.

Chromite assemblages can occur both within and outside chondrules. Chondrules are rounded beads of rock that have textures indicating they cooled from melt, possibly as free-floating melt droplets. In some chondrules, chromite is a major component together

with albitic plagioclase (Ramdohr, 1967; Krot and Rubin, 1993; Krot et al., 1993). Ramdohr (1967, 1973) noted that some chromite-rich chondrules in chondrites are firmly intergrown with the meteorite matrix and are bound by feldspar (or feldspathic glass) at the chondrule-matrix contact, as if they had been welded to the meteorite. Other assemblages form inclusions, which are irregularly shaped, and which could have formed in situ (Rubin 2003, 2004). FCAs of the inclusion type range in size from 200-300 μm across, with 0.2-20μm size euhedral, subhedral, anhedral, and rounded chromite grains surrounded by plagioclase or glass of plagioclase composition (Rubin 2003).

If FCAs did form by shock processes, one might expect other evidence for shock deformation in the chondrites. Petrographic criteria for shock deformation in olivine and feldspar, utilizing an optical microscope, can be used to assign chondrites to one of six shock stages (S1 through S6) representing increasing shock pressure (Stöffler et al., 1991, 2018, 2019). These petrographic criteria include the formation of planar microfractures and undulose-mosaic extinction in olivine, and undulose-mosaic extinction or the formation of a feldspathic glass (maskelynite) for plagioclase (Stöffler et al., 1991, 2019). However, many of the chondrites that contain FCAs also have low-shock stages (S1 or S2) (Rubin, 2003, 2004). This has been interpreted as indicating early shock deformation to produce the FCAs, followed by annealing to obliterate deformation effects (Rubin, 2003, 2004). If a shock melt origin for all FCAs is correct, for a FCA to appear in an unshocked (S1) meteorite would mean that it would have had to have been shocked, and then annealed to remove the obvious effects of shock, with the notable exception of the FCAs themselves (Rubin, 2003, 2004). Rubin (2003, 2004) has suggested that regardless of shock stage, the FCAs can be used as shock indicators.

More recently, electron backscatter diffraction (EBSD) techniques have been used to evaluate shock deformation in chondrites (e.g., Ruzicka and Hugo, 2018; Hugo et al., 2019). These techniques utilize an EBSD detector attached to a scanning electron microscope (SEM) to identify mineral structures and quantify crystal orientations. Such data can be used to study crystal fabrics and deformation (Prior et al., 2009). Ruzicka and Hugo (2018) and Hugo et al. (2019) developed additional EBSD metrics to evaluate the extent of shock deformation, post-shock annealing, and pre-shock deformation temperature, which are important variables for understanding the shock histories of chondrites (Ruzicka et al., 2015).

The purpose of this study is to 1) identify the characteristics of the different assemblages by quantitative EBSD metrics, 2) use the characteristics of these assemblages to determine whether there are any differences between low and high shock stage meteorites, 3) interpret how these assemblages may have formed, and 4) test the model of shock followed by annealing of Rubin (2003).

What was investigated in this study were FCAs found as inclusions within the meteorite samples, notably they presented as irregular shapes, as opposed to chondrules which are spherical. These inclusions contain multiple chromite grains that are associated with feldspathic material (mostly appearing as plagioclase, and maskelynite). This study focused on the FCAs that have been described as “chromite plagioclase assemblages” by Rubin (2003) and “pseudomorphic” or “aggregated chromite assemblages” by Ramdohr (1967, 1973).

2) METHODS AND SAMPLES

2.1 Methodology:

Thin sections of meteorites in the Cascadia Meteorite Laboratory (CML) collection were surveyed using Optical Microscopy (OM) with a Leica DM2500 petrographic microscope with intent to locate FCAs. Many thin sections were surveyed (Annex Table A-1). Samples were selected for further study based on having well-formed feldspathic-chromite assemblages with a variety of textural types in generally unweathered meteorites of differing shock stages. Samples were then prepped and mapped using EBSD, gathering both Large Area Maps (LAMs), as well as Targeted Maps (TMs) from each sample. Assemblage data were then individually analyzed using Oxford Instruments AZtec 4.3, AZtecCrystal 1.1, and Channel 5 software to create various maps, plots, and tables from which other data were extracted.

2.2 Shock Classification:

Olivine shock character data were gathered from each thin section for the purpose of evaluating the shock history of these meteorites. Shock stage was determined for samples that had not previously been classified using a Leica DM2500 petrographic microscope. Based on olivine grains within the samples, conventional shock stage was determined using the criteria of Stöffler et al. (1991, 2019) as the highest shock stage containing at least 25% of the grains observed. Petrographic criteria include the extent of undulatory or mosaic extinction, the number of planar fractures within the grain, and whether the olivine shows recrystallization. Table A-1 shows the conventional shock stage for all meteorites that were studied with optical microscopy. The weighted shock stage was then determined using the methods of Jamsja and Ruzicka (2010). In the

Jamjsa and Ruzicka (2010) method, extinction angles and the number of planar fractures sets together with any evidence for recrystallization are the primary criteria for assigning shock stage to an individual grain. Weighted shock stage is determined by the mean of all assigned olivine shock stage characters for each individual grain, displayed with the standard deviation of the population (Jamsja and Ruzicka, 2010). Olivine grains used for analysis have minimal weathering and alteration, with the key criterion being that they are of sufficient recommended size (≥50 μm in one dimension).

2.3 EBSD Methods:

The SEM-EBSD system used for this work was a Zeiss Sigma Variable Pressure-Field Emission Gun-Scanning Electron Microscope (VP-FEG-SEM), with an Oxford Instruments ULTIM MAX 65 energy dispersive spectrometer (EDS) with silicon-drift detector, and an Oxford Instruments NordlysNano Symmetry Electron Backscatter Detector (EBSD) with 5-diode forward scattered electron detectors. The SEM was used to obtain high resolution Backscatter Electron (BSE) images, chemical maps, and chemical point data of the specific areas of interest within each sample. EBSD data including band contrast and crystal identities and orientations were obtained in map format. Band contrast images represent the intensity differences in Kikuchi images of diffraction data and are typically related to the quality of diffraction patterns. Crystal orientations are commonly portrayed as inverse pole figure (IPF) (x, y, z) maps, which show the orientation of principal crystal axes relative to the x, y, and z sample directions. EBSD data were analyzed with Oxford Instruments AZtec 4.3, Channel5, and AZtecCrystal 1.1 software to determine various metrics including grain orientation spread (GOS), grain reference orientation deviation (GROD) angle, and lattice preferred

orientation (LPO) maps and metrics for olivine, chromite, and plagioclase grains. Additionally, grain size data were collected. GOS metrics derived from Large Area Maps were used to evaluate deformation temperature and annealing in the samples according to the methods of Ruzicka and Hugo (2018) and Hugo et al. (2019). These methods include an assessment of temperature at the time of deformation, given by the EBSD parameter $R_{2\text{-}10}$ for olivine, which is related to the fraction of misorientation rotation directions in the <010> and <001> crystal directions of olivine compared to the total rotation directions in the <100>, <010>, and <001> directions, for misorientation angles between 2 and 10° (Ruzicka and Hugo, 2018). They also include an assessment of annealing (recovery) following deformation, given by the $Sk_{d>50}$ parameter for olivine, which is related to the skewness of GOS values (=mean/median GOS) in olivine grains larger than 50μm across (Ruzicka and Hugo, 2018).

For EBSD work, the SEM accelerating voltage was set to 20 keV, with mapping step sizes ranging from 0.11μm to 0.83μm for the Targeted Maps, and between 2.5-4.5μm for the Large Area Maps. The minimum grain size criterion for all maps was 5 contiguous pixels. All maps (LAM and TM) were gathered in less than 24 hours.

2.4 Study Samples:

Meteorites used in this study for EBSD analysis are: Spade (H6), Estacado (H6), Alfianello (L6), and NWA 13533 (L6) (Table 1). Spade, Estacado, and Alfianello were previously shock-classified (Friedrich et al. 2017), whereas NWA 13533 was classified (group, type) and the shock stage was determined for this study.

Table 1: Meteorites used in this study for EBSD work.

Name	Classification	Conventional Shock Stage
Spade	H6	S4
Estacado	H6	S1
Alfianello	L6	S5
NWA 13533	L6	S4

3) RESULTS

3.1 Textural Types

For this study, we focus on three main textural types of FCAs, Fine Clumped Chromite, Coarse Clumped Chromite, and Chromite Poor. These classifications have been created for this study and are based on quantitative EBSD data as discussed below. The primary criteria used to distinguish textural types are 1) grain sizes of chromite in an assemblage, 2) the number of chromite grains in each area of an assemblage ("clump number density" or simply "clump density"), and 3) the area fraction of chromite pixels in an assemblage. Before discussing quantitative data in detail, examples of the different textural types are first given below.

Fine Clumped Chromite (FCC) – These are assemblages found in compact regions that contain numerous chromite grains less than 5μm in diameter (Fig. 1). Although in clumps, some physical distance occurs between adjacent chromite grains. In these clumps individual chromite grains can be roughly equant or elongate, and elongate grains are typically parallel to other elongate grains (Fig. 1). Some of the assemblage clumps have apparent crystal outlines, and these outlines have been proposed to be the remnant edges of a parent crystal that has since exsolved to form chromite (Ramdohr, 1967, 1973).

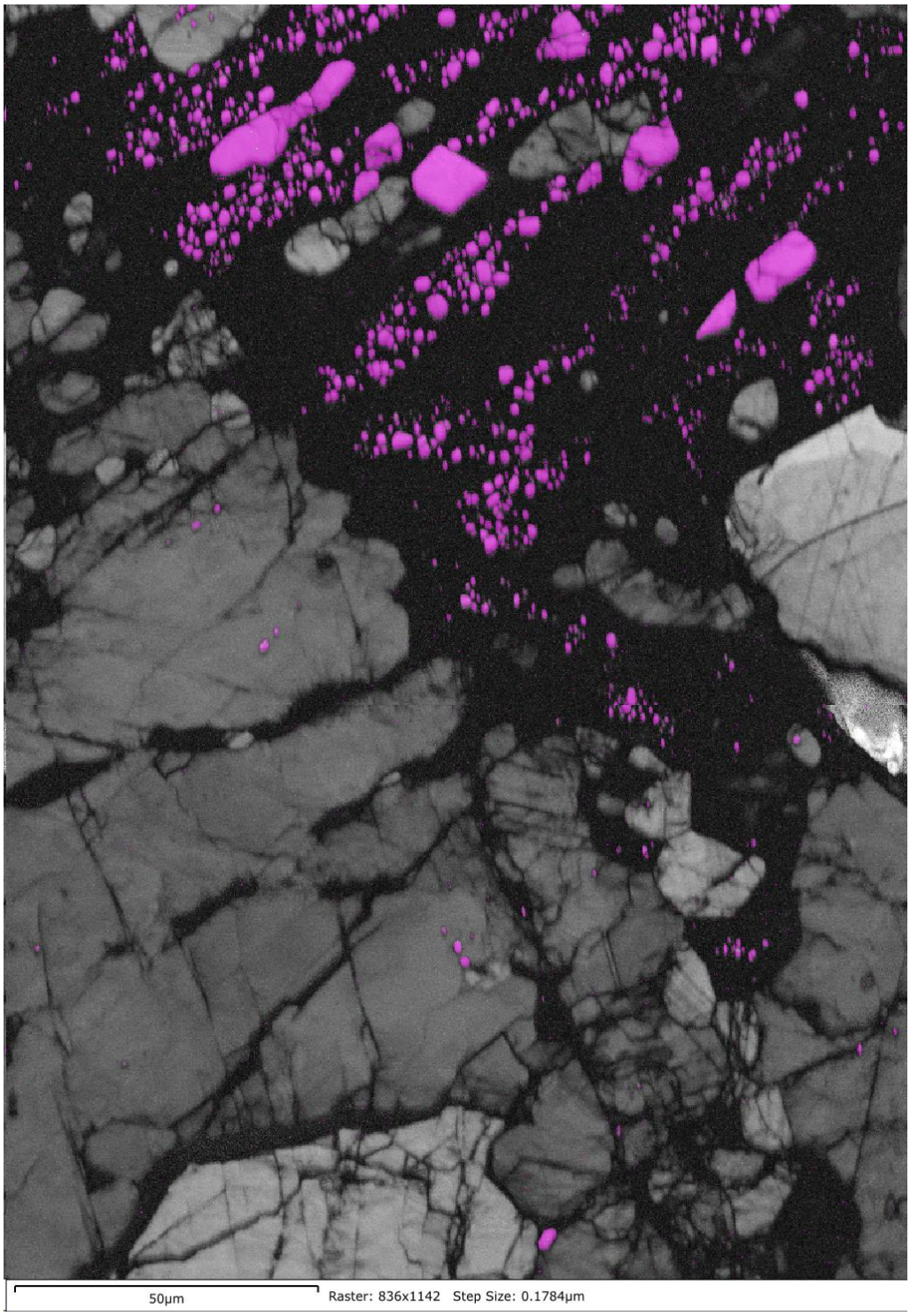

Figure 1: An example of Fine Clumped Chromite (FCC) in NWA 13533. Image: monochrome = band contrast, pink = pixels indexed as chromite. Black areas associated with chromite are maskelynite. Medium grey areas outside the assemblage consist of olivine and pyroxene; the lighter grey area to the middle right consists of metal. EBSD map: 0995-TM4D

Coarse Clumped Chromite (CCC) – This type of assemblage contains chromite crystals often larger than 5µm in diameter size that form compact assemblages with little if any physical distance between adjacent chromite grains (Fig. 2). They could have started as broken or fractured chromite grains that have since, potentially through shock, been cobbled back together to form a clumped pile of chromite surrounded by feldspar (Ramdohr, 1967, 1973). While chromite is a brittle mineral (Ramdohr, 1967), not all chromites in chondrites or FCAs have been found to be heavily fractured. The CCC chromite in Fig. 2, for example, is not especially fractured. (Faint lines crossing the interiors of chromite grains are polishing scratches—A. Ruzicka, personal communication).

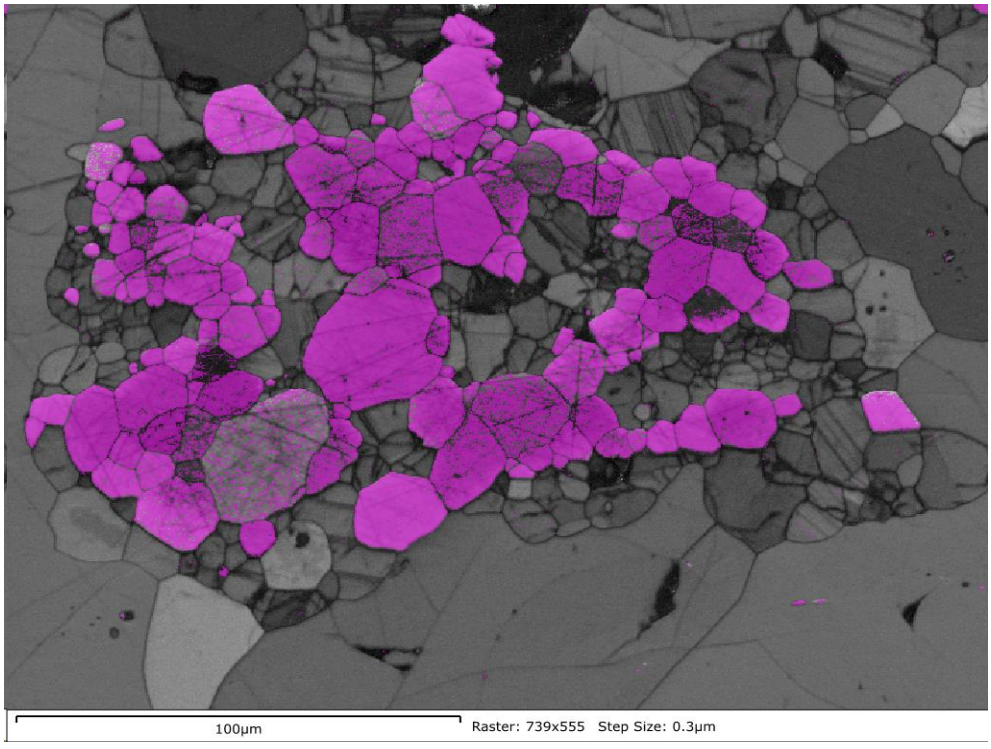

Figure 2: An example of Coarse Clumped Chromite (CCC) in Estacado. Image: monochrome = band contrast, pink = pixels indexed as chromite. Grey areas intergrown with chromite are largely grains indexed as plagioclase; grey areas outside the assemblage consist chiefly of olivine. EBSD map: 0295-TM2B

Chromite Poor (CP) – This assemblage type contains chromite congregated in one area but has more distance between chromite grains, with visibly less chromite than the FCC or CCC assemblages (Fig. 3). This designation can be fitted into the FCC or the CCC category in some instances for some parameters, but CP assemblages are set apart as their own grouping due to the relatively low proportion of chromite.

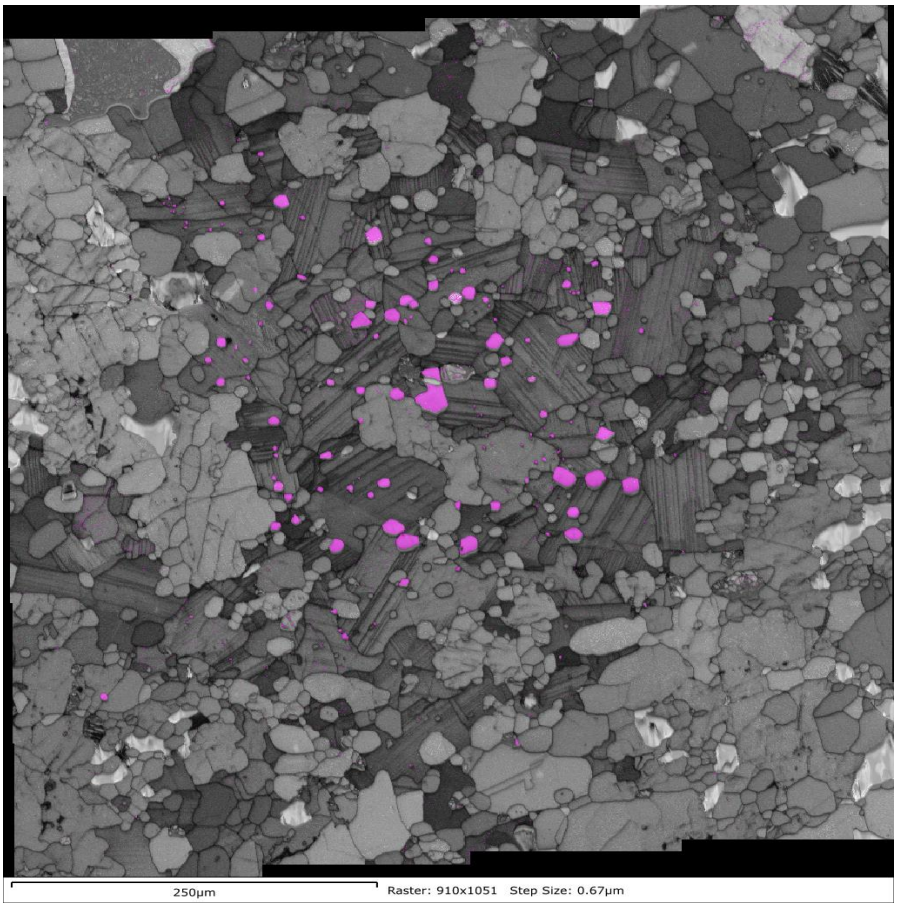

Figure 3: An example of a Chromite Poor (CP) assemblage in Spade. Image: monochrome = band contrast, pink = pixels indexed as chromite. Grains intergrown with chromite consist largely of grains indexed as plagioclase. Grey areas outside the assemblage consist mainly of olivine and pyroxene. EBSD map: 0269-TM1A

3.2 Characterization of Assemblages

Multiple Targeted Maps were taken from each of the four meteorites analyzed with EBSD (Table 2). Each Targeted Map was chosen for containing an FCA. These FCAs vary slightly in texture and make-up. Some maps only had one assemblage,

whereas others had multiple nearby assemblages that were grouped into subsets (Table 2). An assemblage was determined by having a concentration of chromite with feldspathic material surrounding it. Within Alfianello and NWA 13533, feldspar in FCAs is largely maskelynized, but there were some relict plagioclase crystals found within maskelynite (Table 2). These relict plagioclase grains appear cracked in BSE or forescattered diode (FSD) images, in contrast to a smooth appearance for maskelynite. In Spade and Estacado, crystalline plagioclase is present in the FCAs (Table 2), and it is observed to be twinned. The presence of maskelynite (feldspathic glass) as opposed to plagioclase, is indicative of a more highly shocked meteorite.

Table 2: Listing of all Targeted Maps, including metadata and basic data for assemblages.

Meteorite (thin section)	Targeted Map	Whole Map Area (mm^2)	Assemblage Area (mm^2)	Step Size (µm)	n_g plag*	n_g chr*	# of assemblage subsets	Assemblage Mineralogy*
Spade (0269-1A)	TM1A	0.4293	0.2579	0.67µm	2318	126	1	chr + plag
	TM2A	0.3781	0.1195	0.83µm	832	77	2	chr + plag
	TM3A	0.5697	0.1042	0.83µm	832	159	1	chr + plag
Estacado (0295-3C)	TM1B	0.0142	0.0114	0.13µm	670	332	6	chr + plag
	TM2B	0.0369	0.0328	0.30µm	600	350	1	chr + plag
	TM3B	0.3129	0.0128	0.28µm	82	168	1	chr + plag
	TM4B	0.0051	0.0051	0.11µm	1214	232	7	chr + plag
	TM5B	0.0164	0.0123	0.15µm	673	351	6	chr + plag
Alfianello (0496-1A)	TM1C	0.8343	0.0568	0.45µm	--	196	4	chr + mask
	TM2C	0.0411	0.0341	0.25µm	12	2015	13	chr + mask w/ plag
	TM3C	0.0058	0.0035	0.12µm	36	227	2	chr + mask
	TM4C	0.0123	0.0066	0.18µm	66	336	9	chr + mask w/ plag
	TM5C	0.0111	0.0069	0.17µm	206	528	5	chr + mask w/ plag
	TM6C	0.0203	0.0133	0.22µm	13	224	7	chr + mask
NWA 13533 (0995-1)	TM1D	0.1472	0.1472	0.38µm	--	1824	23	chr + mask
	TM4D	0.0304	0.0231	0.18µm	--	614	17	chr + mask
	TM5D	0.0286	0.0231	0.18µm	--	539	4	chr + mask
	TM6D	0.1546	0.1055	0.18µm	203	1848	2	chr + mask

* Chr = chromite, plag = plagioclase, mask = maskelynite

3.3 Assemblage types

In this study, we have found there to be two main groups of FCAs, Fine Clumped Chromite, and Coarse Clumped Chromite. There is an additional group, Chromite Poor, that does not quite fit into the two main groups. Tables 3, 4, and 5 show data for the three groups that help to characterize these assemblage types. Table 6 shows the plagioclase data for each targeted map. In maps containing multiple assemblages and subsets (Table 2), data in these tables are averaged values for the assemblages in each map.

FCC:

Table 3: Chromite data for assemblages in this study that have been classified as Fine Clumped Chromite (FCC). These assemblages have generally the smallest Chromite Coarseness Ratio among FCAs in this study.

Meteorite	Targeted Maps	Assemblage Type	Chromite Coarseness Ratio (% d>5/d>1)	Area Fraction of Chromite (pixel fraction)	Clump Density (grains per mm^2)	LPO # $\Delta_{<100>}$
Estacado (0295-3C)	TM1B	FCC	0	0.21	29049.4	9.51
	TM3B	FCC	0	0.12	13100.7	6.27
	TM4B	FCC	0	0.17	45250.6	5.18
	TM5B	FCC	0.741	0.21	28515.7	10.86
Alfianello (0496-1A)	TM2C	FCC	1.46	0.27	59039.0	6.34
	TM3C	FCC	0	0.29	65117.6	8.17
	TM4C	FCC	1.10	0.33	50978.6	9.74
	TM5C	FCC	0.529	0.39	76733.0	7.81
	TM6C	FCC	3.75	0.25	16815.6	4.45
NWA 13533 (0995-1)	TM1D	FCC	1.54	0.12	12391.4	3.39
	TM4D	FCC	1.69	0.16	26527.3	5.82

CCC:

Table 4: Chromite data for assemblages in this study that have been classified as Coarse Clumped Chromite (CCC). These assemblages have generally the largest Chromite Coarseness Ratio of FCAs in this study.

Meteorite	Targeted Maps	Assemblage Type	Chromite Coarseness Ratio (% d>5/d>1)	Area Fraction of Chromite (pixel fraction)	Clump Density (grains per mm^2)	LPO # $\Delta_{<100>}$
Spade (0269-1A)	TM2A	CCC	44.16	0.23	644.5	4.56
	TM3A	CCC	37.50	0.45	1525.9	4.14
Estacado	TM2B	CCC	61.96	0.55	10674.4	7.48
Alfianello	TM1C	CCC	17.39	0.27	3452.3	3.53
NWA 13533	TM6D	CCC	29.67	0.41	17513.6	1.40

CP:

Table 5: Chromite data for assemblages in this study that have been classified as Chromite Poor (CP). Note these assemblages have the lowest Area Fraction of Chromite of all the Targeted Maps in this study.

Meteorite	Targeted Maps	Assemblage Type	Chromite Coarseness Ratio (% d>5/d>1)	Area Fraction of Chromite (pixel fraction)	Clump Density (grains per mm^2)	LPO # $\Delta_{<100>}$
Spade	TM1A	CP	36.51	0.054	488.5	1.58
NWA 13533	TM5D	CP	2.01	0.09	23361.7	0.88

Table 6: Plagioclase details for the Targeted Maps acquired for this study.

			Grain Size (µm)			**GOS values (degrees)(All d)**		
Meteorite	**Targeted Map**	**# of Grains**	**Mean**	**Max,Min**	**Median**	**Mean**	**Standard Deviation**	**mean/median ratio (All)**
Spade (0269-1A)	TM1A	2318	3.44	63.5, 1.69	2.13	0.66	0.49	1.25
	TM2A	832	5.12	55, 2.10	2.96	0.78	0.59	1.26
	TM3A	832	5.06	76.9, 2.09	2.81	0.73	0.63	1.38
Estacado (0295-3C)	TM1B	670	1.20	18.22, 0.33	0.78	0.62	0.20	1.05
	TM2B	600	2.38	19.27, 0.76	1.27	0.68	0.40	1.19
	TM3B	82	2.10	42.3, 0.7	0.82	0.97	0.66	1.30
	TM4B	1214	0.53	9.92, 0.28	0.36	0.59	0.36	1.13
	TM5B	673	1.01	51, 0.38	0.48	0.51	0.33	1.21
Alfianello (0496-1A)	TM1C	25	1.25	2.34, 0.97	1.15	0.95	0.47	1.20
	TM2C	12	1.51	4.49, 0.63	1.12	1.12	0.60	1.20
	TM3C	36	0.47	1.59, 0.3	0.37	0.88	0.32	1.02
	TM4C	66	0.93	6.33, 0.44	0.56	0.86	0.55	1.17
	TM5C	206	0.63	5.94, 0.42	0.49	0.70	0.32	1.12
	TM6C	13	0.87	2.58, 0.56	0.76	1.06	0.57	1.38
NWA 13533 (0995-1)	TM1D	8	2.32	6.83, 1.14	1.48	1.16	0.51	1.14
	TM4D	28	0.85	2.87, 0.45	0.60	0.78	0.25	1.01
	TM5D	70	0.67	2.69, 0.45	0.53	0.99	0.67	1.17
	TM6D	203	1.31	8.17, 0.64	0.89	0.93	0.33	1.06

As seen in the above tables (3, 4, 5), the FCC category appears to have a very small chromite coarseness ratio, whereas the CCC group has a very large value. Chromite Poor sets itself apart with a lower area fraction of chromite than either the FCC or the CCC group.

3.4 Quantitative EBSD parameters for FCA groups

The plots below show the two distinct groups, FCC and CCC, according to various quantitative parameters. Although there is some overlap between the two main groups in some of the plots, they have different ranges of parameters. The Chromite Poor assemblages can be seen to line up with either the CCC or FCC groups for some parameters, but they do not consistently fall into one of the other two groups.

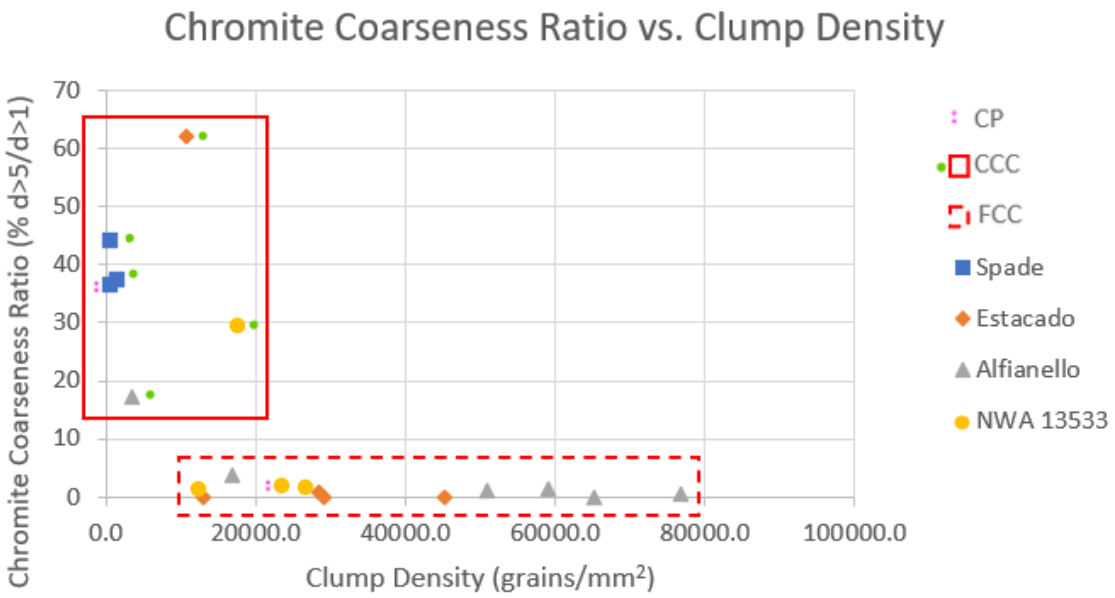

Figure 4: Chromite Coarseness Ratio (grain size) vs. Clump density. d = equivalent grain diameter in microns (μ), d>5/d>1 is the percentage of grains with d>5 compared to all grains with d>1. Green dots next to symbol for meteorite denote CCC, pink double dots denote CP, lack of dots denote FCC. Solid line box shows CCC trend, while dotted line box shows FCC trend.

Grain size and clump density show the distinct difference in the FCC and CCC groups (Fig. 4). CCCs tend to be less 'clumped' (have lower number grain densities) than FCCs, but they overlap some FCCs with the lowest clump density. Figure 4 shows that for these two parameters, the Spade CP assemblage fits into the CCC group, whereas the NWA 13533 CP assemblage fits into the FCC group. In the case of this figure, we see that both of our CP data points have a lower clump density but are varied in their grain size.

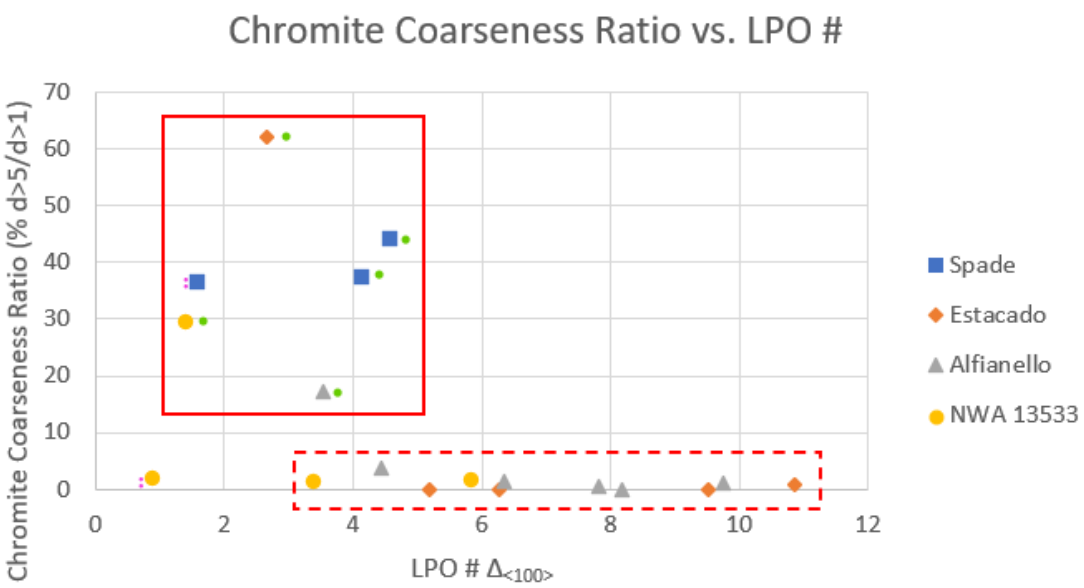

Figure 5: Chromite Coarseness Ratio (grain size) vs. LPO #. Green dots next to symbol for meteorite denote CCC, pink double dots denote CP, lack of dots denote FCC. Solid line box shows CCC trend, while dotted line box shows FCC trend.

Figure 5 shows that there tends to be a higher LPO number (higher degree of chromite lattice preferred orientation) for the FCC group, as opposed to the CCC group. The Spade CP assemblage again fits within the CCC group in terms of chromite LPO and grain size, but the NWA 13533 CP assemblage falls far outside of either the FCC or CCC groups in terms of having weak LPO together with low grain size.

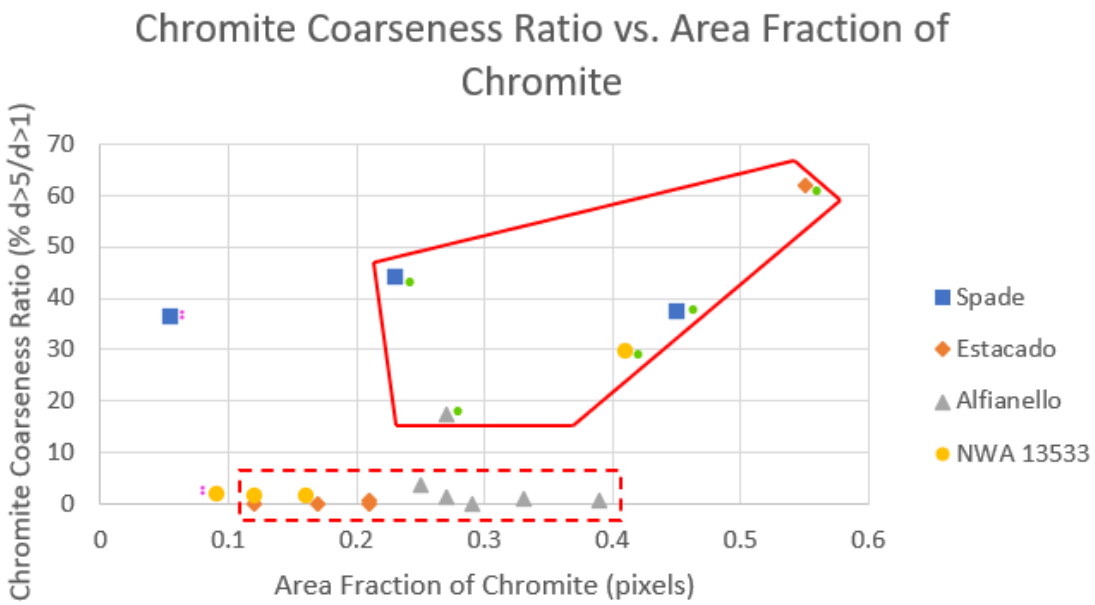

Figure 6: Chromite Coarseness Ratio (grain size) vs. Area Fraction of Chromite. Green dots next to symbol for meteorite denote CCC, pink double dots denote CP, lack of dots denote FCC. Solid line box shows CCC trend, while dotted line box shows FCC trend.

Figure 6 shows both CCC and FCC to have a large and overlapping spread in chromite area fraction, although FCC assemblages tend to have a lower chromite area fraction than CCC. The CP assemblages are set slightly apart from either the CCC or FCC fields, as they have the lowest amount of chromite.

In Fig. 7 and plots to immediately follow, GOS is shown for all grain sizes ("all d"). Although GOS is dependent on grain size (Ruzicka and Hugo, 2018), we will see later that for the chromite grains in FCAs, $GOS_{all\ d}$ is a good measure of the overall deformation extent of chromite.

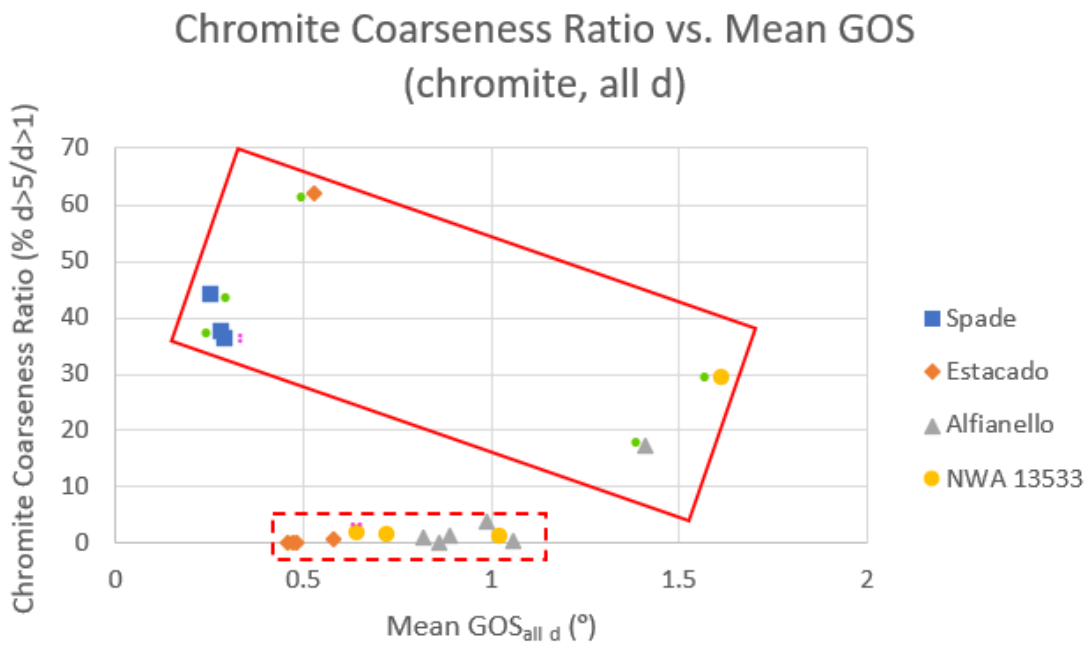

Figure 7: Chromite Coarseness Ratio (grain size) vs. Mean GOS of chromite, all d. d = equivalent grain diameter in microns (µ). Green dots next to symbol for meteorite denote CCC, pink double dots denote CP, lack of dots denote FCC. Solid line box shows CCC trend, while dotted line box shows FCC trend.

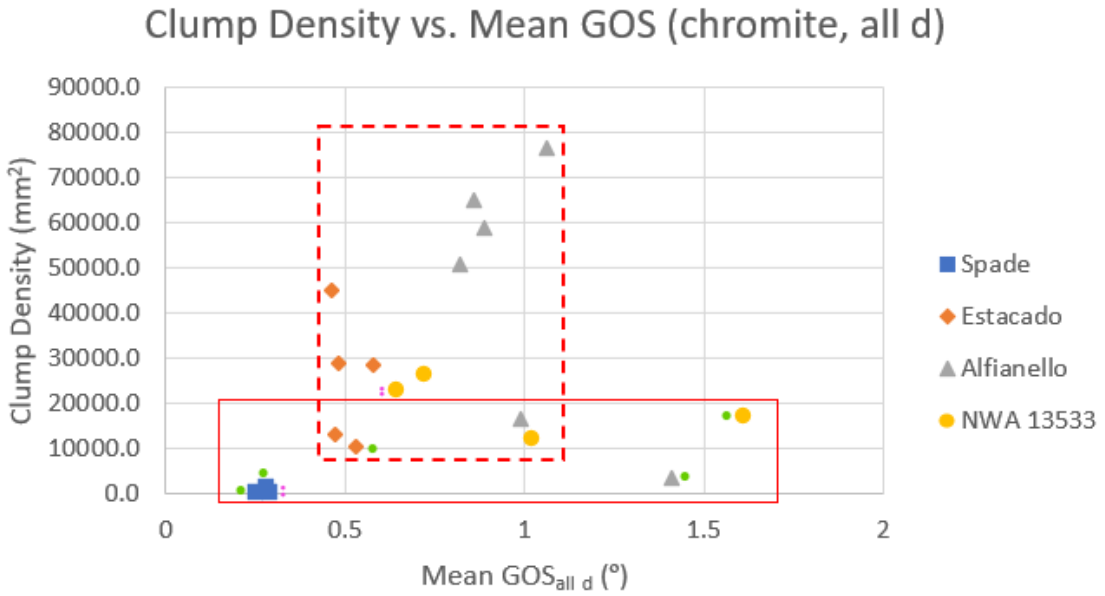

Figure 8: Clump Density vs. Mean GOS of chromite, all d. d = equivalent grain diameter in microns (µ). Green dots next to symbol for meteorite denote CCC, pink double dots denote CP, lack of dots denote FCC. Solid line box shows CCC trend, while dotted line box shows FCC trend.

Figure 8 depicts the clump density of each assemblage verses the mean $GOS_{all\ d}$ showing that there is some overlap in our assemblage groupings. Despite this overlap in the FCC and CCC groups in Figure 8, we can see a distinct difference in average chromite $GOS_{all\ d}$ between our meteorites. Spade and Estacado have a low average $GOS_{all\ d}$ in chromite (~0.25-0.6°) compared to Alfianello and NWA 13533 (~0.7-1.6°).

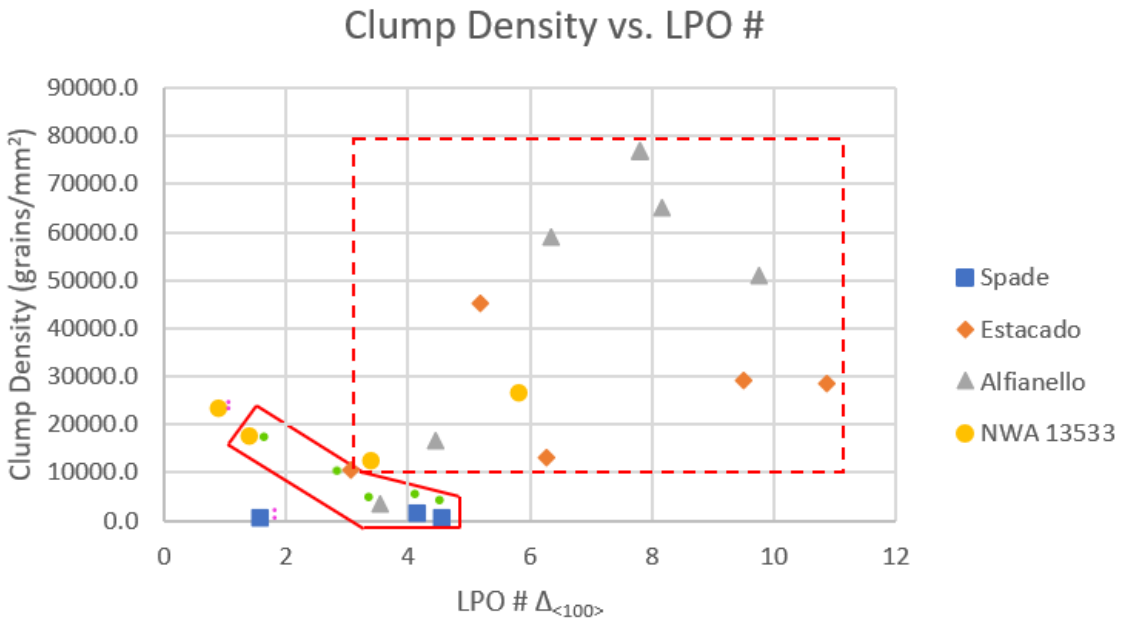

Figure 9: Clump Density vs. LPO #. Green dots next to symbol for meteorite denote CCC, pink double dots denote CP, lack of dots denote FCC. Solid line box shows CCC trend, while dotted line box shows FCC trend.

Figure 9 shows that there is some distinction in the FCC and CCC groups, as well as showing our CPs as outliers. FCCs tend to have the high clump density as well as the higher LPO number. Whereas our CCCs trend on the lower end for both LPO and clump density.

Figures 10, 11, and 12 show the Area Fraction data for each Targeted Map. They show that there is some distinction between the separate assemblage groups, however it's

more muddled than other parameters. This points to area fraction not being a large factor in the creation of the assemblages.

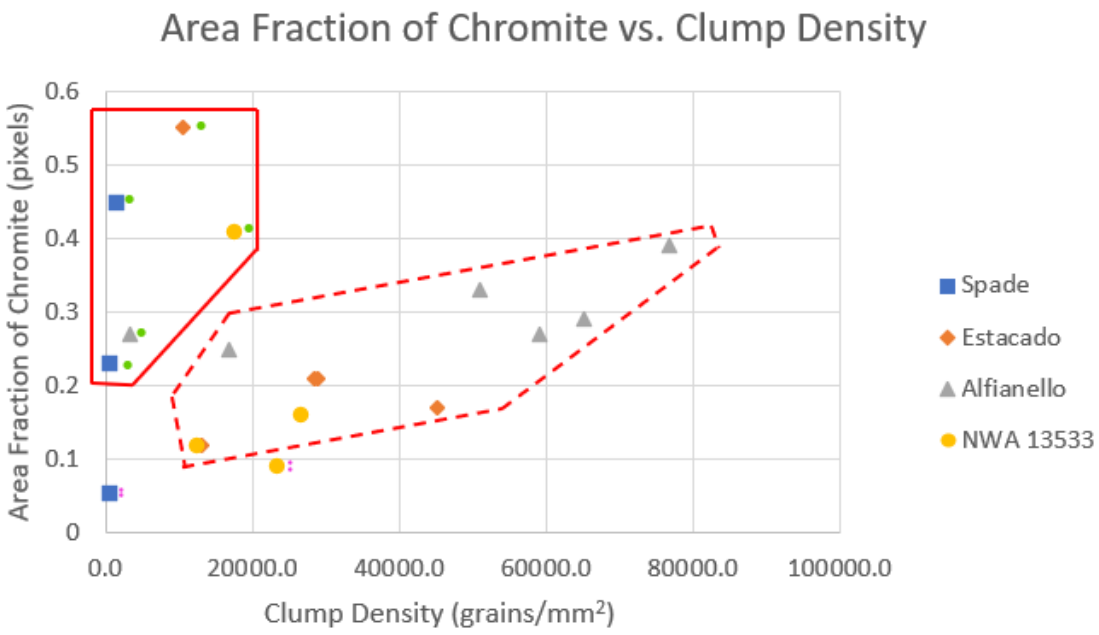

Figure 10: Area Fraction of Chromite vs. Clump Density. Green dots next to symbol for meteorite denote CCC, pink double dots denote CP, lack of dots denote FCC. Solid line box shows CCC trend, while dotted line box shows FCC trend.

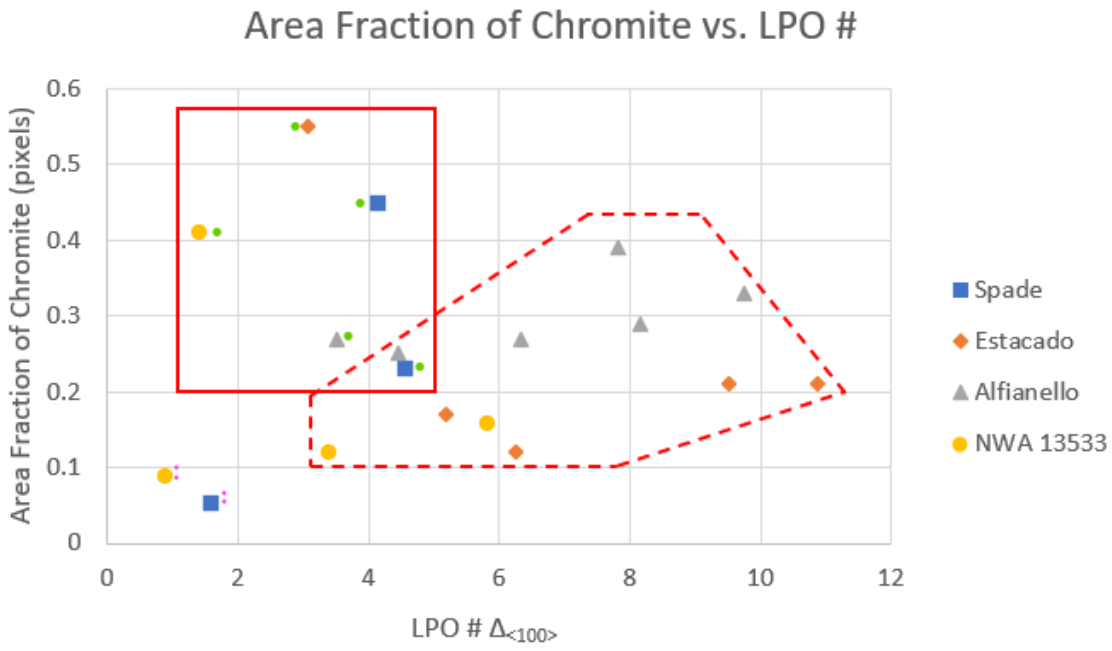

Figure 11: Area Fraction of Chromite vs. LPO#. Green dots next to symbol for meteorite denote CCC, pink double dots denote CP, lack of dots denote FCC. Solid line box shows CCC trend, while dotted line box shows FCC trend.

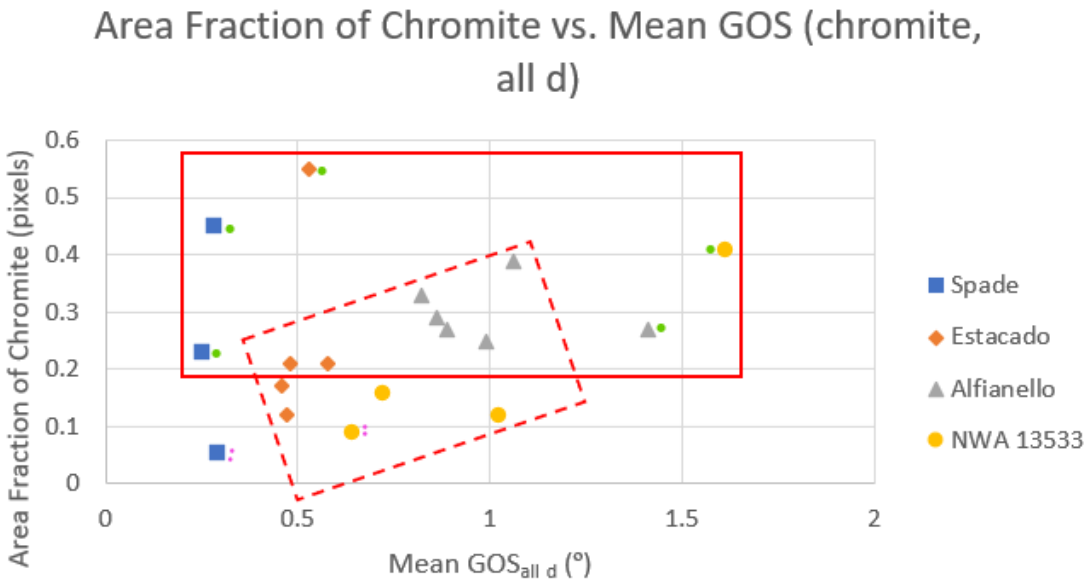

Figure 12: Area Fraction of Chromite vs. Mean GOS of chromite, all d. d = equivalent grain diameter in microns (µ). Green dots next to symbol for meteorite denote CCC, pink double dots denote CP, lack of dots denote FCC. Solid line box shows CCC trend, while dotted line box shows FCC trend.

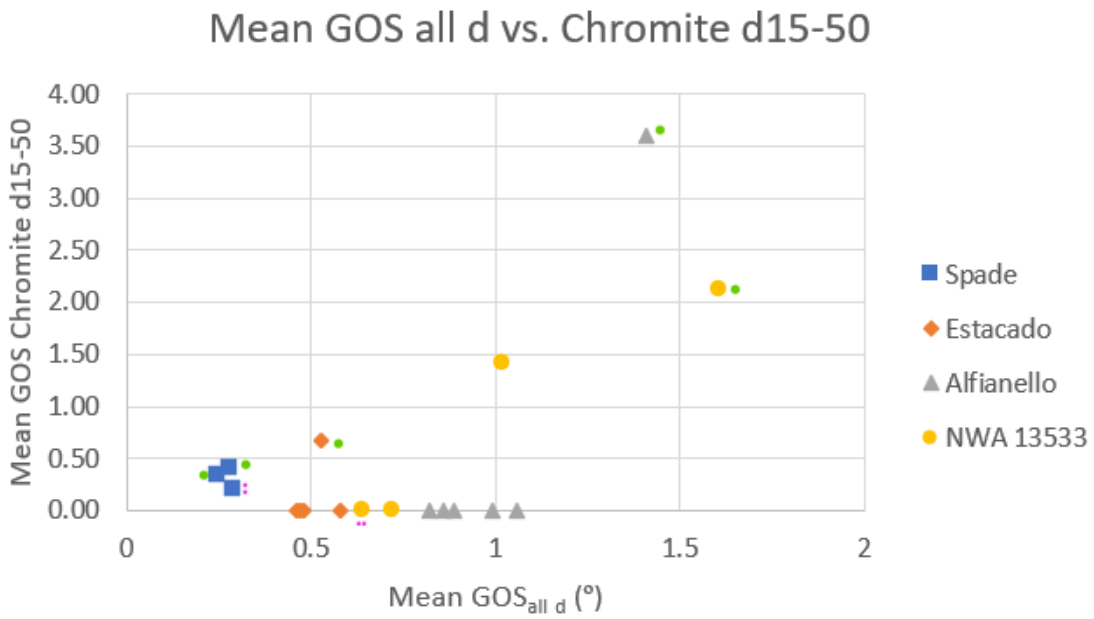

Figure 13: Mean Grain Orientation Spread (GOS) for all d for chromite on the x-axis, versus Chromite d 15-50 on the y-axis. Data points on the x-axis with zero values are artifacts of not having any d15-50 grains. Green dots next to symbol for meteorite denote CCC, pink double dots denote CP, lack of dots denote FCC.

In Figure 13, mean GOS in chromite for d=15-50 grains ($GOS_{d15\text{-}50}$) is plotted against mean GOS in grains of all sizes ($GOS_{all\ d}$). It is seen that not all targeted maps featured chromite grains between 15-50 µm size range, which is not surprising given the diminutive size of grains in some of the FCC assemblages. Aside from such assemblages, Fig. 13 shows that there is a general correlation between chromite $GOS_{d15\text{-}50}$ and $GOS_{all\ d}$.

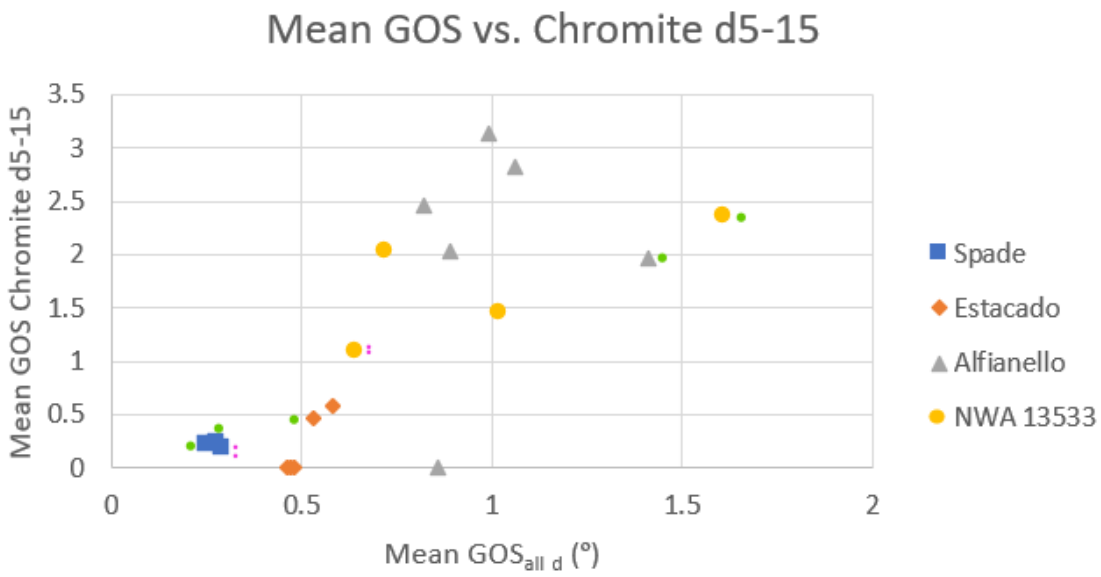

Figure 14: Mean Grain Orientation Spread (GOS) for all d for chromite on the x-axis, versus Chromite d 5-15 on the y-axis. Data points on the x-axis with zero values are artifacts of not having any d5-15 grains. Green dots next to symbol for meteorite denote CCC, pink double dots denote CP, lack of dots denote FCC.

Figure 14 shows mean GOS in chromite for d=5-15 grains (GOS_{d5-15}) against mean GOS in grains of all sizes ($GOS_{all\ d}$). There is now a more obvious positive trend, as more assemblages have grains at the 5-15µm size, with only three targeted maps sitting on the x-axis. The positive trend occurs both for FCC and CCC assemblages, but they may have different slopes (less steep for CCCs, steeper for FCCs).

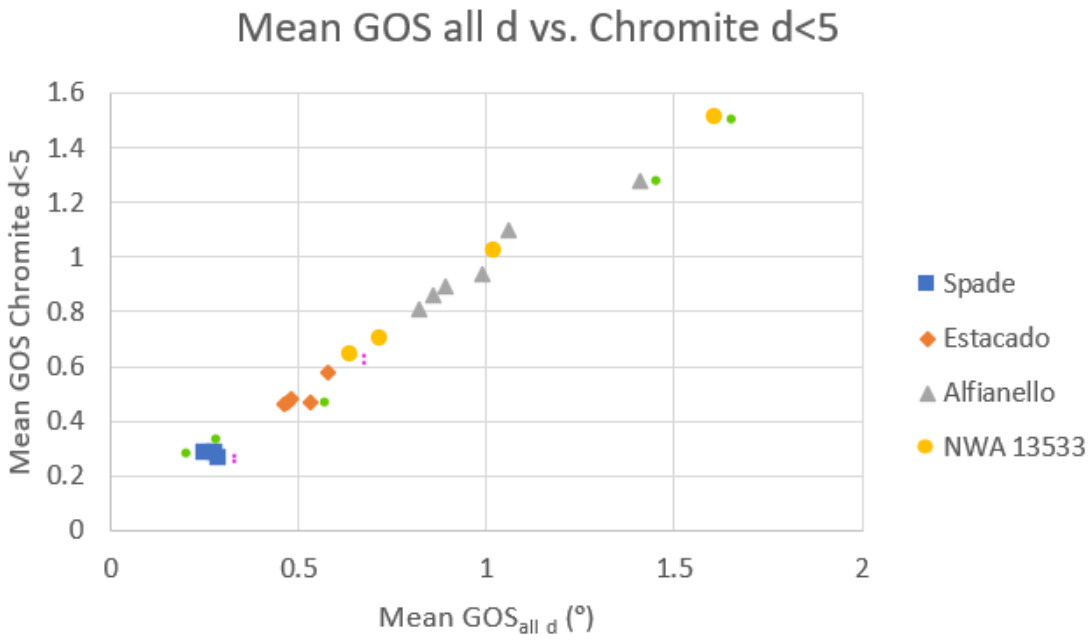

Figure 15: Mean Grain Orientation Spread (GOS) for all d for chromite on the x-axis, versus Chromite d <5 on the y-axis. Green dots next to symbol for meteorite denote CCC, pink double dots denote CP, lack of dots denote FCC.

In Figure 15, mean GOS in chromite for d<5 grains ($GOS_{d<5}$) is plotted against mean GOS in grains of all sizes. This linear correlation can be taken as evidence that the GOS all d parameter largely reflects the smallest (d<5) grains. This is true for FCC as well as CCC. Two CCC assemblages, one each from Alfianello and NWA 13533, have the largest chromite GOS values among the FCAs studied, whereas two other CCC assemblages, both from Spade, have the lowest GOS values. There is no obvious difference in chromite GOS between CCC and FCC assemblages. Instead, assemblages in the Alfianello and NWA 13533 tend to have higher chromite GOS than assemblages in Spade and Estacado.

The plagioclase data (Table 6) shows the relative coarseness of the feldspathic grains in Spade and Estacado, in comparison to the very small grains found in Alfianello and NWA 13533. The small grains in the high shock meteorites are due to relict

plagioclase grains that were not fully maskelynized. Alfianello and NWA 13533 were shocked hard enough that the feldspathic material was transformed to a glass, but not entirely, leaving behind a few grains.

3.5 Orientation and deformation data for example FCA assemblages

Figures 16-21 show orientation and deformation data for chromite in particular assemblages of different types. Inverse Pole Figure (IPF) maps show the crystal orientations of each chromite grain using a false color scheme, together with a monochrome band contrast image. In these maps the orientation of the <100> direction in chromite is shown relative to a sample coordinate system (x=left-right in the plane of the section, y=up-down in the plane of the section, z=normal to the section). Two types of pole figure plots are shown. One plots the orientation of each pixel with the corresponding color in the associated IPF map (pole figure plot with IPF colors). The other is a density plot based on 15º halfwidth contouring assuming one point per grain (contoured pole figure plot). The contoured pole figures especially highlight whether there is a lattice preferred orientation (LPO) of chromite grains. As chromite is a cubic mineral, there are three crystallographically equivalent <100> directions, so a single orientation will show as three distinct spots in a contoured <100> pole figure.

Grain Orientation Spread (GOS) and Grain Reference Orientation Deviation (GROD) angle maps show deformation of each chromite grain using a false color scheme together with a monochrome band contrast image. GOS indicates the average misorientation, whereas GROD angle shows the deviation in orientation within a crystal relative to the average orientation. GOS maps are shown with maximum values set to

15°, whereas GROD angle maps are shown with maximum values set to 20°. In these maps blue corresponds to minimum values, green to intermediate values, and red to maximum values.

Data for two example FCC assemblages are shown in Figure 16 and 17. The assemblages in NWA 13533 (TM1) (Fig. 16) and Alfianello (TM2) (Fig. 17) both consist of chromite groupings with sharp edges, all set in maskelynite. In NWA 13533, the chromite groupings form lath-like shapes. In Alfianello, the groupings have various polyhedral outlines. Both assemblages are dominated by small chromite crystallites, although there are some larger grains in the Alfianello assemblage that tend to be aligned.

Within each grouping of the two FCC assemblages, IPF colors are similar but vary somewhat, indicating a high degree but not perfect LPO. The pole figure plots for Alfianello indicate that there is one dominant orientation of chromite (a set of three spots), indicating a dominant LPO approaching a single orientation for all chromite groupings in this map (Fig. 17). The contoured pole figure plot for NWA 13533 indicates a somewhat more complex situation, characterized by a girdle of two <100> directions around a third dominant <100> direction (Fig. 18). This suggests rotation of a cube around a single axis that is fixed in direction. This could be related to the spread of chromite clumps in Figure 16, as there are more clumped groups that are going in many directions, as opposed to one large clump of chromite in the assemblage in Figure 17. The fan shape for clumps seen in Figure 16 is one that implies crystallization from a single point, analogous to the radiating pattern seen in radial pyroxene chondrules in chondrites (A. Ruzicka, Personal Communication).

Both of the FCC assemblages feature chromite crystals with low overall GOS values (Fig. 16, 17). A few crystallites, especially in the Alfianello assemblage, are more deformed (Fig. 17). In the latter, this includes most obviously the larger grains, but also some of the smaller crystallites.

Data for two CCC assemblages are shown in Figures 18 and 19. Both assemblages, in NWA 13533 (TM6) (Fig. 18) and in Estacado (TM2) (Fig. 19), consist of chromite grain groupings in chain-like patterns. These chains have irregular edges, marked by the edges of chromite crystals. The chromite grains are adjacent to maskelynite in NWA 13533 and within plagioclase in Estacado. In the Estacado assemblage, chromite grains are granular and often meet in triple junctions (Fig. 19). In the NWA 13533 assemblage, chromite grains also tend to be equant, though less granular, and often meet in triple junctions. A large difference from Estacado is that the CCC grains in NWA 13533 are more highly fractured, with some parts of the assemblage appearing to be brecciated (Fig. 18).

In contrast to the FCCs, the CCCs in NWA 13533 and Estacado do not show a strong chromite LPO, as indicated by a variety of IPF colors and a spatially random distribution in the pole figure plots (Fig. 18, 19). However, the LPO is higher for the Estacado assemblage (Fig. 19) than for the NWA 13533 assemblage (Fig. 18). Generally low LPO is typical of this assemblage type (Fig. 5, 9, 11).

The two CCC assemblages differ significantly in chromite deformation. In figure 18, the GROD angle 20 map for the CCC in NWA 13533 shows that there are many grains within the clump that have seen deformation (shown as blue grains with green to red in and around them). Conversely, Figure 17 for the CCC in Estacado is almost solidly

blue, with only one solid green grain, and very few blue grains showing some green around the edges (see scale bar).

Data for the two CP assemblages found in this study are shown in Figures 20 and 21. Both assemblages tend to have generally low LPO strength for chromite and low GOS for chromite. They also differ from one another, one being a larger map (Fig. 21), that tends to align itself closer with the CCC group, while the smaller map aligns more with the FCC group. The CP group also differs texturally, with the Spade TM showing plagioclase surrounding the chromite, while the NWA 13533 TM has maskelynite enclosing the chromite.

FCC

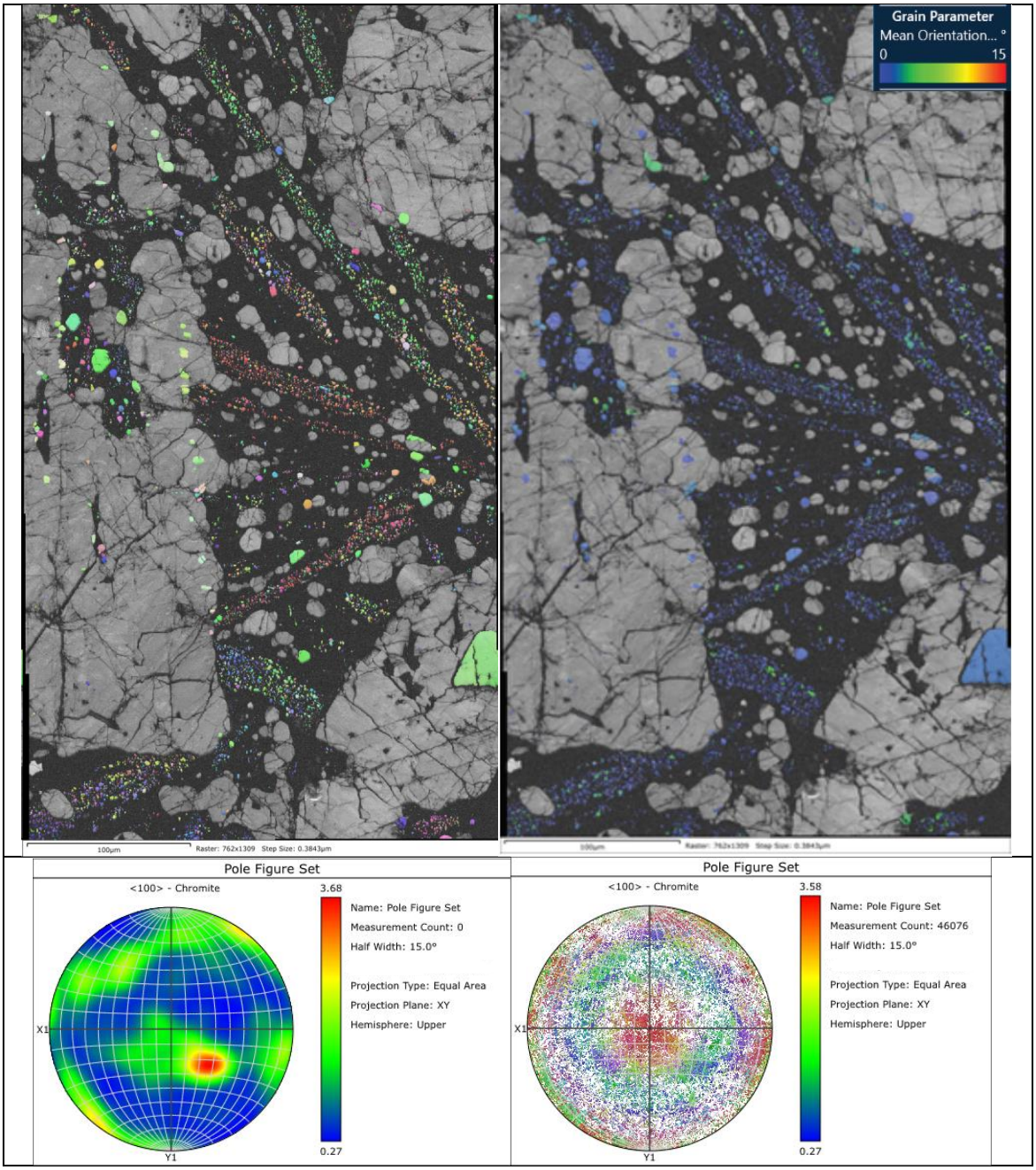

Figure 16: NWA 13533 (TM1), IPFx (top left) and GOS15 (top right) maps (colors) together with band contrast (monochrome), with contoured pole figure plot (bottom left), as well as scattered pole figure plot in IPFx colors (bottom right).

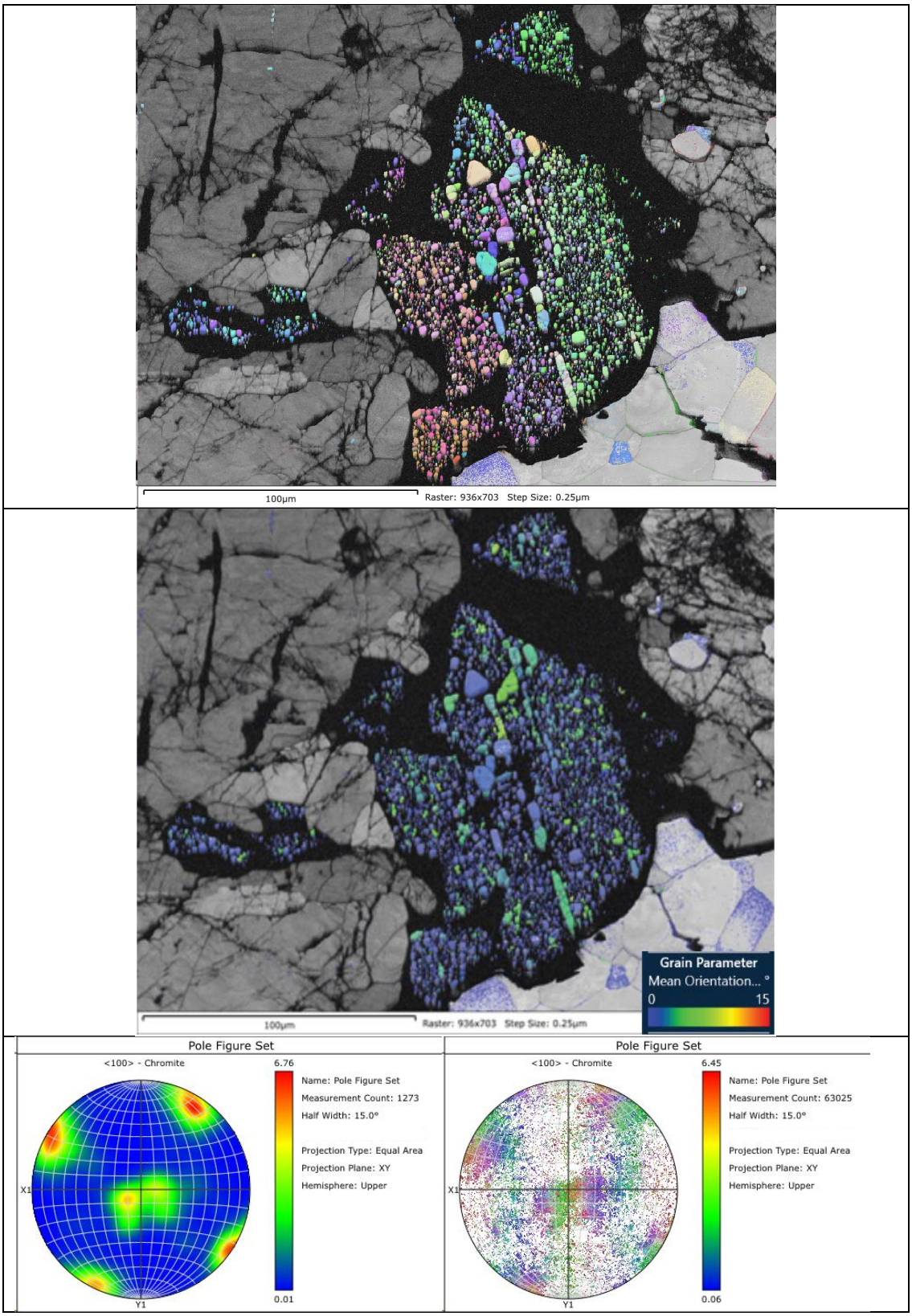

Figure 17: Alfianello (TM2), IPFx (top left) and GOS15 (top right) maps (colors) together with band contrast (monochrome), with contoured pole figure plot (lower left) and scattered pole figure plot in IPFx colors (lower right).

CCC

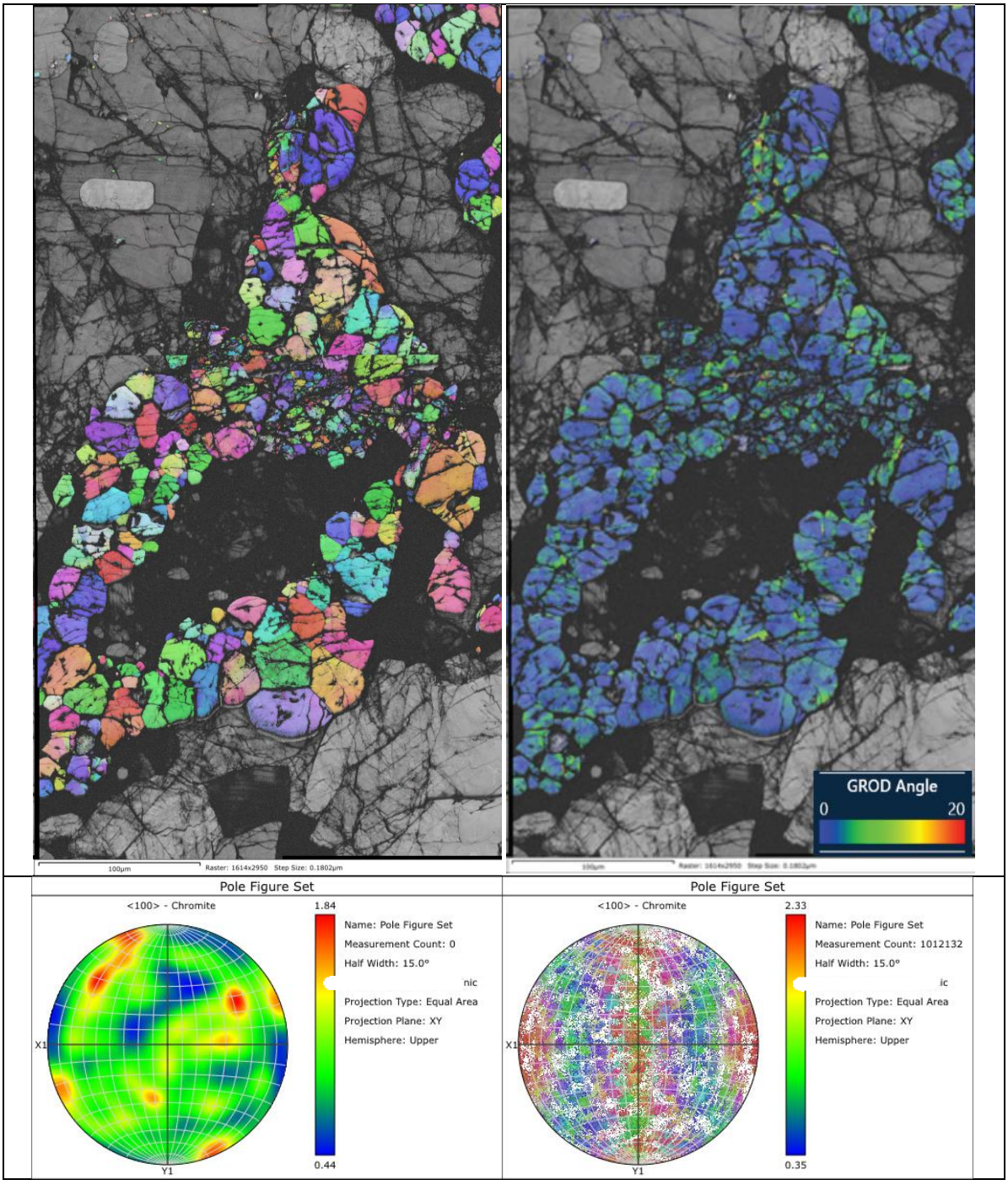

Figure 18: NWA 13533 (TM6), IPFx (top left) and GROD angle20 (top right) maps together with band contrast (monochrome), with contoured pole figure plot (lower left), as well as scattered pole figure plot in IPFx colors (lower right).

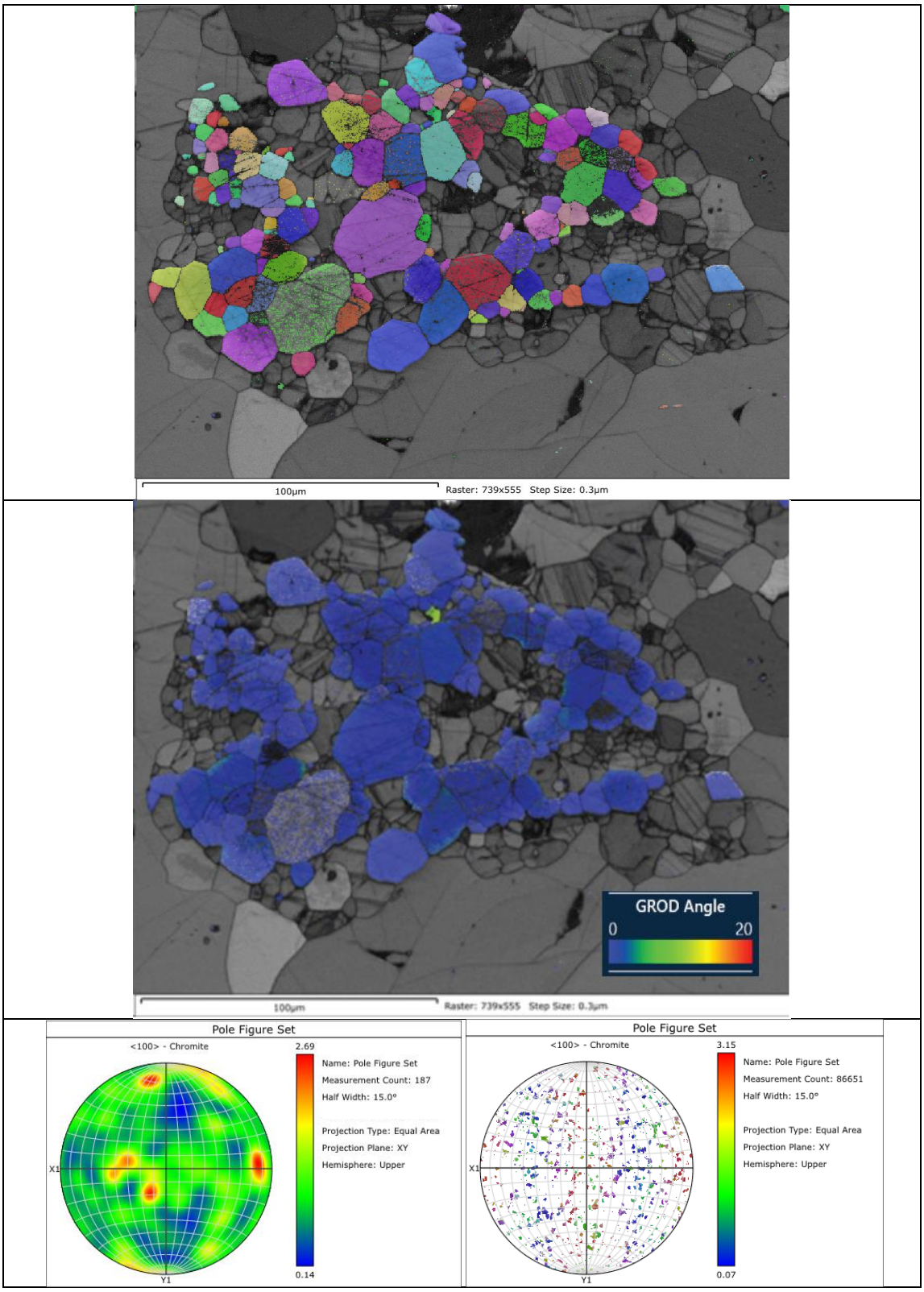

Figure 19: Estacado (TM2), IPFx (top) and GROD angle20 (middle) maps together with band contrast (monochrome), with contoured pole figure plot (lower left) and scattered pole figure plot in IPFx colors (lower right). Some artifacts were removed from the pole figures as to give accurate numbers.

CP

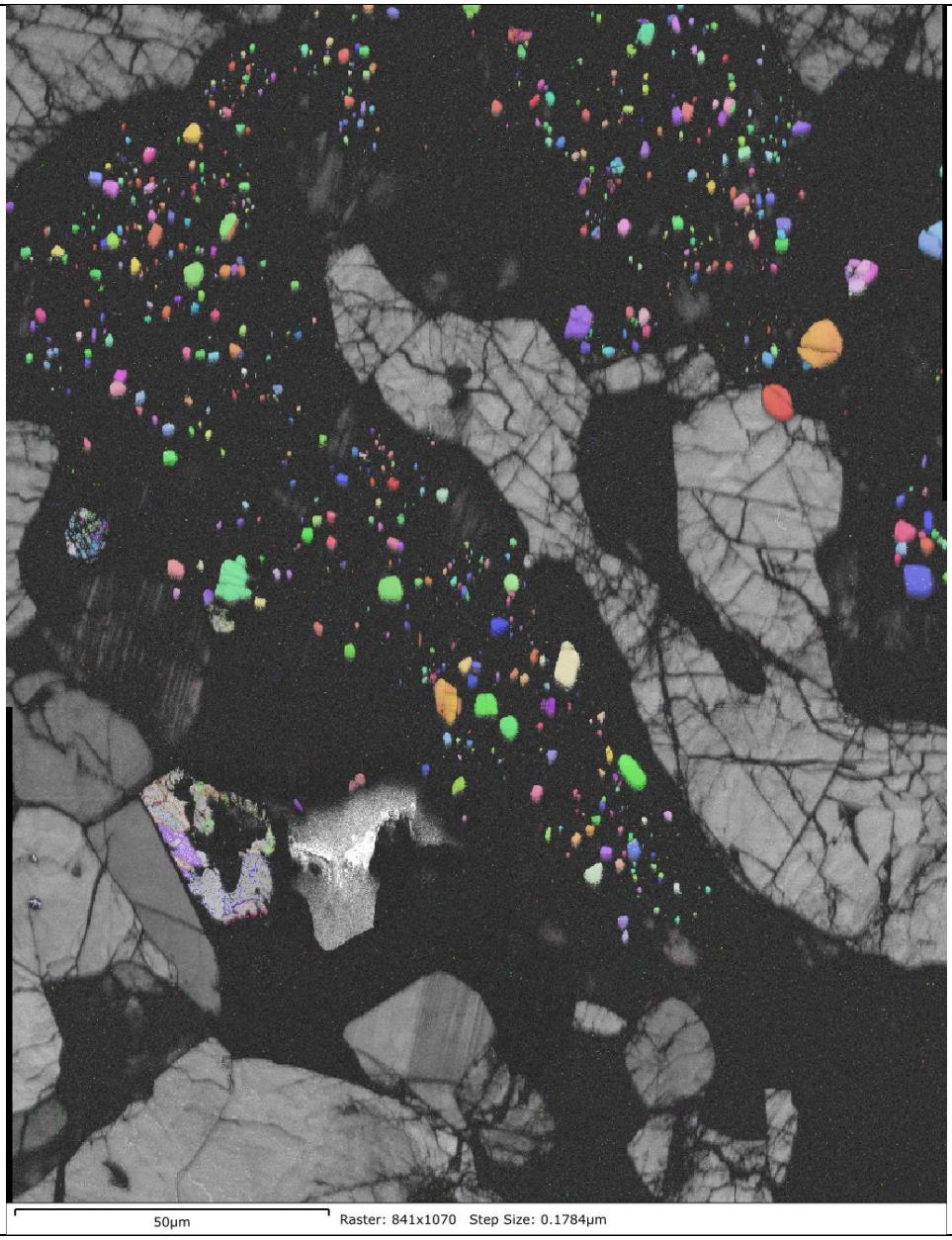

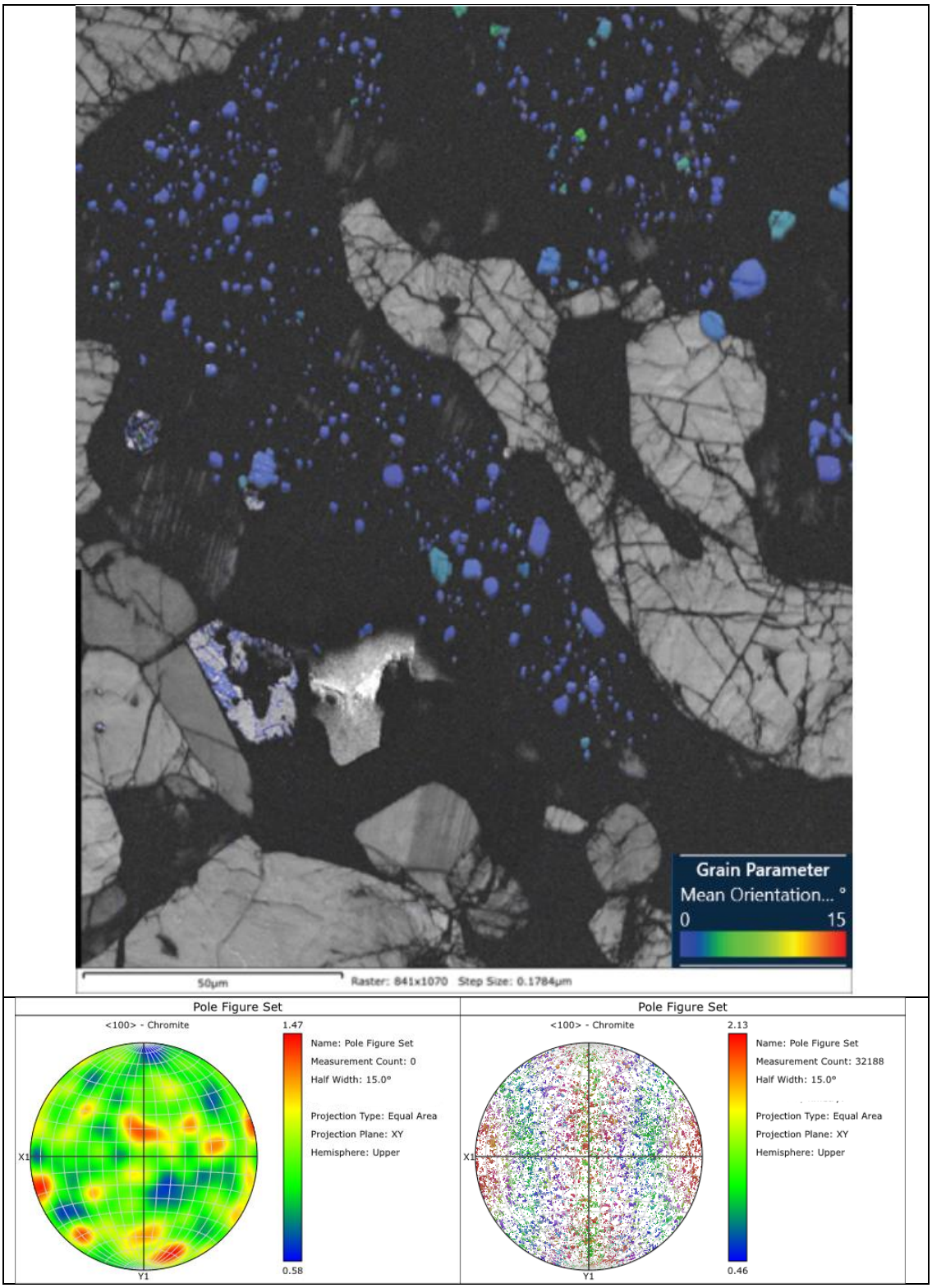

Figure 20: NWA 13533 (TM5), IPFx (top) and GOS15 (middle) maps together with band contrast (monochrome), with a 1 point-per-grain contoured pole figure plot (lower left) and all-pixels scattered pole figure plot in IPFx colors (lower right).

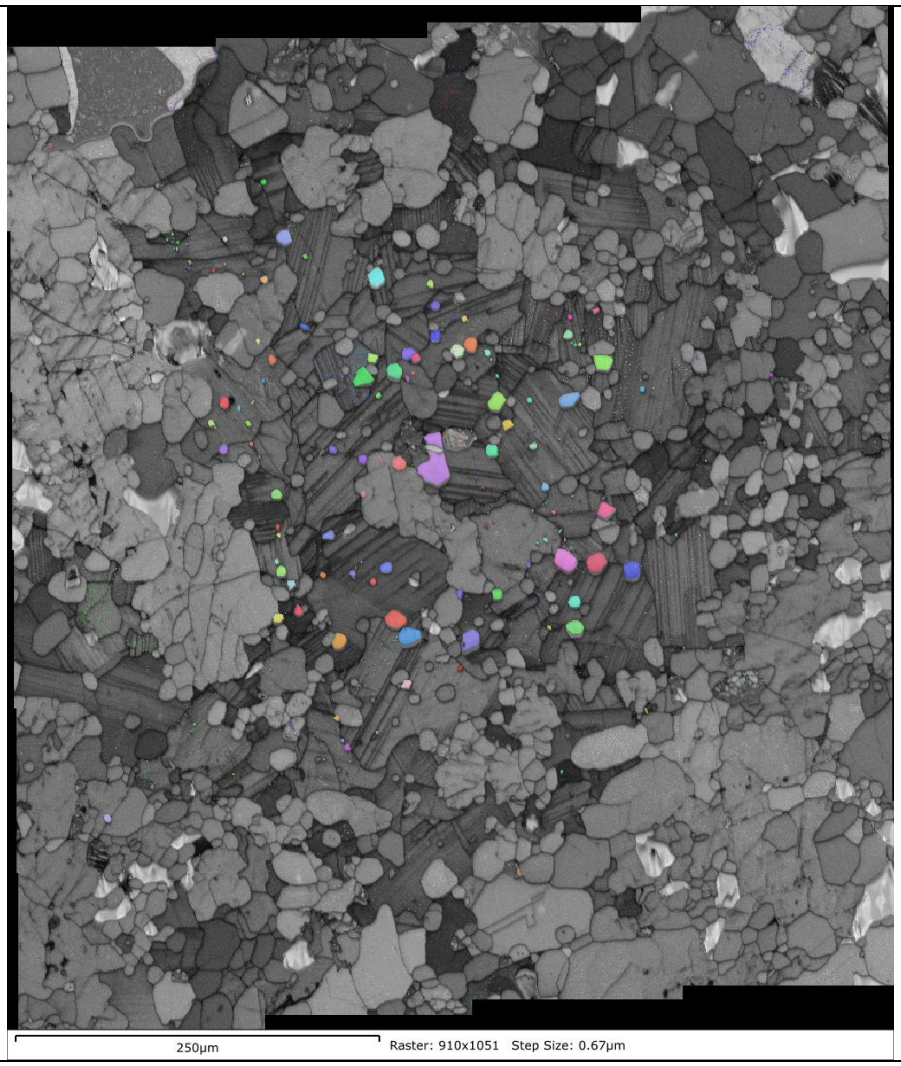
250µm
Raster: 910x1051 Step Size: 0.67µm

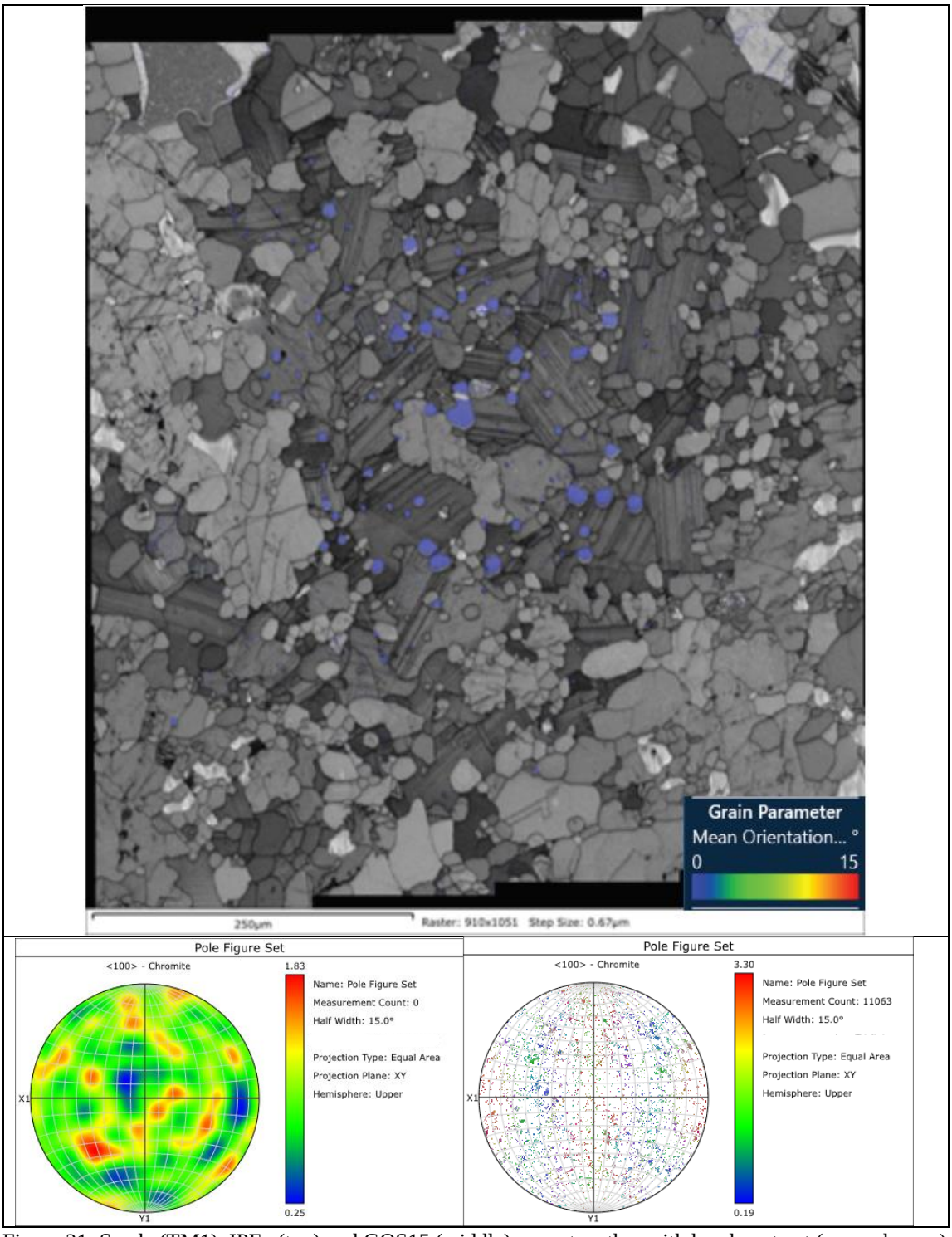

Figure 21: Spade (TM1), IPFx (top) and GOS15 (middle) maps together with band contrast (monochrome), with contoured pole figure plot (lower left) and scattered pole figure plot in IPFx colors (lower right).

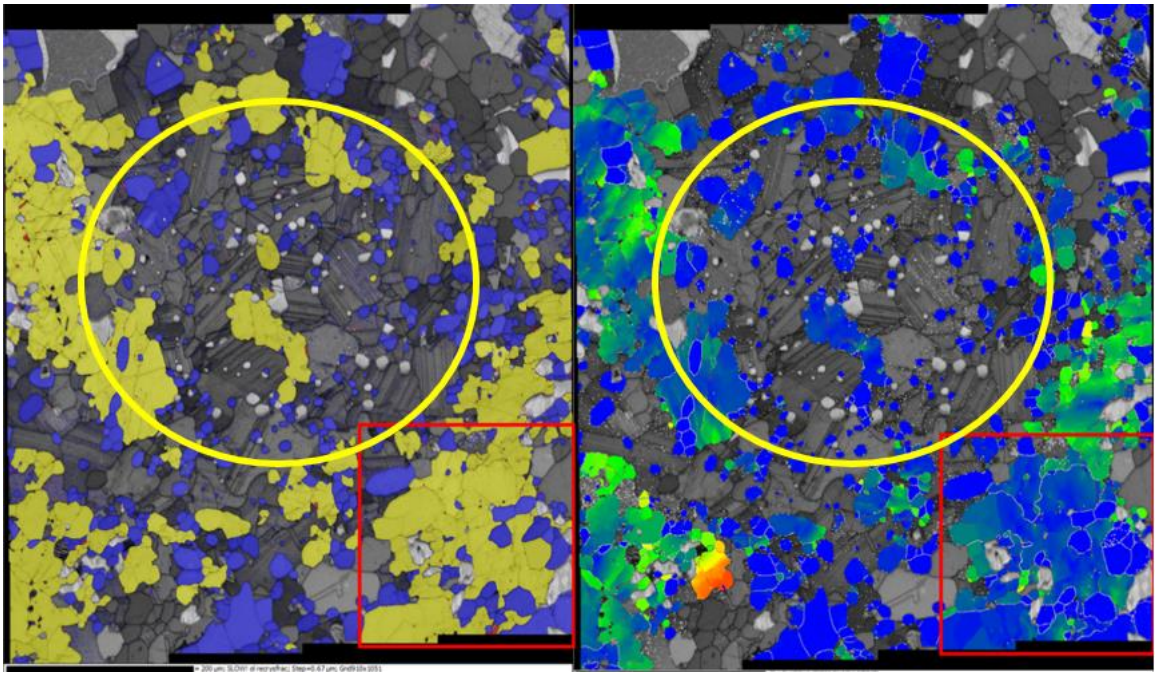

Figure 22: The map on the left (Spade TM1) shows the recrystallization of the olivine. Inside the red box the blue grains are the recrystallized grains, while yellow denotes structured grains. The map on the right (Spade TM1) shows the GROD angle20 map. Inside the red box the dark blue grains are grains that have not been deformed, while the green-blue grains have been deformed. The yellow circle highlights the Feldspathic Chromite Assemblage in this map.

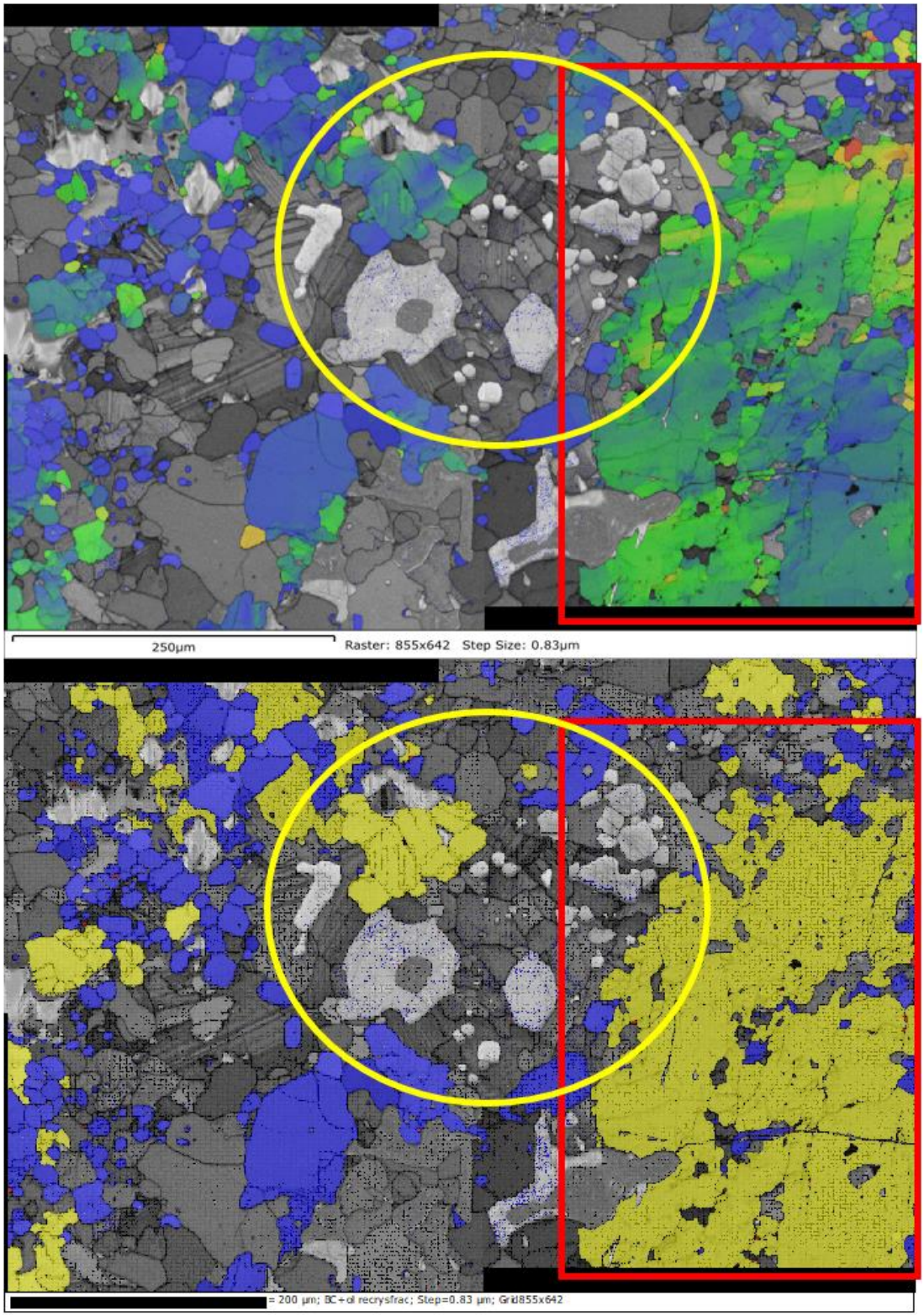

Figure 23: The map on the top (Spade TM1) shows the GROD angle20 map. Inside the red box at the top, dark blue grains are grains that have not been deformed, while the green-blue grains have been deformed. The map on the bottom (Spade TM1) shows the recrystallization of the olivine. Inside the red box at the bottom, the blue grains are the recrystallized grains, while yellow denotes structured grains. The yellow circle highlights the Feldspathic Chromite Assemblage in this map.

Figures 22 and 23 show two targeted maps taken from Spade, TM1 and TM2. Both figures are olivine maps, that show the recrystallization that Spade experienced. The left side map in Figure 22 shows a recrystallization map derived using Channel5 data. The blue grains are the recrystallized grains, meaning they are largely undeformed grains, while the yellow represents the structured grains that have been deformed, with sub-grain boundaries. The blue grains could represent the recrystallization of previously deformed grains, or grains that were never deformed in the first place. The bottom map in Figure 23 is the same as stated previous. The association of weakly-deformed grains, shown in the GROD angle 20 maps accompanying the recrystallization maps, with heavily deformed grains indicates either that olivine was recrystallized or that it was crystallized from a melt. This will be further discussed later in this Thesis.

3.3 LAM & mini-LAM data

The meteorites chosen for this study appear to vary significantly in deformation and thermal history. Data for olivine based on OM and EBSD Large Area Maps are shown in Table 6 and Fig. 24. Alfianello and NWA 13533 fit well into the group 3, type 6 meteorites as defined by Ruzicka & Hugo (2018) and Hugo et al. (2019), which have high shock stage (S4-S5), low $R_{2\text{-}10}$ values, and low $Sk_{d>50}$ values. These were interpreted to have been strongly shocked while cold initially, and quickly cooled after shock (Ruzicka and Hugo, 2018; Hugo et al., 2019). Spade is shown to have an elevated rotation parameter ($R_{2\text{-}10}$) but a low skewness parameter ($Sk_{d>50}$) (Table 6). In this regard it resembles St. Severin (LL6), which was interpreted to have been shocked while hot, but which cooled quickly afterwards (Hugo et al. 2019). Estacado has an $R_{2\text{-}10}$ value

between that of Spade and Alfianello and NWA 13533, as well as a higher $Sk_{d>50}$ value (Table 7, Fig. 24). Based on Ruzicka and Hugo (2018) and Hugo et al. (2019), this could indicate that Estacado experienced deformation at an elevated temperature followed by a significant amount of post-shock annealing (A. Ruzicka, personal communication). More details on the apparent deformation and thermal histories for the four meteorites are given in the Discussion.

Table 7: Olivine data including shock stage (weighted and conventional), and the EBSD parameters R_{2-10} and $Sk_{d>50}$ based on Large Area Maps. The implied thermal history based on the EBSD parameters is shown following Ruzicka and Hugo (2018). Shock stage data for Spade, Estacado, and Alfianello after Friedrich et al. (2017).

Meteorite	Map	Step Size (µm)	Weighted Shock Stage	Conventional Shock Stage	R_{2-10}	$Sk_{d>50}$	Thermal History*
Spade (0269-1A)	mini LAM	2.5	2.39	S4	0.748	1.065	high temp, low annealing
	LAM	4			0.695	1.062	high temp, low annealing
Estacado (0295-3C)	LAM	4	1.28	S1	0.605	1.451	high temp, high annealing
Alfianello (0496-1A)	LAM	4	4.18	S5	0.383	1.082	low temp, low annealing
NWA 13533 (0995-1)	LAM	4.5	3.73	S4	0.357	1.100	low temp, low annealing

* Temp = temperature

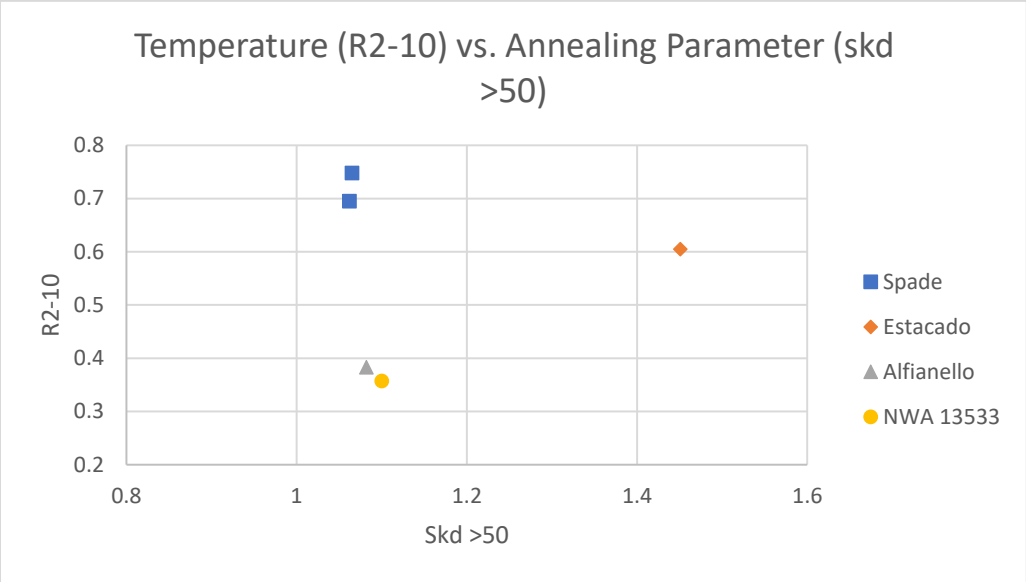

Figure 24: Temperature (R_{2-10} parameter) vs. Annealing ($Sk_{d>50}$) parameter.

Tables 8 and 9 and Figures 25 and 26 present data for GOS in the 3 major phases highlighted for this study, olivine, chromite, plagioclase. No GOS data were obtained for chromite in the LAM dataset for Spade, because in this dataset metal grains were often mis-indexed as chromite. Figures 27, 28, 29, and 30 show GOS maps for olivine in the mini-LAM for Spade and the three LAMs for Alfianello, Estacado, and NWA 13533, using a uniform false color scale for GOS.

The GOS maps show that most olivine grains in Estacado are weakly deformed (dominantly blue colors, Fig. 28), whereas many olivine grains in Alfianello (Fig. 29) and NWA 13533 (Fig. 30) are significantly deformed (dominantly green colors). A few of the grains in Estacado have higher GOS values (green, yellow in Fig. 28). In Spade, many olivine grains are significantly deformed (green) and many others are weakly deformed (blue) (Fig. 27).

Mean GOS values in olivine and chromite for the coarsest grains (d>50 μm) are similar in Estacado and Alfianello but tend to be higher for olivine than chromite in Spade and NWA 13533 (Fig. 25). In comparing coarse (d>50 μm) grains of olivine and plagioclase in Spade and Estacado, mean GOS values appear to be higher in olivine (Table 9) but there are too few data for plagioclase to be sure.

For moderately small (d=5-15 μm) grains, the mean GOS values in Spade and Estacado for olivine and chromite are similar, but in Alfianello and NWA 13533 the GOS values are significantly lower in olivine than in chromite (Fig. 26). When comparing moderately small grains of olivine and plagioclase in Spade and Estacado, the mean GOS values are notably lower in olivine than in plagioclase (Table 9).

Table 8: Mean Grain Orientation Spread (GOS) values for equivalent grain sizes greater than 50 µm and for equivalent grain sizes of 5-15 µm for olivine and chromite, based on LAM and mini-LAM data.

Meteorite	Map	Mean GOS olivine (d>50)	Mean GOS olivine (d5-15)	Mean GOS chromite (d>50)	Mean GOS chromite (d5-15)
Spade (0269-1A)	mini LAM	2.76	0.55	1.2x	0.37
	LAM	2.75	0.90	--	--
Estacado (0295-3C)	LAM	0.70	0.53	0.75	0.55
Alfianello (0496-1A)	LAM	4.36	3.23	4.18	1.62
NWA 13533 (0995-1)	LAM	4.71	3.46	3.16	1.97

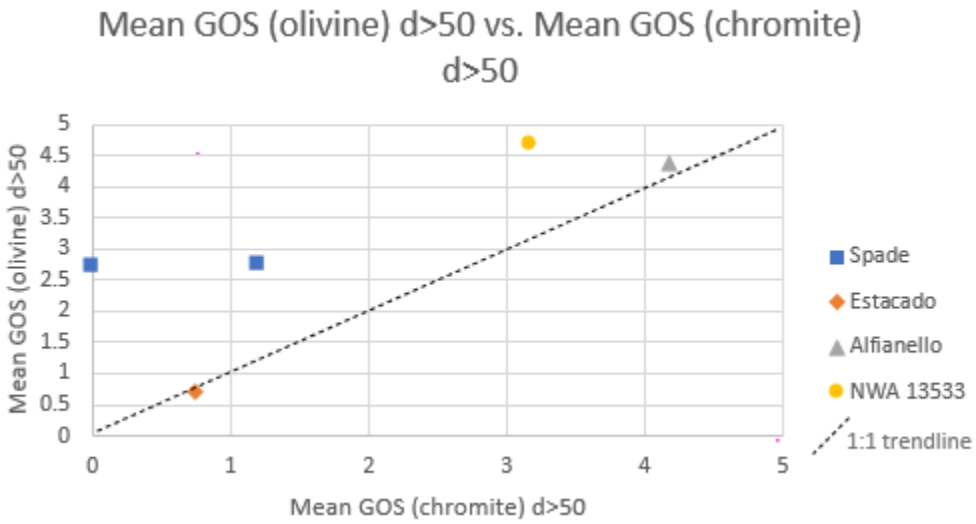

Figure 25: Mean Grain Orientation Spread (GOS) of grain sizes (d) greater than 50 for olivine versus chromite in all four samples Large Area Maps (LAM). The zero-GOS value for the Spade point is an artifact, as metal was mis-indexed as chromite and the GOS value for chromite was arbitrarily set to zero.

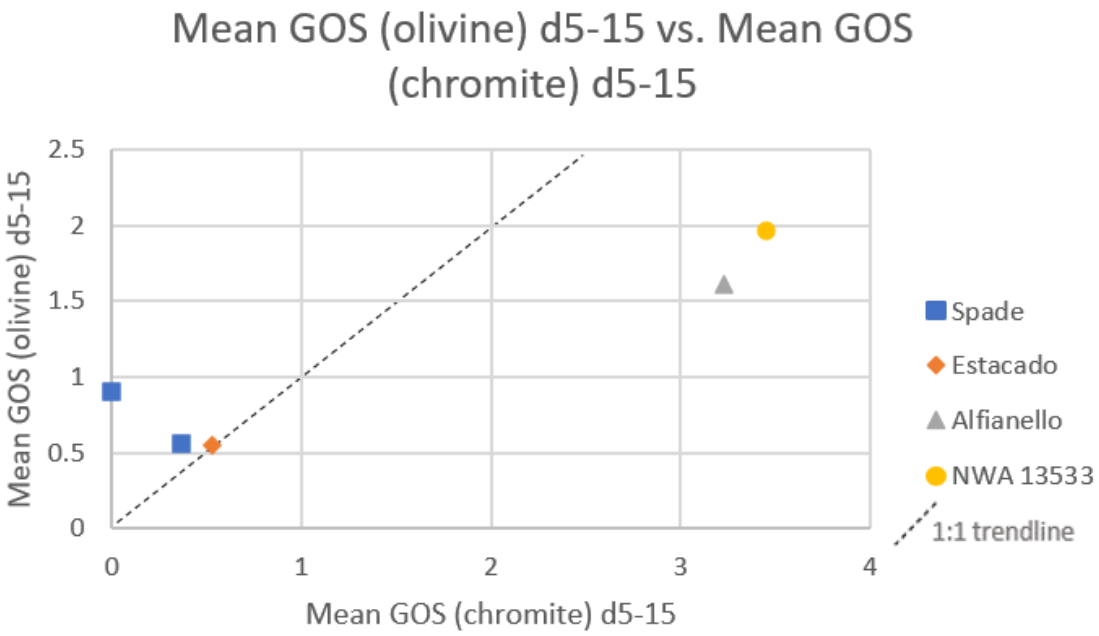

Figure 26: Mean Grain Orientation Spread (GOS) of grain sizes (d) 5-15 for olivine verses chromite in all four samples Large Area Maps (LAM). The zero-GOS value for the Spade point is an artifact, as metal was mis-indexed as chromite and the GOS value for chromite was arbitrarily set to zero.

Table 9: Mean GOS table for all Targeted Maps and Large Area Maps. Shows the grain size (d>50 & d5-15) and standard deviation of GOS for Olivine, Chromite, and Plagioclase.

Meteorite	Map	olivine (d>50) +/- St Dev	olivine (d5-15) +/- St Dev	chr (d>50) +/- St Dev	chr (d5-15) +/- St Dev	plag (d>50) +/- St Dev	plag (d5-15) +/- St Dev
Spade (0269-1A)	TM1A	3.06 +/-1.84	0.40 +/-1.75	--	0.18 +/-0.04	1.72 +/-1.49	0.69 +/-0.62
	TM2A	2.69 +/-1.51	0.49 +/-0.80	--	0.22 +/-0.20	0.49 +/-n/a	0.90 +/-0.54
	TM3A	4.08 +/-2.71	0.49 +/-0.76	--	0.23 +/-0.14	1.91 +/-n/a	0.69 +/-0.45
	mini LAM	2.76 +/-1.68	0.55 +/-0.61	1.2 +/-0.65	0.37 +/-0.45	1.15 +/-0.98	0.94 +/-0.56
	LAM	2.75 +/-1.57	0.88 +/-0.91	--	--	0.84 +/-0.14	0.93 +/-0.55
Estacado (0295-3C)	TM1B	--	0.43 +/-0.13	--	--	--	0.64 +/-0.16
	TM2B	0.38 +/-0.14	0.39 +/-0.10	--	1.47 +/-0.21	--	0.85 +/-0.62
	TM3B	--	0.31 +/-0.10	--	--	--	0.89 +/-0.34
	TM4B	--	--	--	--	--	0.82 +/-0.44
	TM5B	--	0.68 +/-0.85	--	0.58 +/-n/a	0.75 +/-n/a	0.61 +/-0.36
	LAM	0.697 +/-0.73	0.53 +/-0.35	0.75 +/-0.49	0.55 +/-0.39	1.15 +/-0.53	1.11 +/-0.75
Alfianello (0496-1A)	TM1C	5.34 +/-0.38	3.61 +/-2.55	--	1.97 +/-1.49	maskelynite	maskelynite
	TM2C	4.12 +/-n/a	3.27 +/-1.99	--	2.04 +/-1.65	maskelynite	maskelynite
	TM3C	--	4.44 +/-1.52	--	--	maskelynite	maskelynite
	TM4C	3.73 +/-n/a	2.34 +/-0.91	--	2.46 +/-n/a	maskelynite	2.77 +/-n/a
	TM5C	--	4.53 +/-2.64	--	2.83 +/-n/a	maskelynite	1.13 +/-n/a
	TM6C	2.54 +/-1.10	4.1 +/-2.15	--	3.14 +/-2.24	maskelynite	maskelynite
	LAM	4.36 +/-1.74	3.23 +/-2.13	4.18 +/-2.21	1.62 +/-1.81	--	1.64 +/-0.77
NWA 13533 (0995-1)	TM1D	3.23 +/-0.62	1.93 +/-1.12	--	1.45 +/-1.05	maskelynite	6.83 +/-n/a
	TM4D	--	2.19 +/-0.99	--	2.04 +/-0.81	maskelynite	maskelynite
	TM5D	3.84 +/-n/a	2.94 +/-1.73	--	1.09 +/-0.63	maskelynite	maskelynite
	TM6D	4.07 +/-2.04	3.52 +/-1.74	--	2.37 +/-1.53	maskelynite	0.94 +/-0.25
	LAM	4.71 +/-1.97	3.46 +/-2.07	3.16 +/-1.11	1.97 +/-1.89	--	1.56 +/-0.73

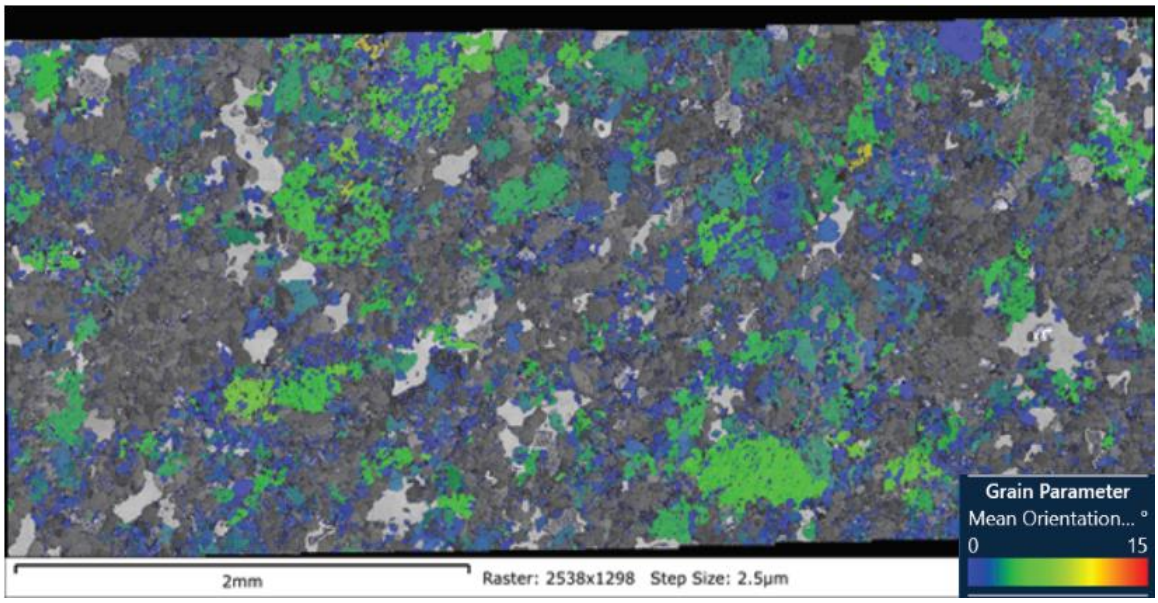

Figure 27: Spade mini-LAM GOS15 map for olivine (colors) and band contrast (monochrome).

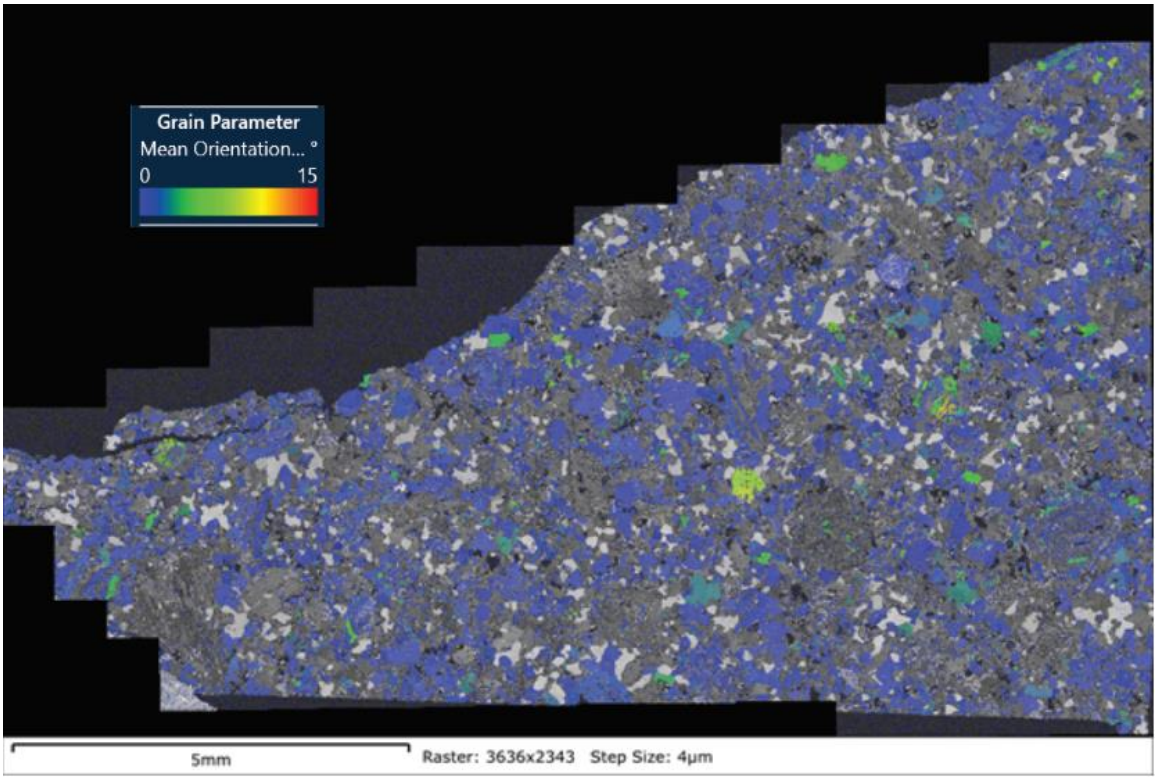

Figure 28: Estacado LAM GOS15 map for olivine (colors) with band contrast (monochrome).

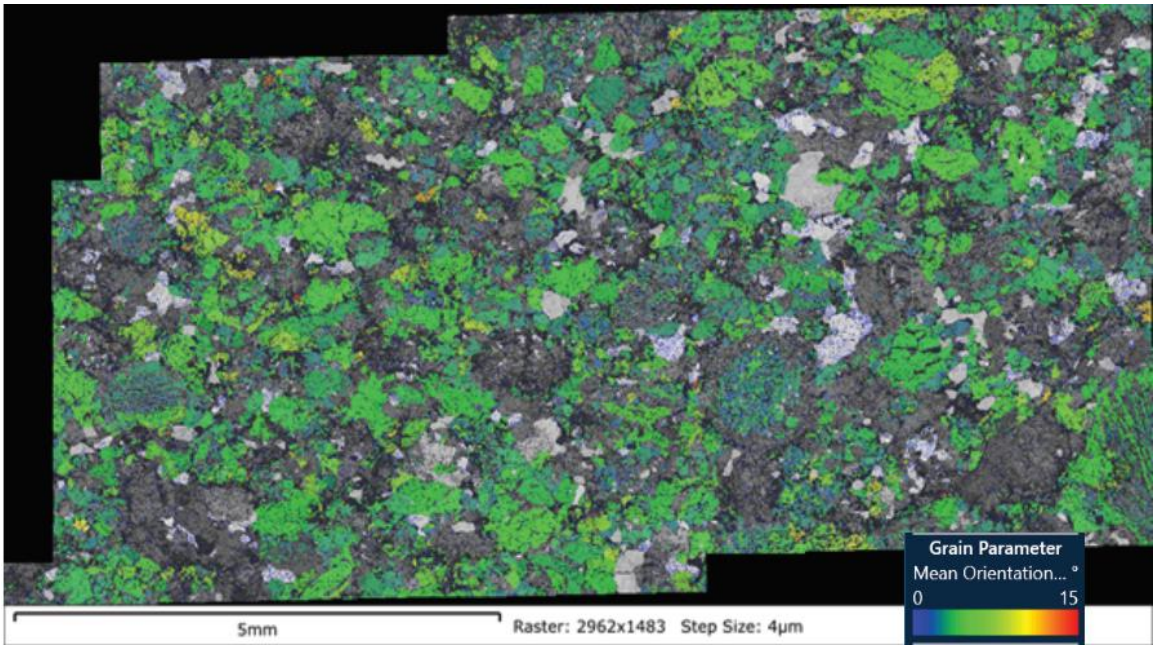

Figure 29: Alfianello LAM GOS15 map for olivine (colors) and band contrast (monochrome).

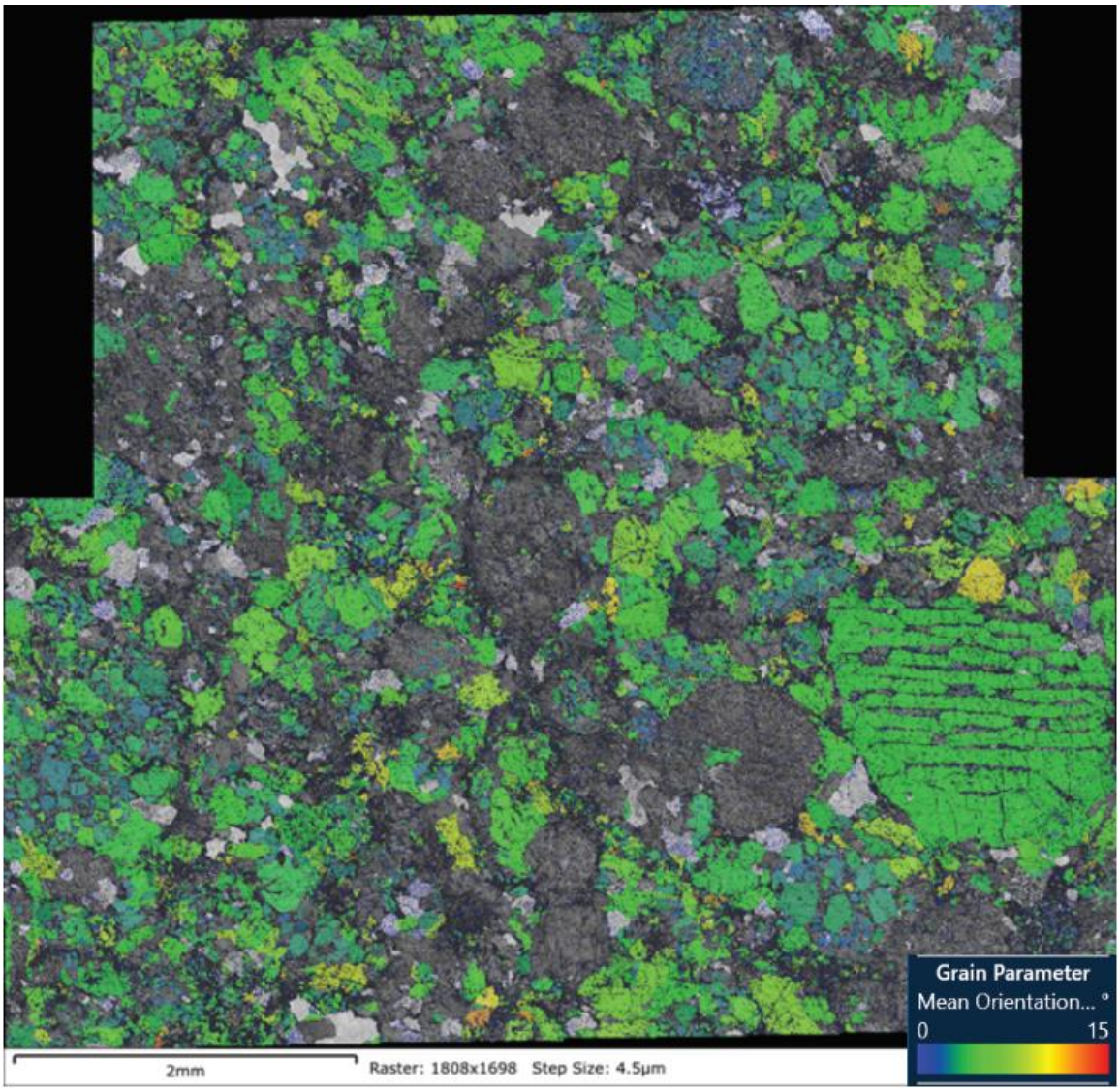

Figure 30: NWA 13533 LAM GOS15 map for olivine.

4) DISCUSSION

4.1 General Meteorites (deformation-thermal history)

Olivine LAM data suggest that the four meteorites can be grouped into three different categories for shock and thermal histories (Table 6). **1)** Spade was deformed at high temperatures and did not experience much post-shock annealing afterwards. Like St. Severin (Hugo et al., 2019), Spade may have been excavated from an interior portion of the parent body while it was experiencing thermal metamorphism and placed near the top surface of the body. The histories for Spade and St. Severin could have been generally similar but they represent different parent bodies (H for Spade, LL for St. Severin). **2)** Alfianello and NWA 13533 were deformed at low temperatures and did not experience much post-shock annealing. Like Leedey, Bruderheim, and Morrow County for the L-group (Ruzicka and Hugo, 2018) and Elbert for the LL group, Alfianello and NWA 13533 could have been shocked while the L parent body was cold. **3)** Like Spade, Estacado could have been shocked while the parent body was undergoing thermal metamorphism, but unlike Spade, Estacado was annealed after shock. This could indicate that the source materials for Estacado remained buried in a warm body after deformation.

4.2 Spade

Spade gives the impression of a strongly shocked meteorite that caused localized melting that created the FCAs that are found there. The olivine adjacent to the FCAs appears to be recrystallized, not annealed after deformation as has been previously proposed for Spade overall (Rubin and Jones, 2003). This indicates intense deformation, as olivine recrystallization is associated with shock stage S6 (Stöffler et al. 1991, 2018;

Fritz et al., 2017). Figure 16 is strong evidence for Spade having not been annealed, given that its annealing parameter (Skd_{50}) is relatively low (~1.06-1.07 for both LAM and mini LAM, Table 6). The small (d=5-15) chromite grains in Spade have low mean GOS (<0.4°) and have especially low mean GOS values (~0.18-0.23) in the three FCAs examined (Table 8, Fig. 14). These GOS values are the lowest in the meteorites examined for this grain size range. Similarly, the smallest (d<5) grains in FCAs from Spade have the lowest GOS values among any assemblage examined (Fig. 15). Given that Spade was evidently strongly shocked and not significantly annealed, low GOS values for the smaller chromites including those in FCAs could indicate that the small chromites formed by crystallization from melts, and that the FCAs in Spade formed at least in part by crystallization from melt pockets. This is consistent with the plagioclase normal Na-Ca zoning (Ca-rich cores, Na-rich rims) that was found in the EDS maps of these FCAs. For larger (d>50) grains, Spade shows a much higher mean GOS in olivine compared to chromite, but for smaller (d=5-15) grains, GOS values in olivine and chromite are similar (Fig. 25, 26, Table 8). This may indicate that the larger olivines in Spade often have relict deformation, but that the smaller olivine grains could have either been recrystallized, as shown by some olivine adjacent FCAs, or crystallized from a melt, as in the FCAs themselves (Fig. 22, 23).

4.3 NWA & Alfianello

Both NWA 13533 and Alfianello appear to have been strongly shocked from a cold initial state and quickly cooled afterwards. They give the impression of strongly shocked meteorites with FCAs created by localized melting. The presence of

maskelynite, which only appears in strongly shocked meteorites (Stöffler et al., 1991), and which could have crystallized from melts (Chen and El Goresy, 2000) and is concentrated in FCAs, supports this idea. Within the maskelynite is the presence of ragged plagioclase patches, which appear to represent relict plagioclase grains. The presence of relict plagioclase indicates that at least some portion of the FCAs was not melted.

GOS values in olivine and chromite grains of different sizes in NWA 13535 and Alfianello are the highest in the four meteorites examined (Table 7; Fig. 25, 26). This includes elevated GOS values in chromite for the FCAs themselves (Table 8). Although the high GOS values generally support the idea that NWA 13533 and Alfianello were strongly shocked, elevated GOS in FCA chromite raises the question of whether all the chromite in these assemblages crystallized from a melt. It would seem either that some of the chromite in the FCAs from these meteorites is also relict, or that chromite in FCAs was deformed after it crystallized from a melt.

4.4 Estacado

Estacado shows evidence of a shock followed by annealing. If the FCAs found in this meteorite formed by shock melting, this was followed by the crystallization of plagioclase from these melts (as proposed here for Spade) or was followed by the crystallization of plagioclase from maskelynite. The plagioclase grains found in the FCAs are fairly coarse, which suggests that the plagioclase crystallized out of the melts. However, normal zoning was not observed for plagioclase in EDS maps. Such normal zoning could have been obliterated during annealing, so the lack of such zoning is not

necessarily an argument against melt crystallization. Estacado has consistently low GOS values in minerals (though not as low as Spade), which could have been lowered during the annealing event. This is called 'recovery', when the GOS values are lowered by the movement of dislocations within crystals, a process proposed for some type 6 ordinary chondrites (Ruzicka and Hugo, 2018). Mean GOS values are similar between olivine, chromite, and plagioclase in Estacado (Table 8), although somewhat higher in plagioclase compared to the other two minerals based on the Large Area Map. This could indicate that annealing lowered the GOS values in all these minerals in Estacado, especially for olivine and chromite.

4.5 FCA comparison across all meteorites

There are five main parameters that were used to characterize the assemblages utilized in this study. These parameters help to craft the origin story of these objects, here we will talk about each textural type in terms of these parameters. In the four meteorites chosen, eighteen targeted maps were acquired and further analyzed. Altogether, the data suggest that there are two main types of chromite-rich assemblages in type 6 chondrites, fine clumped chromite (FCC) and coarse clumped chromite (CCC), with chromite-poor (CP) forming a third, smaller, group. Below is the comparison of the parameters for the three assemblage types (LPO, Chromite Coarseness Ratio, and Clump Density), as well as the parameters that do not seem to factor into assemblage origin (Area Fraction of Chromite, and GOS).

FCC:

A model for the origin of Fine Clumped Chromites relies heavily on three of the five parameters, specifically the LPO, clump density, and grain coarseness ratio. GOS parameters give information on how the assemblages were processed and is discussed after the other parameters.

Most of the FCC assemblages have a high (>5) chromite LPO number. This leads to one of two conclusions, 1) the subsets taken in these assemblages are pseudomorphs that exsolved from a high pressure precursor phase, or 2) they represent single grains of chromite that are spongy. This means that the grains are connected in 3 dimensions with a good amount of space between the grains. If the second possibility is correct, then the chromite would have to be extremely spongy, with more non-chromite than chromite in any given slice of the meteorite. However, the apparent euhedral shapes of some of the chromite grains is strong evidence against the grains being spongy. Available evidence therefore supports the suggestions of Ramdohr (1967, 1973) that some chromite assemblages, including the FCC type described here, formed by the decomposition of unstable precursor grains. Ramdohr (1967, 1973) suggested that the precursor phase could be a pyroxene rich in the kosmochlor ($NaCrSi_2O_6$) component. Brearley et al. (1991) studied a chromite-rich inclusion in an L6 chondrite (Los Martinez) that has fine oriented chromite set in plagioclase, similar to FCC, and on the basis of preferred orientation and other features suggested that fine chromite and plagioclase exsolved from an unknown metastable phase that itself had crystallized from a melt.

The FCCs used for this study have a high clump density, especially in those examples with high LPOs. This suggests these assemblages are the product of

precipitation from a melt that did so in such a way that the result is many chromite grains in one concentrated space such as is seen in the targeted maps. Conversely, this could also imply that the inferred precursor grain was so loaded with normative chromite, that the grains produced were small enough to allow many grains to be packed closely together in a fairly compact area.

The FCC assemblages are not resolved by the area fraction of said assemblages. They have a variety of chromite area fractions, as well as a variety of GOS. GOS seems to mostly relate to the host meteorite and can indicate that this assemblage is not distinguished by GOS, but by the history experienced by the host meteorite.

CCC:

The origin of Coarse Clumped Chromites, much like the FCCs, relies on the same three of the five parameters. CCCs are most likely some sort of aggregates of pre-existing grains, or grain clumps that crystallized from a melt that was enriched in normative chromite. The low clump density of the CCC group could be attributed to their potential aggregate origin, as they have fewer, but larger, grains to 'clump'. Clump density is found using the area of an assemblage divided by the number of chromite grains found in that assemblage. CCCs tend to have fewer, but larger, chromite grains and are concentrated closer together, as there is usually little to no space between chromite grains.

Much like the FCCs, the CCCs are not resolved by the area fraction. They trend towards a high to moderate area fraction which leads to two possible conclusions, 1) these were pre-existing chromite grains that were clumped together as a result of shock or 2) they could also be crystallized from a melt after shock and then clumped together.

CP:

The origins of the Chromite Poor assemblages are less clear. Both CP assemblages were found to be typically low in almost all parameters. The LPO of these assemblages is the lowest off all 18 Targeted Maps. However, they overlap with the CCC and FCC groups in terms of the grain coarseness ratio and GOS. These assemblages were found in Spade and NWA 13533, which points to theses assemblages being crystallized from a melt.

GOS:

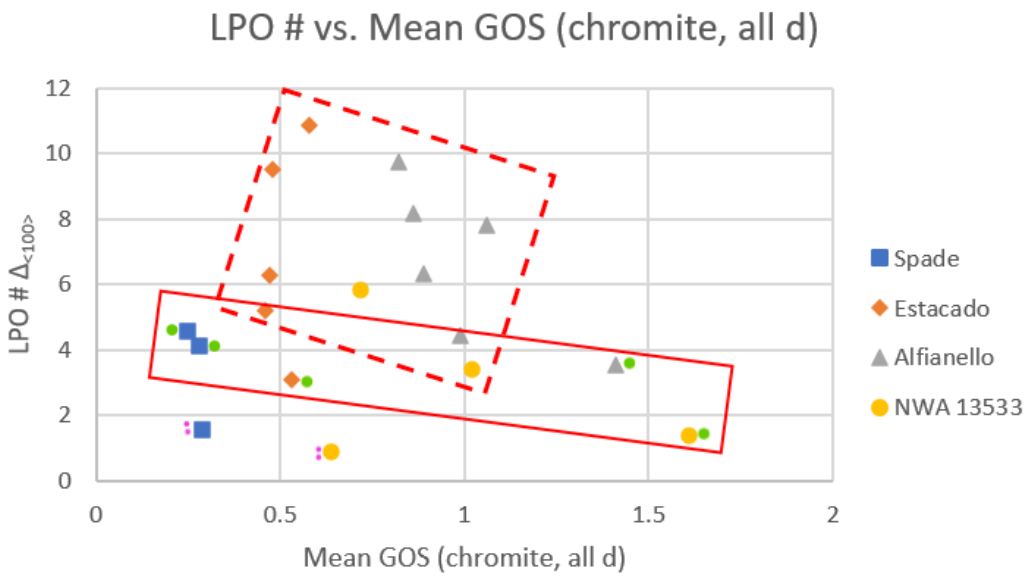

Figure 31: LPO # vs. Mean GOS of chromite, all d. d = equivalent grain diameter in microns (μ). Green dots next to symbol for meteorite denote CCC, pink double dots denote CP, lack of dots denote FCC. Solid line box shows CCC trend, while dotted line box shows FCC trend.

This parameter is the only one that does not strongly relate to assemblage type. The GOS data taken for these assemblages appears to have more of a correlation to the shock stage and thermal history of the meteorites host body. This implies that the chromites crystallized from a shock melt due to the deformation that the host body experienced. This could mean that there was more of an aggregational origin for these

assemblages, but this doesn't line up well with the FCC group. There is always the possibility of a second shock event having happened, but this is not a model that works for Spade. With the FCCs not fitting into an aggregational origin, therefore we gravitate to the idea that these assemblages were created due to exsolution from a precursor phase.

Figures 7, 8, and 31 compare mean GOS (all d) for chromite against chromite coarseness ratio, clump density, and LPO #. Figures 7 and 8 show that texture (grain size and clumping) of the FCC objects didn't change much during the annealing process. This could mean that the chromite grains couldn't grow due to already being encased in plagioclase. Interpretation of the data for CCCs are hampered by having studied relatively few assemblages of this type. However, the CCC assemblages in Spade and Estacado are notably coarser than in Alfianello and NWA 13533 (Fig. 7). Clump densities in Estacado are similar to those of Alfianello and NWA 13533, whereas that in Spade is somewhat lower. This implies that annealing could have caused grain coarsening in Alfianello CCCs without much changing the clump density, by adding to coarser grains from the smaller, possibly similar to an Ostwald ripening process. Spade CCCs may have formed differently, by crystallization from a melt, leading to both coarser grains and a lower clump density. If correct this would imply two origins for CCCs, namely crystallization in Spade, and aggregation ion the other three meteorites.

With Figures 7 & 8 showing the comparisons of GOS against two of the three main parameters in determining the assemblage types of the FCAs, there is one important parameter unaccounted for. Figure 31 shows GOS versus LPO, the FCC group shows no significant difference between Estacado, Alfianello, and NWA 13533. Meaning that once more, the annealing that Estacado experienced didn't make much of a difference in FCC

LPO. This is likely for the reason that the chromite was encased in feldspathic material, implying that the plagioclase crystallized from maskelynite (if that's what it was originally), and annealing couldn't change the orientation of the chromite. The CCC group shows higher LPO in Spade than in Alfianello and NWA 13533. This could imply that crystallization allowed the chromite crystals to attach and become more crystallographically oriented, by one chromite growing on top of another, in a process called topotactic growth. Once more, this implies that there are two different origins for the CCC group, one being crystallization (seen in Spade), and the other being aggregation of pre-existing grains (seen in Alfianello and NWA 13533).

The GOS data shows that Spade and Estacado were deformed during their shock events, while the parent body interiors were being metamorphosed. Meanwhile Alfianello and NWA 13533 were deformed after the parent body interiors were metamorphosed. The high $Skd_{>50}$ value for Estacado suggests that the post deformation annealing brought down the overall GOS value for the olivine.

4.6 What is the bigger picture?

The bigger picture that we can see with these four meteorites, while they are very different meteorites with their own unique origin, is the characteristic that they share. The obvious difference in high and low shock meteorites is the GOS in chromite. For our low shock meteorites (Spade and Estacado) we see evidence that either **1)** annealing removed signs of deformation and healed the cracks made via shock (which is likely in Estacado), or **2)** the grains crystallized from a melt after most deformation had already happened (which is likely in Spade). For our high shock meteorites (NWA 13533 and Alfianello),

the FCAs were likely produced as a result of the strong shock these meteorites experienced, with no complications of post-shock annealing, although localized melting during strong shock might still be involved.

If these FCA objects are formed by shock melting, as was inferred by Rubin (2003), then what differences do we see between the high and low shock meteorites? There appears to be no difference in many of the measured parameters (chromite coarseness ratio, LPO, area fraction of chromite, and clump density) between the high and the low shocked meteorites. There are some real differences between assemblage types, but aside from those, there is no differences (outside of GOS) between the high and low shock meteorites. The large difference that we do see between the high and low shock meteorites studied for this paper is their GOS values. The mean GOS values tend to be higher for the high shock meteorites, and lower for the low shock meteorites.

Rubin (2003) states that these FCAs form under high shock conditions, and Alfianello and NWA 13533 fit this model. It is likely that Estacado was annealed, and despite this, the FCAs found within the sample were not destroyed in the process. The chromite in Estacado appears to not have been largely affected at all by annealing, the GOS value for chromite was lowered, but other than that there appears to be no other changes. Annealing changed the GOS values of olivine, lowered them from what they were pre-annealing, but that was the only real change due to annealing. Spade does not fit this model. It was shocked at high temperatures but shows no evidence of annealing. The plagioclase in Spade is zoned, which means it could not have been completely equilibrated, which is a side effect of annealing. The chromite in Spade is also somewhat zoned, but not completely equilibrated. Both of these instances point to annealing not

being a factor for Spade. In Spade, it appears that both chromite-poor (CP) and coarse clumped chromite (CCC) assemblages were able to form by crystallization from local melt pockets.

The conclusion that can be made from this study is that Rubin's (2003) model is supported by our findings for most meteorites, but not all. Of the four meteorites used in this study, three of them fit Rubin's model (Estacado, Alfianello, and NWA 13533), with Spade being an outlier.

References:

Bischoff, A., and Keil, K., (1984), Al-rich objects in ordinary chondrites: Related origin of carbonaceous and ordinary chondrites and their constituents: v. 48, p. 693–709.

Brearley A.J., Casanova I., Miller M.L., and Keil K. (1991), Mineralogy and possible origin of an unusual Cr-rich inclusion in the Los Martinez (L6) chondrite: Meteoritics & Planetary Science, v. 26, p. 287-300.

Friedrich J.M., A. Ruzicka, R.J. Macke, J.O. Thostenson, R.A. Rudolph, M.L. Rivers and D.S. Ebel (2017), Relationships among physical properties as indicators of high temperature deformation or post-shock thermal annealing in ordinary chondrite: *Geochimica et Cosmochimica Acta*, v. 203, p. 157-174.

Fritz, J., Greshake, A., and Fernandes, V.A. (2017), Revising the shock classification of meteorites: *Meteoritics & Planetary Science*, v. 52, p. 1216-1232.

Jamsja, N., and Ruzicka, A., (2010), Shock and thermal history of Northwest Africa 4859, an annealed impact-melt breccia of LL chondrite parentage containing unusual igneous features and pentlandite: *Meteoritics and Planetary Science*, v. 45, p. 828–849, doi:10.1111/j.1945-5100.2010.01056.x.

Hugo, R.C., Ruzicka, A.M. and Rubin, A.E., (2019), Mesoscale and microscale shock effects in the LL 6 S4 chondrites Saint-Séverin and Elbert: A tale of two breccias: *Meteoritics & Planetary Science*. doi 10.1111/maps.13304

Krot A. and M.A. Ivanova (1992), Cr-rich chondrules and inclusions in ordinary chondrites: *Lunar and Planet Science Conference* XXIII, p. 729-730.

Krot, A.N., and Rubin, A.E., (1993), Chromite-Rich Mafic Silicate Chondrules in Ordinary Chondrites: Formation by Impact Melting: *Lunar and Planetary Science Conference* XXIV, p. 827-828.

Prior, D.J., Mariani, E. and Wheeler, J., (2009), EBSD in the earth sciences: applications, common practice, and challenges: *Electron backscatter diffraction in materials science*, p. 345-36). Springer, Boston, MA.

Ramdohr, P., (1967), Chromite and chromite chondrules in meteorites-I: v. 31, p. 1961–1967.

Ramdohr, P. (1973), The Opaque Minerals in Stony Meteorites: Elsevier Publishing Co, Amsterdam, p. 245.

Rubin, A.E., (2003), Chromite-plagioclase assemblages as a new shock indicator; Implications for the shock and thermal histories of ordinary chondrites: *Geochimica et Cosmochimica Acta*, v. 67, p. 2695–2709, doi:10.1016/S0016-7037(03)00107-8.

Rubin, A.E., (2004), Postshock annealing and postannealing shock in equilibrated ordinary chondrites: Implications for the thermal and shock histories of chondritic asteroids: *Geochimica et Cosmochimica Acta*, v. 68, p. 673–689, doi:10.1016/S0016-7037(00)00452-6.

Rubin, A.E., and Jones R.H. (2003), Spade: An H-chondrite impact-melt breccia that experienced post-shock annealing: *Meteoritics & Planetary Sciences*, v. 38, p. 1507-1520.

Ruzicka, A.M., and Hugo, R.C., (2018), Electron backscatter diffraction (EBSD) study of seven heavily metamorphosed chondrites: Deformation systematics and variations in pre-shock temperature and post-shock annealing: *Geochimica et Cosmochimica Acta*, v. 234, p. 115–147, doi:10.1016/j.gca.2018.05.014.

Stöffler, D., Keil, K., and Edward R.D, S., (1991), Shock metamorphism of ordinary chondrites: *Geochimica et Cosmochimica Acta*, v. 55, p. 3845–3867, doi:10.1016/0016-7037(91)90078-J.

Stöffler D., Hamann C., and Metzler K., (2018), Shock metamorphism of planetary silicate rocks and sediments: Proposal for an updated classification system. *Meteoritics & Planetary Science* 53: p. 5–49.

Stöffler D., Hamann C., and Metzler K., (2019), Addendum to "Stöffler, D., Hamann, C., and Metzler, K., Shock metamorphism of planetary silicate rocks and sediments: Proposal for an updated classification system": Meteoritics & Planetary Science 53, 5–49, 2018. *Meteoritics & Planetary Science* 54: p. 946-949.

Appendix A: Optical Microscopy

Table A-1: All thin section samples investigated for this study. Those with an * were chosen for further analysis, with bolded samples being the four chosen for this study.

CML #	Meteorite Name	Classification	Conventional Shock Stage	FCA Present? Y/N
0018-2*	--	unclassified	--	Y
158	--	unclassified	--	Y
0269-1A*	**Spade**	**H6**	**S4**	**Y**
0295-3C*	**Estacado**	**H6**	**S1**	**Y**
0414*	Jungo 001		S1	Y
0417	NWA 5962		--	Y
0496-1A*	**Alfianello**	**L6**	**S5**	**Y**
0594-4A*	--	unclassified	--	Y
0646-1-1*	Tamdakht	H5	S3	Y
0649*	Jungo 004		S3	Y
788	Yucca 050	H3-6	S3	Y
789	--	unclassified	--	N
800	NWA 8645	L5	S4	Y
802	--	unclassified	--	Y
803-3A*	--	unclassified	--	Y
804	NWA 11229	L6	S4	Y
805	NWA 10312	H5	S3	N
806	Trapeang Ronoas	H4	S1	N
811	--	unclassified	--	N
812	NWA 11913	H5	S2	N
813	NWA 11914	H5	S2	N
815	NWA 10458	L5	S3	N
817	NWA 11915	LL4-6	S2	N
823	--	unclassified	--	N
824	--	unclassified	--	Y
825	--	unclassified	--	Y
826	--	unclassified	--	N
830	--	unclassified	--	N
835	Bison	LL6	--	Y
841	--	unclassified	--	N
842	--	unclassified	--	Y
843	--	unclassified	--	Y
844	--	unclassified	--	N
845	--	unclassified	--	Y
846	NWA 10313	L6	S4	Y
847	Yucca 043	H3-6	S4	N
848	NWA 11230	L6	S4	Y
853	NWA 10816	LL5	S3	N

854	NWA 10828	H4	--	Y
864	--	unclassified	--	N
866	--	unclassified	--	Y
867	--	unclassified	--	Y
869	--	unclassified	--	Y
870	--	unclassified	--	Y
871	--	unclassified	--	Y
872	--	unclassified	--	Y
873	--	unclassified	--	Y
891	--	unclassified	--	Y
896	--	unclassified	--	Y
897	--	unclassified	--	Y
900	--	unclassified	--	Y
901	--	unclassified	--	Y
902	--	unclassified	--	Y
912	--	unclassified	--	N
921	--	unclassified	--	Y
939	--	unclassified	--	N
940	NWA 12431	LL3	--	N
941	NWA 12432	H5	--	Y
942	--	unclassified	--	Y
944	--	unclassified	--	Y
945	--	unclassified	--	Y
946	--	unclassified	--	Y
947	--	unclassified	--	Y
953	NWA 5421	LL3.7	--	Y
956	--	unclassified	--	N
967	--	unclassified	--	Y
974	--	unclassified	--	Y
978	NWA 11905	LL3	S3	Y
983	NWA 11291	LL3	--	Y
984	NWA 10220	LL3	S1	Y
985	NWA 8575	L/LL3	S1	Y
995-1*	**NWA 13533**	**L6**	**S4**	**Y**
997	Bluff (a)	L5	S4	Y
1001	NWA 12434	L3	S4	Y
1004	NWA 12380	L3	S2	N
1014	Bovedy	L3	--	Y
1016-1*	Ber-Gheluai	H5	--	Y
1019-1*	Dalgety Downs	L4	--	Y
1070	Selma	H4	--	N
1071	Broken Hill	L6	--	N
1117	--	unclassified	--	Y
1118	--	unclassified	--	N
1119	--	unclassified	--	Y

Appendix B: EDS-EBSD false color maps of each targeted map (TM). Each image is a composite map with different colors attached to different elements (obtained by EDS, color bar shown below), and a band contrast EBSD image shown in monochrome. In these maps, feldspathic material shows as dark purple, chromite as pink, olivine as bright green, low-Ca pyroxene as dark green to tan, high-Ca pyroxene as brown-red, low-Ni metal as light blue, high-Ni metal as dark blue, troilite as yellow-green, phosphate as orange, and holes as black.

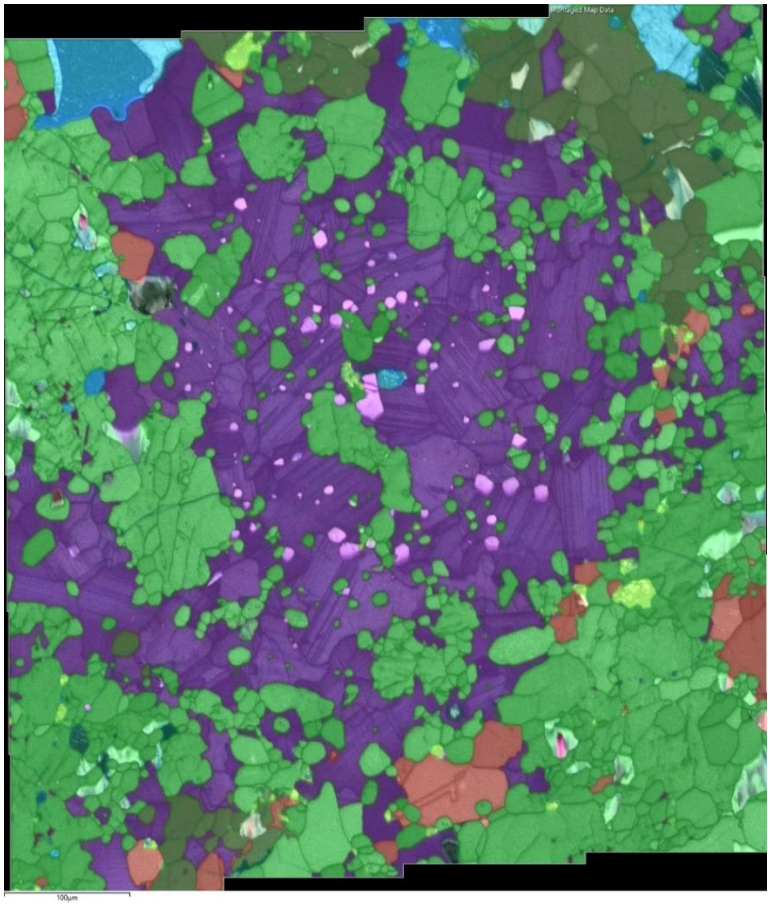

Spade TM1

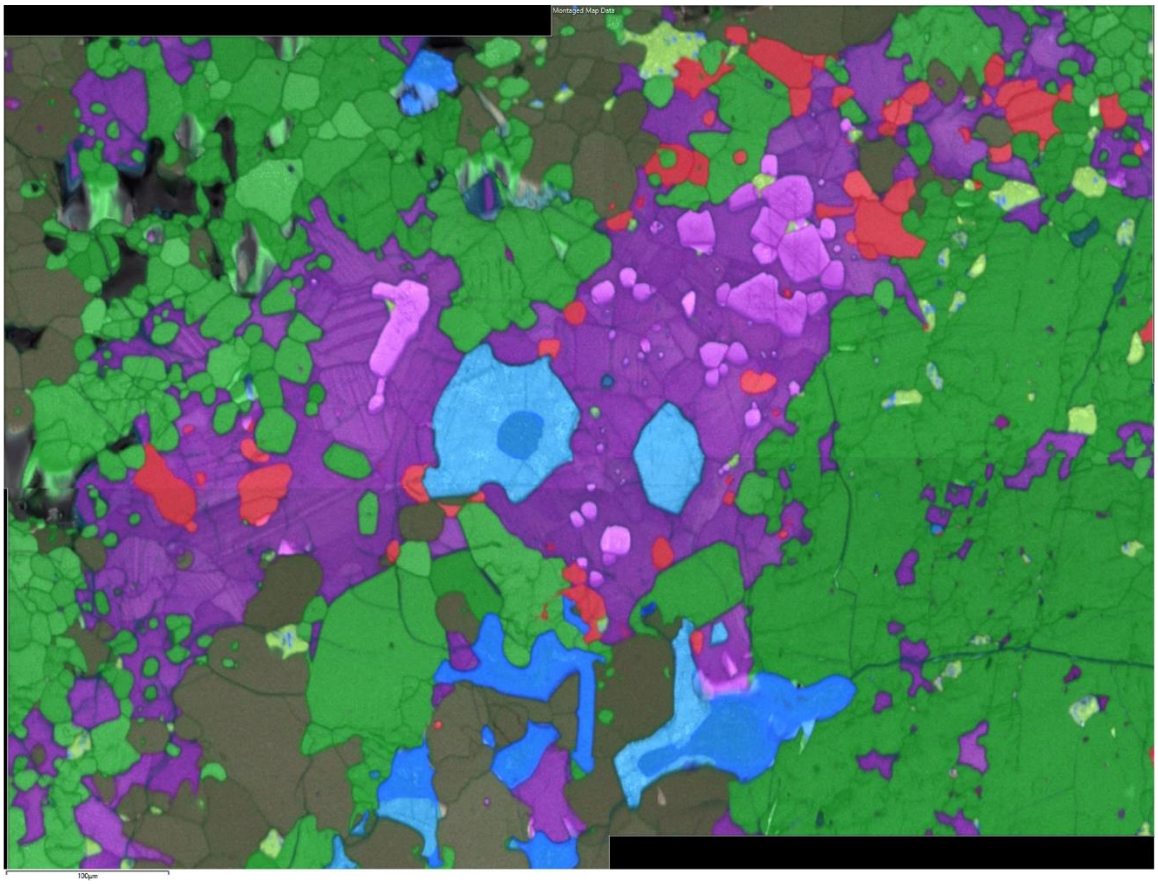

Spade TM2

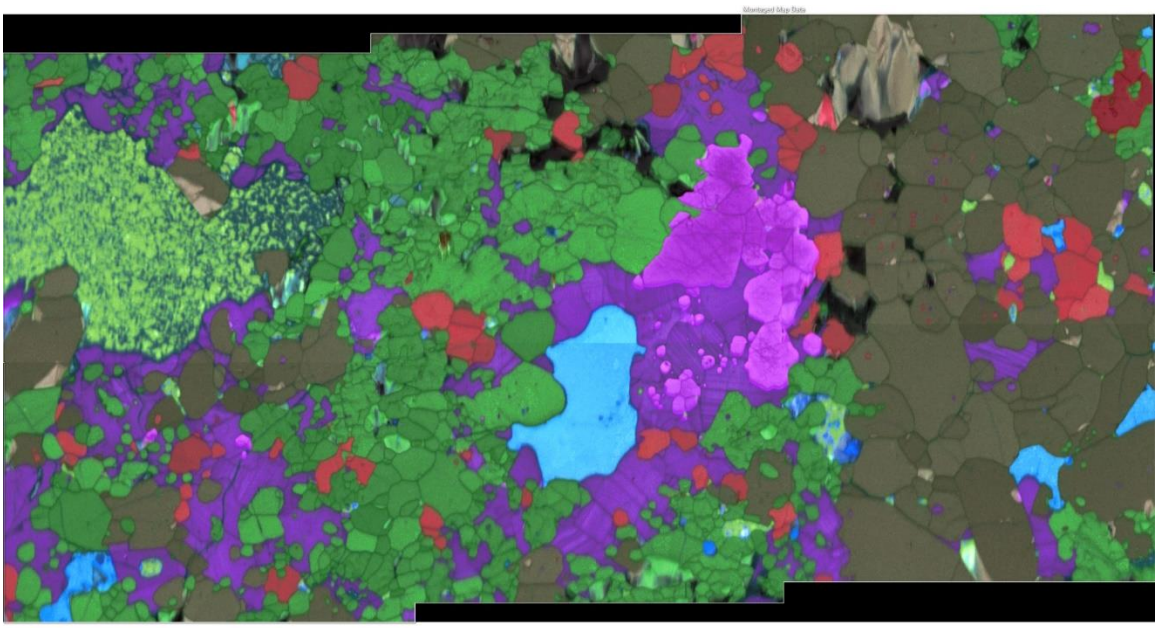

Spade TM3

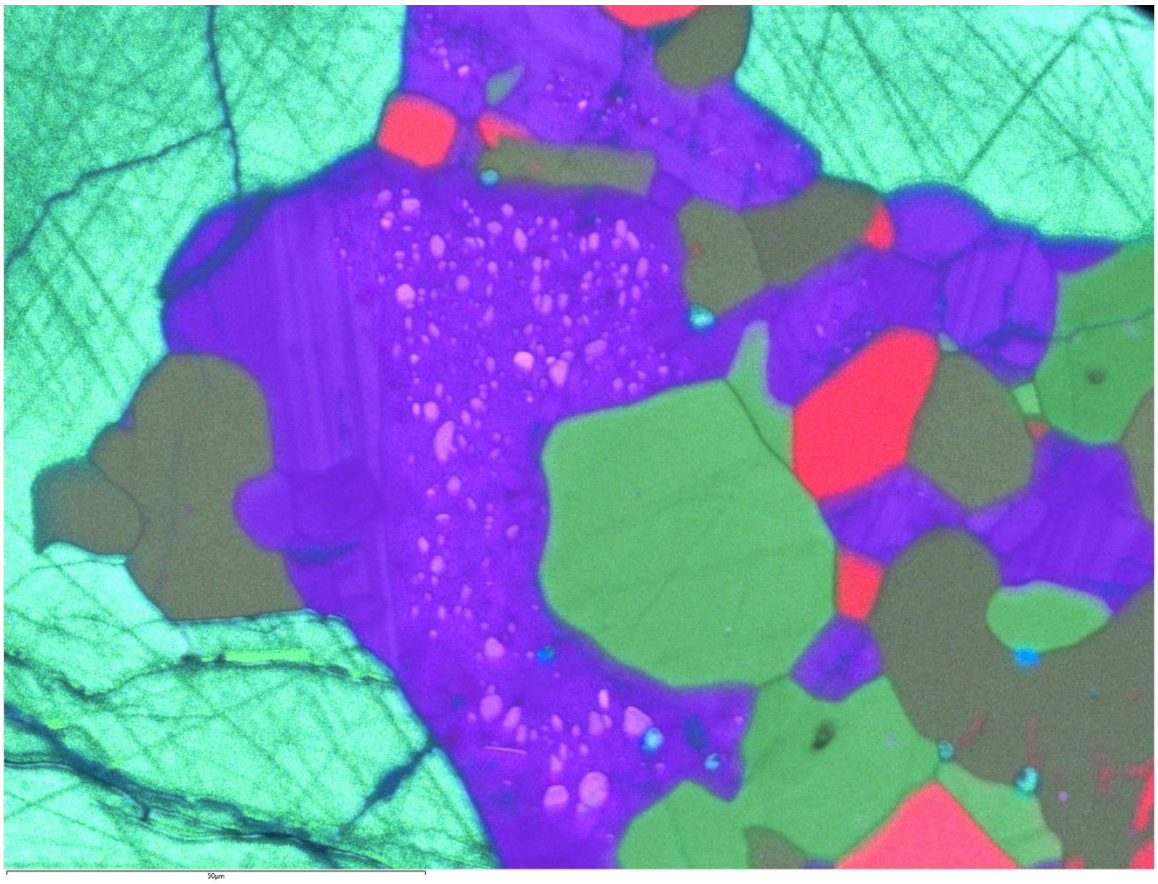

Estacado TM1

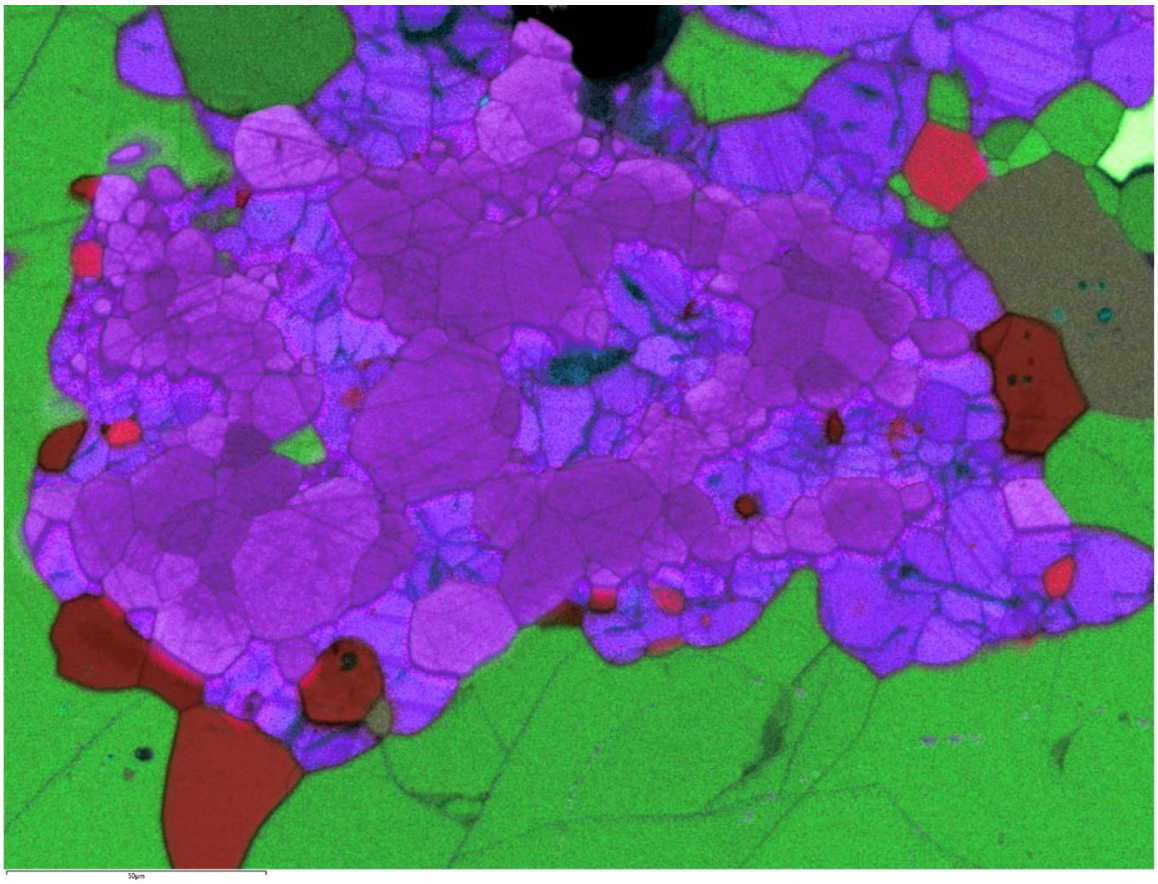

Estacado TM2

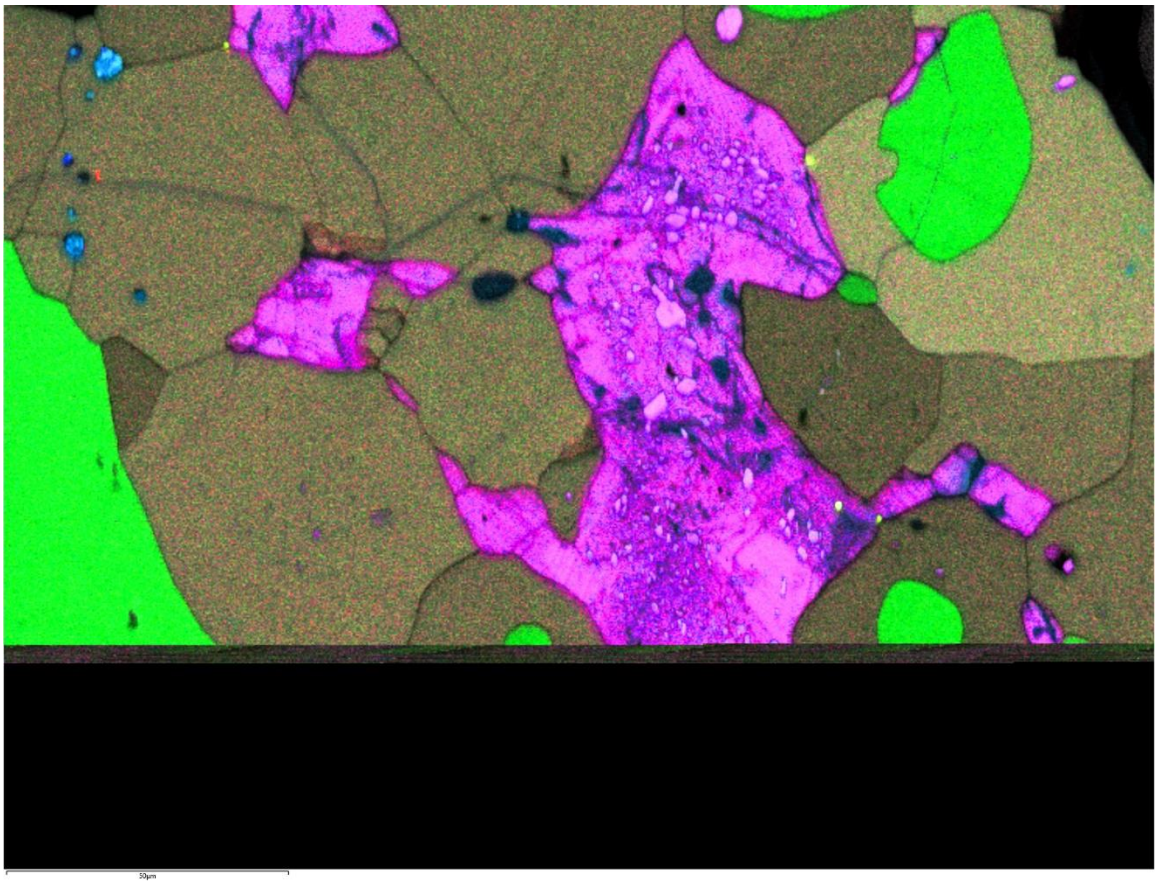

Estacado TM3

Estacado TM4

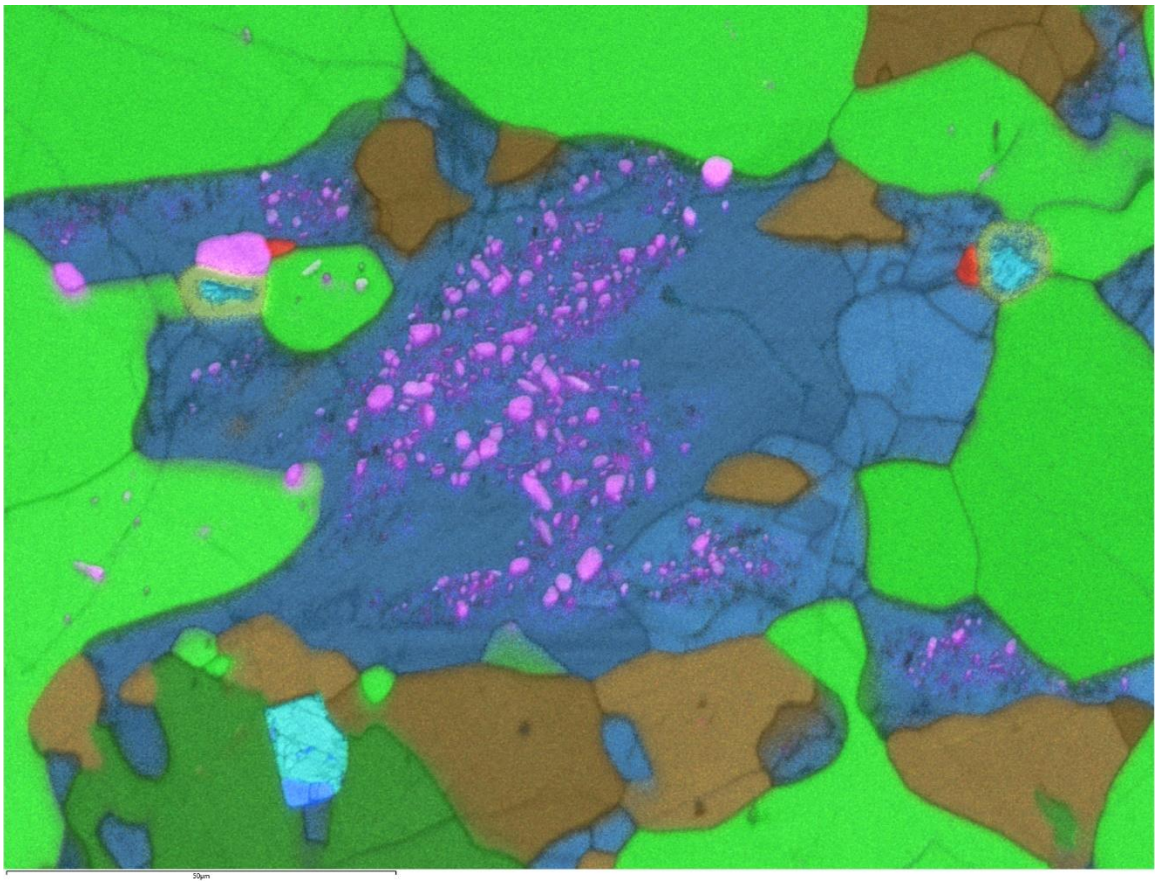

Estacado TM 5

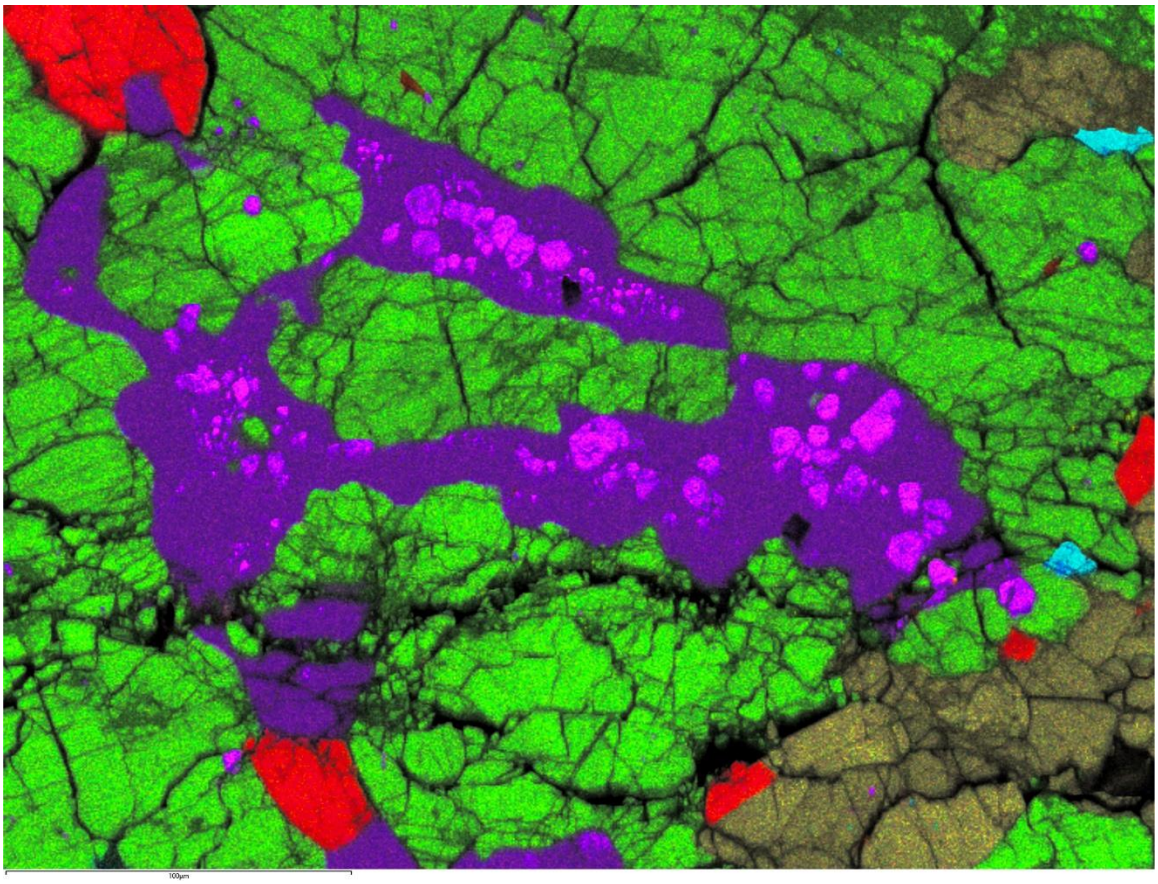

Alfianello TM1

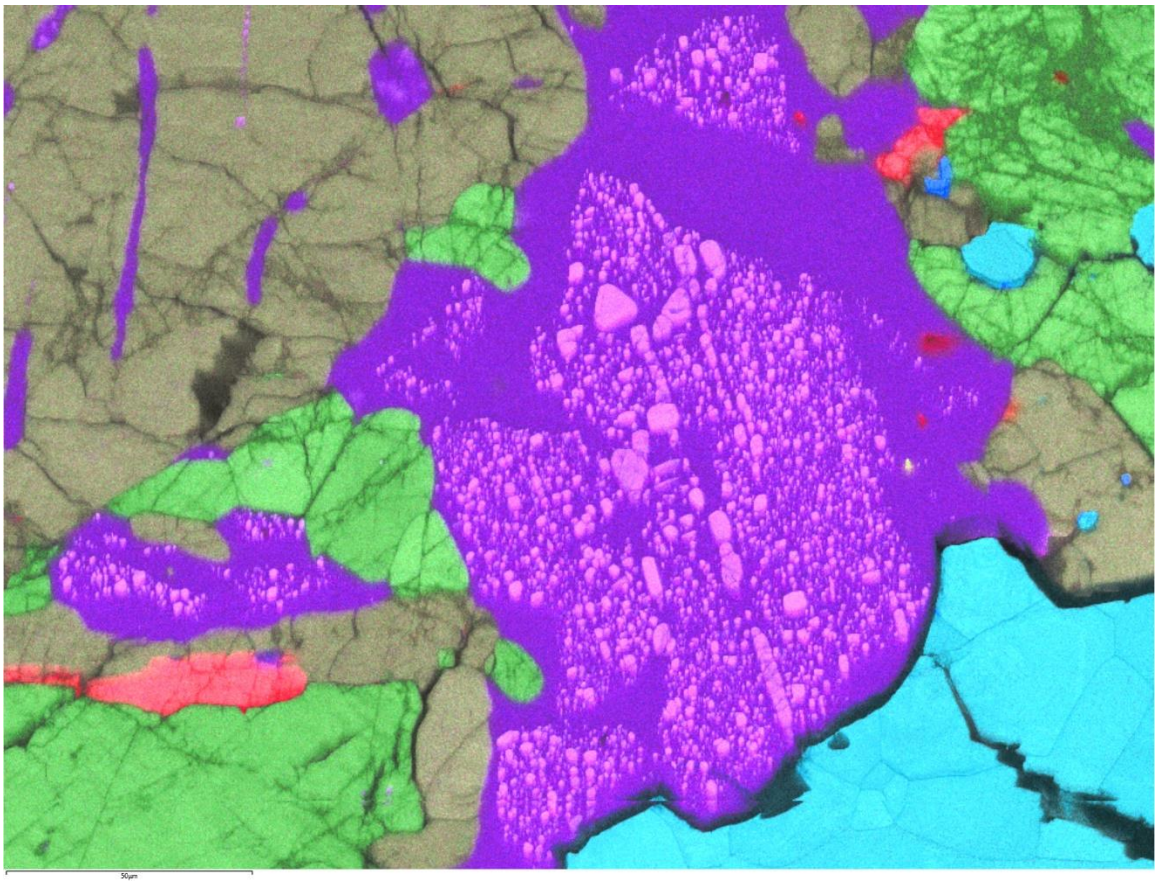

Alfianello TM2

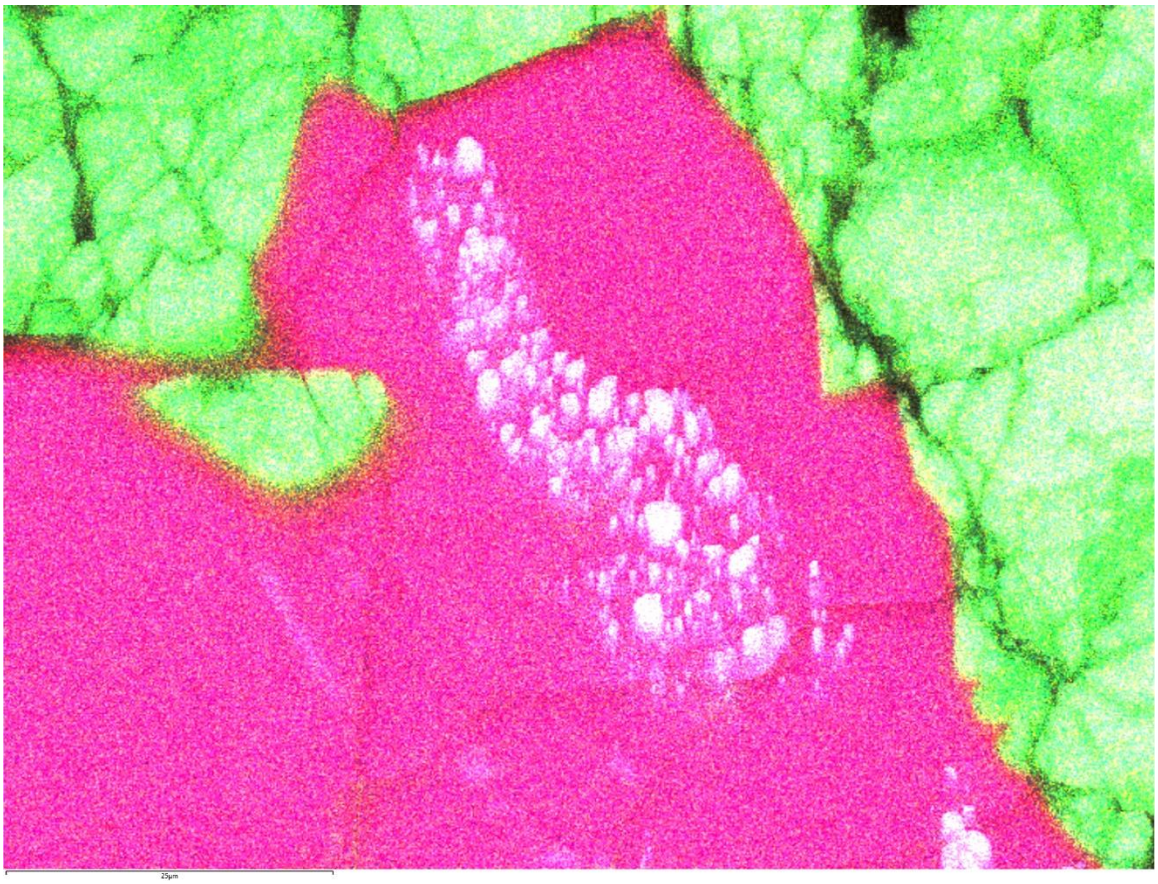

Alfianello TM3

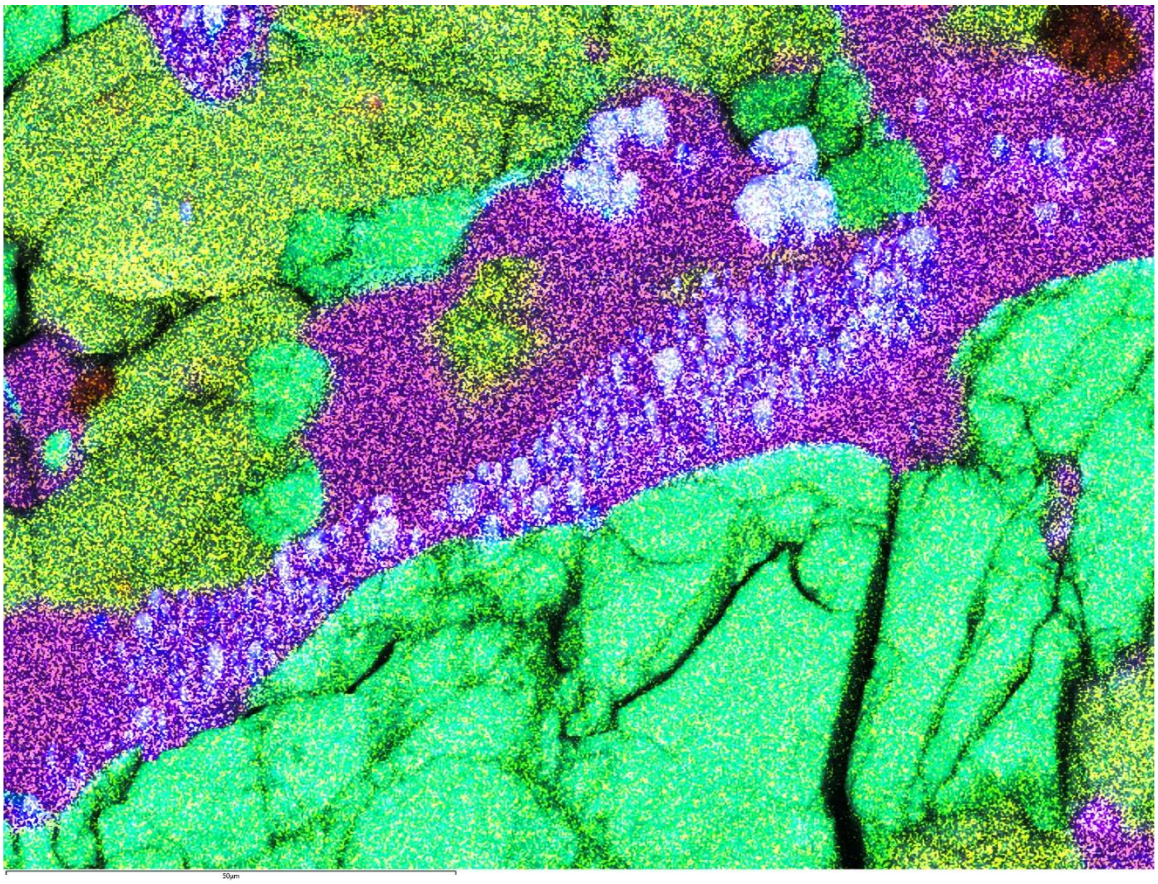

Alfianello TM4

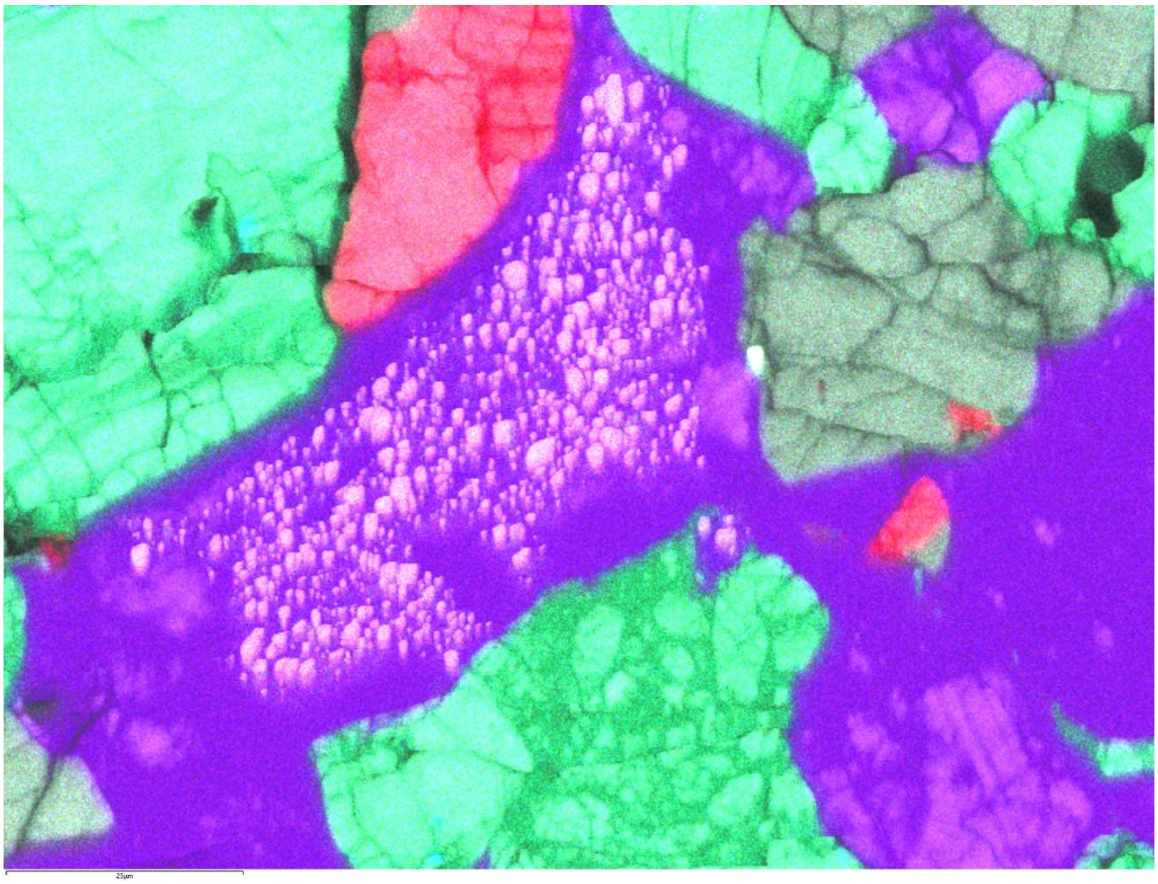

Alfianello TM5

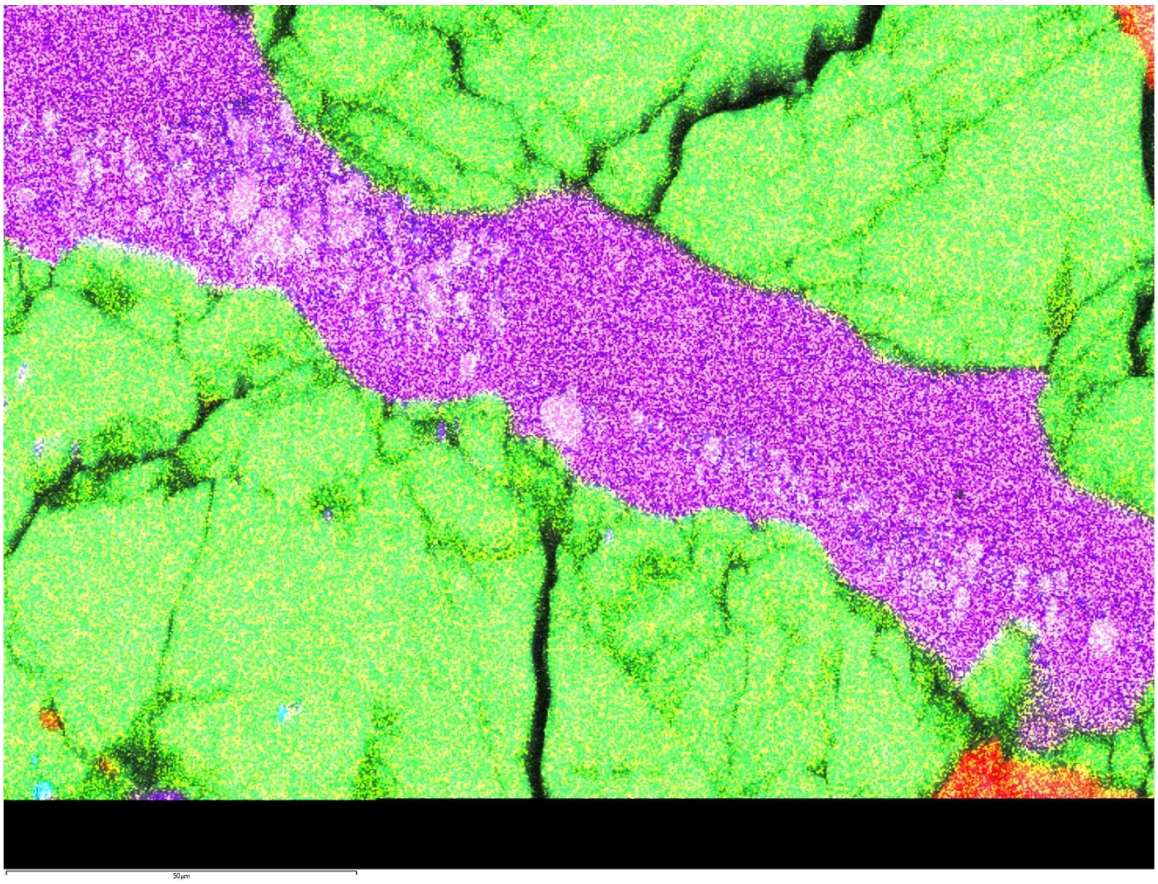

Alfianello TM6

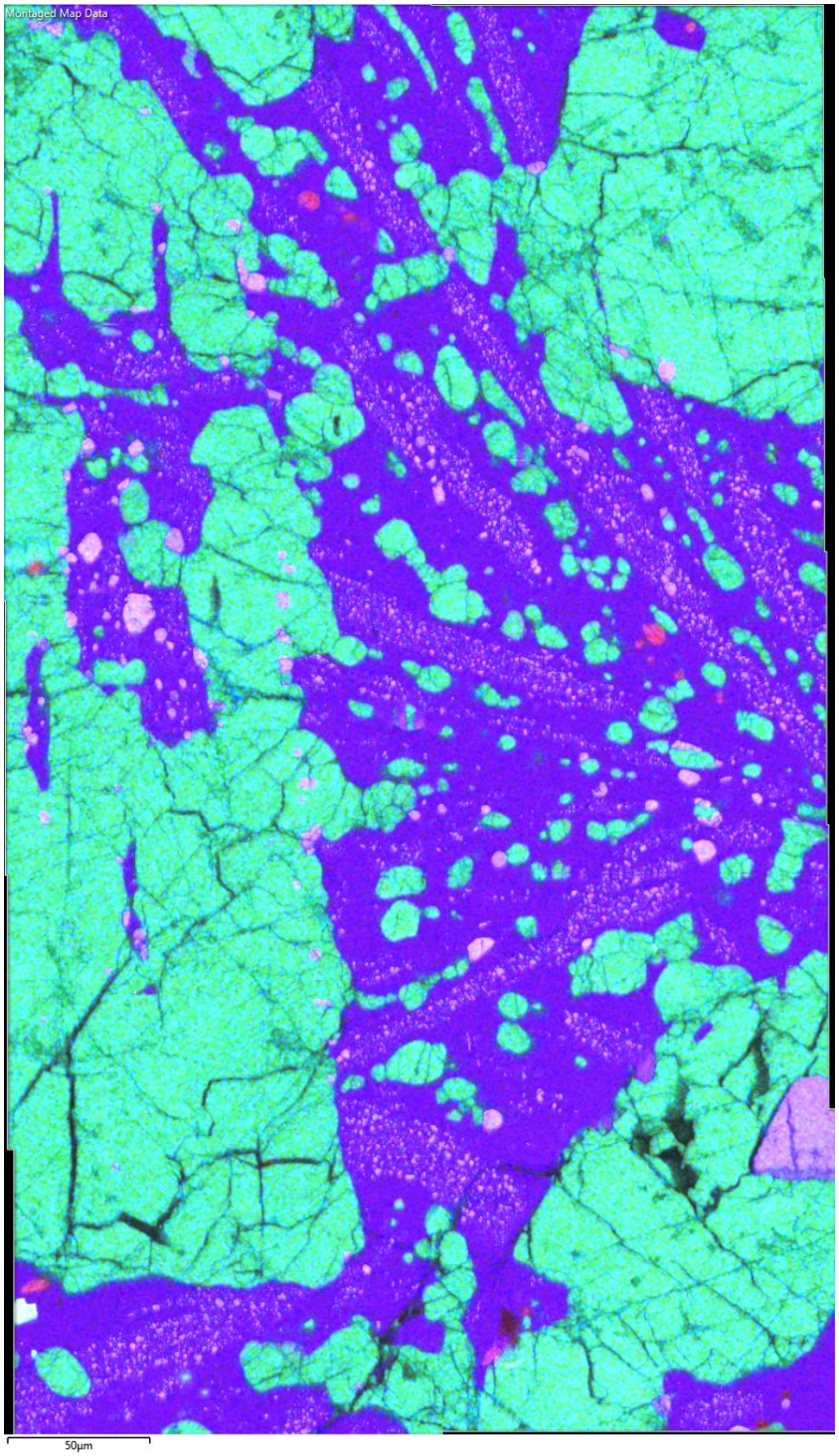

NWA 13533 TM1

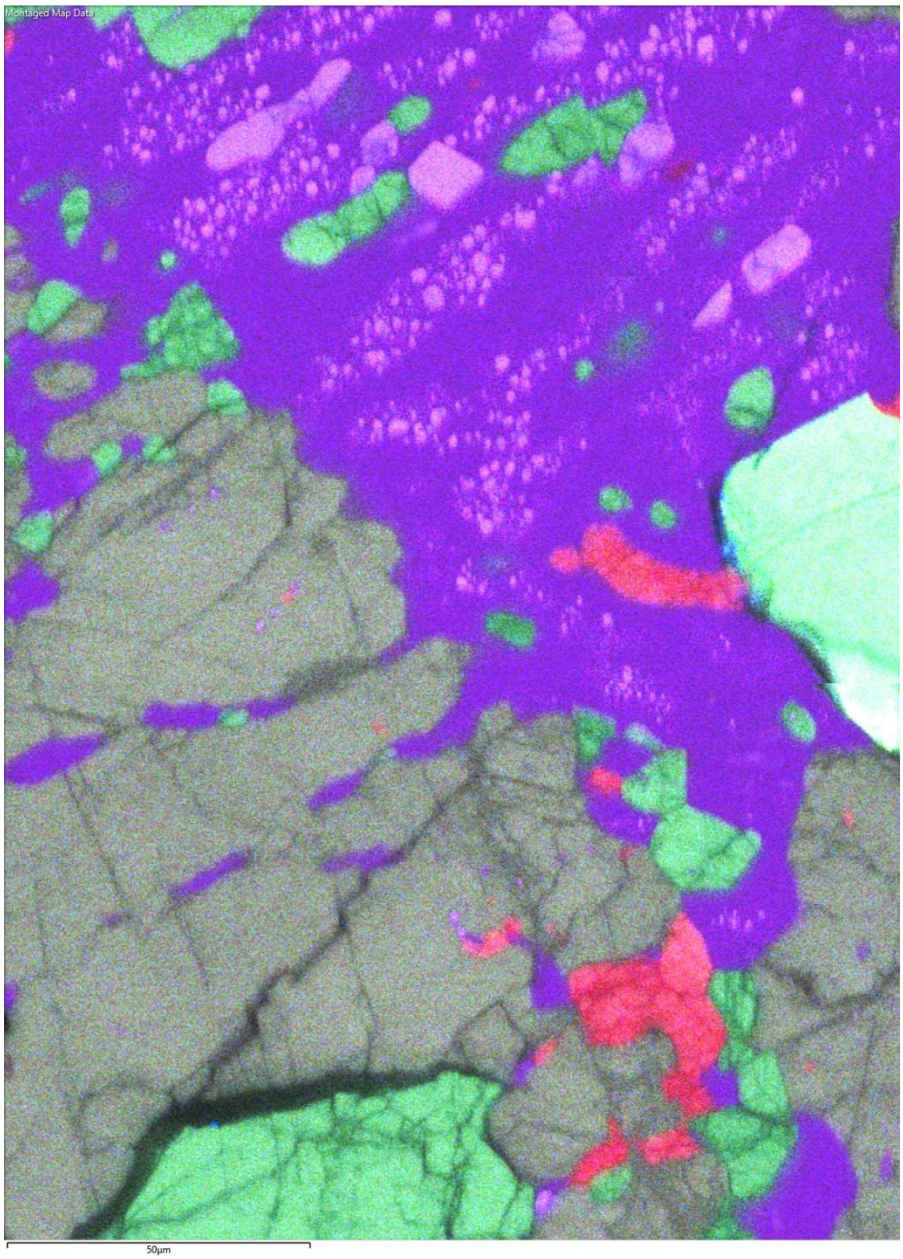

NWA 13511 TM4

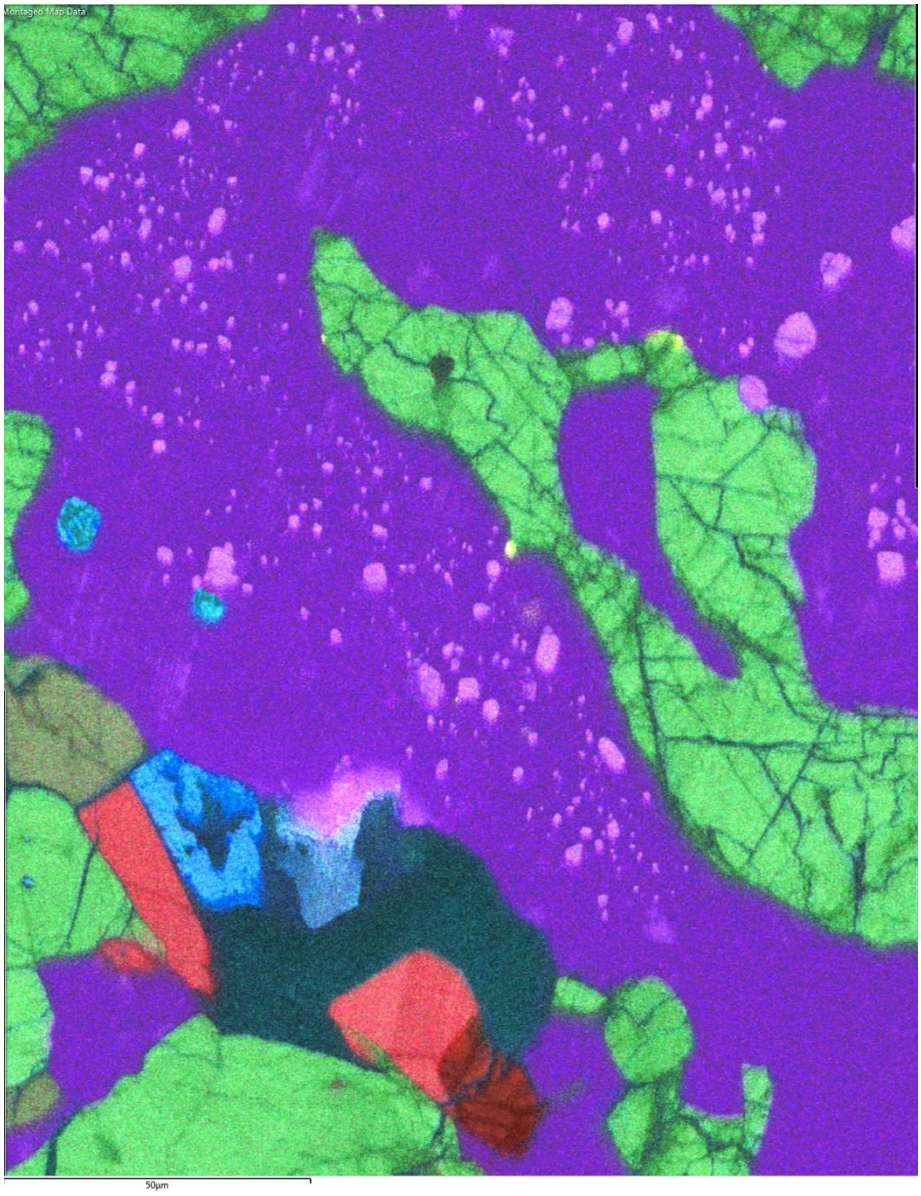

NWA 13533 TM5

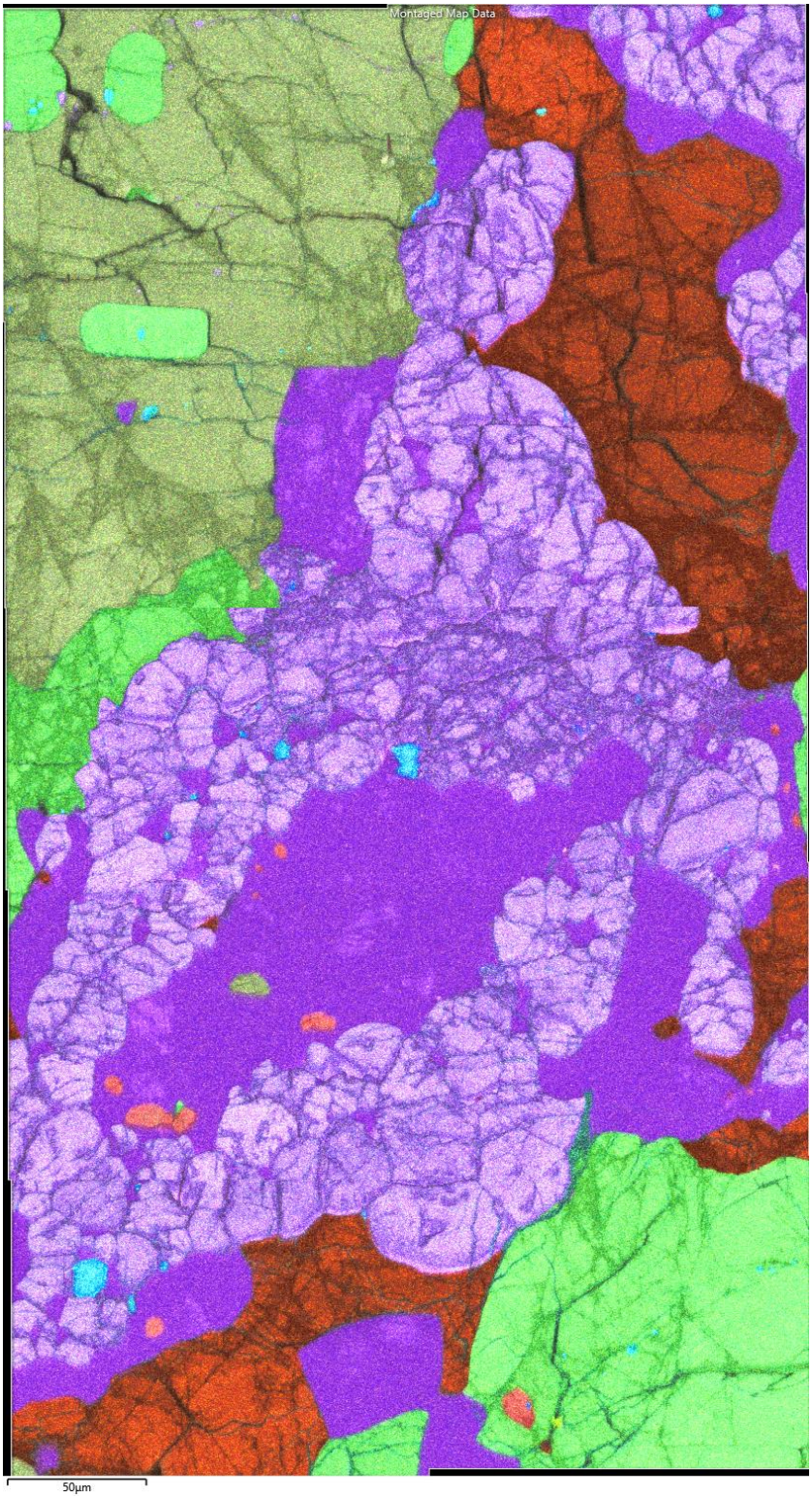

NWA 13533 TM6

Appendix C: Subsets and other data

SPADE (0269-1A)

	Density of Chromite		Area of subset		Grain Data			
TM1	**µm²**	**mm²**	**µm²**	**mm²**	**Average**	**Std Deviation**	**Area Fraction of chr**	**LPO # $\Delta_{<100>}$**
Subset 1 (All)	0.002	1616.2	67448.1	0.067	5.42	3.67	0.054	1.67

	Density of Chromite		Area of subset		Grain Data			
TM2	**µm²**	**mm²**	**µm²**	**mm²**	**Average**	**Std Deviation**	**Area Fraction of chr**	**LPO # $\Delta_{<100>}$**
Subset 1	0.002	2077.8	28398.6	0.028	8.65	7.32	0.208	3.2
Subset 2*	0.001	801.5	2495.8	0.002	24.1	19.1	0.482	24.06*
Subset 3 (All)	0.002	1977.1	30856.6	0.031	9.15	8.10	0.230	3.06

	Density of Chromite		Area of subset		Grain Data			
TM3	**µm²**	**mm²**	**µm²**	**mm²**	**Average**	**Std Deviation**	**Area Fraction of chr**	**LPO # $\Delta_{<100>}$**
Subset 1 (All)	0.004	3989.3	30080.5	0.0301	7.32	9.47	0.446	10.92

ESTACADO (0295-3C)

	Density of Chromite		Area of subset		Grain Data			
TM1	**µm²**	**mm²**	**µm²**	**mm²**	**Average**	**Std Deviation**	**Area Fraction of chr**	**LPO # $\Delta_{<100>}$**
Subset 1	0.19	188328.4	1263.7	0.001264	1.06	0.62	0.237	11.69
Subset 2	0.24	242190.9	185.8	0.000186	0.86	0.46	0.130	13.15
Subset 3*	0.19	192284.9	46.8	0.000047	0.70	0.30	0.085	10.48
Subset 4*	0.24	235014.9	34.0	0.000034	0.87	0.42	0.166	12.52
Subset 5	0.18	179899.9	1717.6	0.001718	1.06	0.66	0.218	10.43
Subset 6*	0.16	162702.6	36.9	0.000037	0.83	0.28	0.096	11.23
Subset 7 (All)	0.18	180892.4	1835.3	0.001835	1.04	0.64	0.212	9.74

	Density of Chromite		Area of subset		Grain Data			
TM2	**µm²**	**mm²**	**µm²**	**mm²**	**Average**	**Std Deviation**	**Area Fraction of chr**	**LPO # $\Delta_{<100>}$**

Subset 1 (All)	0.024	24450.1	14314.9	0.014	3.55	4.04	0.554	7.57

	Density of Chromite		Area of subset		Grain Data			
TM3	**µm²**	**mm²**	**µm²**	**mm²**	**Average**	**Std Deviation**	**Area Fraction of chr**	**LPO # $\Delta_{<100>}$**
Subset 1 (All)	0.073	72754.7	2309.1	0.002	1.29	0.62	0.116	6.65

	Density of Chromite		Area of subset		Grain Data			
TM4	**µm²**	**mm²**	**µm²**	**mm²**	**Average**	**Std Deviation**	**Area Fraction of chr**	**LPO # $\Delta_{<100>}$**
Subset 1	0.364	364371.3	279.9	0.00028	0.62	0.34	0.144	8.16
Subset 2	0.210	209859.4	81.0	0.00008	0.79	0.41	0.129	23.58
Subset 3	0.310	309885.9	109.7	0.00011	0.74	0.37	0.165	11.21
Subset 4	0.232	232197.4	86.1	0.00009	0.70	0.48	0.130	14.86
Subset 5	0.295	294611.7	465.0	0.00047	0.68	0.43	0.151	8.09
Subset 6	0.185	184630.8	211.2	0.00021	0.83	0.72	0.172	14.84
Subset 7*	0.075	75017.6	26.7	0.00003	2.30	2.40	0.480	26.03
Subset 8 (All)	0.003	2579.9	89918.8	0.08993	0.73	0.53	0.165	5.77

	Density of Chromite		Area of subset		Grain Data			
TM5	**µm²**	**mm²**	**µm²**	**mm²**	**Average**	**Std Deviation**	**Area Fraction of chr**	**LPO # $\Delta_{<100>}$**
Subset 1	0.199	199343.3	85.3	0.00009	1.02	0.53	0.205	14.48
Subset 2	0.158	157905.0	1646.6	0.00165	1.10	0.70	0.210	13.54
Subset 3	0.214	213810.6	126.3	0.00013	0.89	0.44	0.163	9.67
Subset 4	0.149	148530.3	127.9	0.00013	0.60	0.24	0.040	12.29
Subset 5	0.143	142708.9	77.1	0.00008	0.83	0.92	0.162	11.54
Subset 6	0.226	225835.6	44.3	0.00004	0.85	0.41	0.158	15.76
Subset 7 (All)	0.159	158771.8	2210.8	0.00221	1.05	0.75	0.208	11.67

ALFIANELLO (0496-1A)

	Density of Chromite		Area of subset		Grain Data			
TM1	**µm²**	**mm²**	**µm²**	**mm²**	**Average**	**Std Deviation**	**Area Fraction of chr**	**LPO # $\Delta_{<100>}$**
Subset 1	0.030	29749.7	2319.3	0.0023	2.83	2.31	0.310	6.71
Subset 2	0.012	11857.9	3120.3	0.0031	4.82	3.07	0.302	2.57

Subset 3	0.020	20450.2	1760.4	0.0018	2.94	2.78	0.259	4.59
Subset 4	0.025	25184.8	2144.1	0.0021	2.55	1.69	0.184	5.30
Subset 5 (All)	0.021	20975.7	9344.1	0.0093	3.15	2.54	0.269	4.02

	Density of Chromite		**Area of subset**		**Grain Data**			
TM2	**μm^2**	**mm^2**	**μm^2**	**mm^2**	**Average**	**Std Deviation**	**Area Fraction of chr**	**LPO # $\Delta_{<100>}$**
Subset 1	0.20	200565.5	304.3	0.00030	1.25	0.62	0.307	12.67
Subset 2	0.19	185378.3	172.7	0.00017	1.07	0.50	0.202	12.34
Subset 3	0.25	254368.5	90.5	0.00009	1.12	0.44	0.287	12.87
Subset 4	0.24	241708.3	625.1	0.00062	1.15	0.53	0.304	12.47
Subset 5	0.22	218918.6	1682.1	0.00168	1.14	0.59	0.283	11.17
Subset 6	0.24	241066.5	892.4	0.00089	1.05	0.47	0.250	10.22
Subset 7	0.21	211573.0	378.4	0.00038	1.15	0.49	0.259	9.49
Subset 8	0.21	210740.1	522.3	0.00052	1.21	0.57	0.293	9.18
Subset 9	0.23	227560.8	2541.6	0.00254	1.10	0.55	0.273	13.04
Subset 10	0.22	220987.1	448.3	0.00045	1.04	0.47	0.225	12.99
Subset 11	0.21	207918.6	226.2	0.00023	1.15	0.59	0.258	8.79
Subset 12	0.04	38889.6	1003.5	0.00100	2.39	1.93	0.285	8.26
Subset 13	0.18	177273.8	9894.9	0.00989	1.17	0.74	0.267	7.38
Subset 14 (All)	0.18	181044.2	11136.9	0.01113	1.17	0.72	0.266	6.61

	Density of Chromite		**Area of subset**		**Grain Data**			
TM3	**μm^2**	**mm^2**	**μm^2**	**mm^2**	**Average**	**Std Deviation**	**Area Fraction of chr**	**LPO # $\Delta_{<100>}$**
Subset 1	0.35	351507.8	631.3	0.000629	0.86	0.61	0.303	7
Subset 2*	0.18	178359.1	33.8	0.000034	0.87	0.50	0.135	12.87
Subset 3 (All)	0.34	343014.3	664.5	0.000662	0.86	0.60	0.295	6.96

	Density of Chromite		**Area of subset**		**Grain Data**			
TM4	**μm^2**	**mm^2**	**μm^2**	**mm^2**	**Average**	**Std Deviation**	**Area Fraction of chr**	**LPO # $\Delta_{<100>}$**
Subset 1	0.18	179137.4	72.7	0.00007	0.86	0.31	0.117	10.41
Subset 2	0.27	270153.2	392.8	0.00039	0.96	0.46	0.241	9.9
Subset 3	0.23	233623.0	321.4	0.00032	1.14	0.59	0.301	12.9
Subset 4	0.00	2085.7	47043.3	0.04699	1.29	0.84	0.384	16.15
Subset 5	0.22	221382.5	786.9	0.00079	1.24	0.75	0.364	14.47
Subset 6	0.08	77429.3	129.3	0.00013	2.13	1.27	0.364	6.21
Subset 7	0.07	70696.4	141.6	0.00014	2.45	2.46	0.631	9.06
Subset 8*	0.13	132350.2	53.0	0.00005	1.58	1.10	0.368	10.7
Subset 9	0.12	116144.0	112.1	0.00011	1.30	0.71	0.196	7.21

Subset 10 (All)	0.20	195821.3	1717.9	0.00172	1.21	0.84	0.333	10.71

	Density of Chromite		Area of subset		Grain Data			
TM5	**µm²**	**mm²**	**µm²**	**mm²**	**Average**	**Std Deviation**	**Area Fraction of chr**	**LPO # $\Delta_{<100>}$**
Subset 1	0.27	266509.7	611.1	0.00061	1.04	0.72	0.337	9.07
Subset 2	0.29	284788.9	536.8	0.00054	1.02	0.77	0.364	12.39
Subset 3	0.25	251070.7	67.7	0.00007	1.08	0.46	0.266	16.12
Subset 4	0.30	296767.4	471.4	0.00047	0.97	0.59	0.302	12.69
Subset 5*	0.12	117508.8	25.5	0.00003	1.77	0.58	0.306	23.1
Subset 6 (All)	0.29	291646.6	1808.9	0.00181	1.06	0.76	0.388	7.8

	Density of Chromite		Area of subset		Grain Data			
0496-1A TM6	**µm²**	**mm²**	**µm²**	**mm²**	**Average**	**Std Deviation**	**Area Fraction of chr**	**LPO # $\Delta_{<100>}$**
Subset 1	0.10	99789.3	630.6	0.00063	1.61	1.18	0.310	8.3
Subset 2	0.13	128188.7	545.4	0.00055	1.41	0.91	0.283	6.58
Subset 3	0.15	153329.2	612.3	0.00061	1.23	0.70	0.241	4.99
Subset 4*	0.00	0.0	141.9	0.00014	--	--	#VALUE!	23.65
Subset 5*	0.06	63155.2	79.1	0.00008	1.03	0.35	0.058	13.13
Subset 6*	0.08	78817.7	50.7	0.00005	1.79	1.84	0.355	10.52
Subset 7*	0.10	101048.4	79.1	0.00008	1.58	0.97	0.265	9.71
Subset 8 (All)	0.10	104790.9	2135.0	0.00214	1.40	0.94	0.253	4.6

NWA 13533 (0995-1)

	Density of Chromite		Area of subset		Grain Data			
0995-1 TM1	**µm²**	**mm²**	**µm²**	**mm²**	**Mean**	**Std Deviation**	**Area Fraction of chromite**	**LPO # $\Delta_{<100>}$**
Subset 1	0.073	72837.3	1427.8	0.0014	1.38	0.41	0.118	10.41
Subset 2	0.049	49194.2	426.9	0.0004	1.41	0.47	0.085	11.67
Subset 3	0.091	90579.7	309.1	0.0003	1.29	0.41	0.130	19.77
Subset 4	0.066	65833.7	1427.8	0.0014	1.37	0.47	0.109	9.49
Subset 5	0.086	86462.5	323.8	0.0003	1.33	0.34	0.127	11.46
Subset 6*	0.049	49407.1	161.9	0.0002	1.17	0.27	0.055	17.3
Subset 7	0.075	74728.3	294.4	0.0003	1.38	0.41	0.122	9.73
Subset 8	0.051	51297.7	721.3	0.0007	1.28	0.35	0.071	9.85
Subset 9	0.072	72257.9	1619.2	0.0016	1.37	0.40	0.116	11.52
Subset 10	0.087	87429.1	1692.8	0.0017	1.43	0.49	0.157	10.94
Subset 11	0.107	107265.4	279.7	0.0003	1.38	0.36	0.168	13.23

Subset 12	0.079	79088.3	986.2	0.0010	1.40	0.49	0.137	9.52
Subset 13	0.088	88315.2	294.4	0.0003	1.31	0.35	0.126	12.95
Subset 14*	0.044	43672.4	206.1	0.0002	1.26	0.25	0.056	12.63
Subset 15*	0.026	26128.8	191.4	0.0002	1.17	0.27	0.030	11.83
Subset 16	0.045	45289.9	485.8	0.0005	1.39	0.42	0.073	8.58
Subset 17	0.082	81521.7	2723.2	0.0027	1.42	0.57	0.149	9.52
Subset 18	0.073	73326.4	927.4	0.0009	1.34	0.40	0.114	13.86
Subset 19	0.074	73596.0	176.6	0.0002	1.17	0.20	0.085	8.37
Subset 20	0.048	47954.0	250.2	0.0003	1.29	0.30	0.066	10.58
Subset 21	0.082	81921.4	500.5	0.0005	1.39	0.39	0.132	13.87
Subset 22	0.074	74404.8	618.2	0.0006	1.21	0.26	0.089	12.64
Subset 23	0.079	79113.9	1162.9	0.0012	1.42	0.45	0.138	6
Subset 24 (All)	0.074	73862.4	17207.6	0.0172	1.37	0.45	0.121	4.25

	Density of Chromite		**Area of subset**		**Grain Data**			
TM4	**µm²**	**mm²**	**µm²**	**mm²**	**Mean**	**Std Deviation**	**Area Fraction of chromite**	**LPO # $\Delta_{<100>}$**
Subset 1	0.21	209399.0	334.2	0.00033	1.21	0.61	0.302	12.04
Subset 2	0.17	171415.0	653.3	0.00065	1.09	0.46	0.187	8.82
Subset 3	0.16	159220.5	94.2	0.00009	1.18	0.64	0.221	11.41
Subset 4*	0.14	141023.8	63.8	0.00006	1.17	0.40	0.169	13.11
Subset 5	0.15	151121.8	410.2	0.00041	1.24	0.70	0.242	8.88
Subset 6	0.16	158434.2	492.2	0.00049	1.33	0.74	0.286	9.54
Subset 7	0.14	142938.2	671.5	0.00067	1.25	0.61	0.217	8.75
Subset 8	0.18	176279.8	255.2	0.00026	1.13	0.67	0.231	9.93
Subset 9	0.17	171479.7	215.7	0.00022	1.04	0.45	0.168	8.68
Subset 10	0.19	191949.1	72.9	0.00007	0.95	0.57	0.181	16.35
Subset 11	0.10	103591.6	164.1	0.00016	1.04	0.47	0.106	16.11
Subset 12	0.12	119656.6	200.5	0.00020	0.86	0.28	0.076	10.34
Subset 13	0.09	92994.0	279.5	0.00028	0.95	0.34	0.071	9.71
Subset 14*	0.01	6093.6	164.1	0.00016	5.42	--	0.142	13.12
Subset 15*	0.00	0.0	164.1	0.00016	--	--	#VALUE!	26.14
Subset 16*	0.03	31338.6	63.8	0.00006	8.88	4.79	0.647	21.68
Subset 17*	0.02	20249.6	197.5	0.00020	3.86	5.76	0.442	15.4
Subset 18*	0.01	11752.0	85.1	0.00009	0.70	--	0.004	26.08
Subset 19	0.13	134245.9	4573.0	0.00457	1.19	0.76	0.209	6.26
Subset 20 (All)	0.09	85840.6	8316.4	0.00832	1.22	0.95	0.156	6.05

	Density of Chromite		Area of subset		Grain Data			
TM5	**μm²**	**mm²**	**μm²**	**mm²**	**Mean**	**Std Deviation**	**Area Fraction of chromite**	**LPO # $\Delta_{<100>}$**
Subset 1	0.072	72150.1	180.4	0.0002	1.86	1.19	0.267	3.77
Subset 2*	0.014	14175.0	211.9	0.0002	2.17	2.37	0.094	10.59
Subset 3	0.068	67761.7	2216.7	0.0022	1.12	0.60	0.086	2.75
Subset 4	0.063	62974.2	5931.3	0.0059	1.09	0.72	0.085	0.98
Subset 5 (All)	0.063	63199.7	8540.4	0.0085	1.13	0.73	0.089	0.78

	Density of Chromite		Area of subset		Grain Data			
TM6	**μm²**	**mm²**	**μm²**	**mm²**	**Mean**	**Std Deviation**	**Area Fraction of chromite**	**LPO # $\Delta_{<100>}$**
Subset 1	0.025	24789.8	71444.8	0.071	2.36	3.89	0.403	1.45
Subset 2	0.015	15277.9	5040.3	0.005	3.92	4.60	0.435	6.79
Subset 3 (All)	0.024	24163.0	76485.1	0.076	2.43	3.93	0.405	1.4

SPADE (0269-1A)

TM1	**pixel**	**%**	**grain count:**	**Total # of chr grain pixels**	**Prevailing Grain Size**
Subset 1 (All)	150223	0.1571	109	8150	</= 13

TM2	**pixel**	**%**	**grain count:**	**Total # of chr grain pixels**	**Prevailing Grain Size**
Subset 1	41201	0.0751	59	8573	</= 15, ~31, ~33
Subset 2*	3614	0.0066	2	1741	No prevailing
Subset 3 (All)	44815	0.0816	61	10314	~22, ~33, ~38

TM3	**pixel**	**%**	**grain count:**	**Total # of chr grain pixels**	**Prevailing Grain Size**
Subset 1 (All)	43657	0.0528	120	19491	24-30, 38-46, ~74

ESTACADO (0295-3C)

TM1	pixel (all, µm2)	(chromite grain # density) %	grain count:	Total # of chr grain pixels	Prevailing Grain Size
Subset 1	74798	0.0891	238	17743	</= 2.5
Subset 2	10987	0.0131	45	1432	</= 1, ~2.1, ~2.5
Subset 3*	2774	0.0033	9	237	No prevailing
Subset 4*	2041	0.0024	8	339	No prevailing
Subset 5	101648	0.1211	309	22198	</= 2.5
Subset 6*	2177	0.0026	6	210	No prevailing
Subset 7 (All)	108640	0.1294	332	22984	</=1.7, ~2.5

TM2	pixel (all, µm2)	(chromite grain # density) %	grain count:	Total # of chr grain pixels	Prevailing Grain Size
Subset 1 (All)	159053	0.3878	350	88164	</= 16

TM3	pixel (all, µm2)	(chromite grain # density) %	grain count:	Total # of chr grain pixels	Prevailing Grain Size
Subset 1 (All)	30253	0.0738	168	3521	</= 2.3

TM4	pixel (all, µm2)	(chromite grain # density) %	grain count:	Total # of chr grain pixels	Prevailing Grain Size
Subset 1	22396	0.0546	102	3218	</= 0.6, ~1.5
Subset 2	6497	0.0158	17	838	No prevailing
Subset 3	8780	0.0214	34	1445	No prevailing
Subset 4	6893	0.0168	20	894	No prevailing
Subset 5	37220	0.0907	137	5634	</= 1.9
Subset 6	16906	0.0412	39	2900	No prevailing
Subset 7*	2127	0.0052	2	1022	No prevailing
Subset 8 (All)	71926	17.54	232	11895	</= 1.6, ~2.9

TM5	pixel (all, µm2)	(chromite grain # density) %	grain count:	Total # of chr grain pixels	Prevailing Grain Size
Subset 1	3796	0.0052	17	778	No prevailing

Subset 2	73177	0.1004	260	15386	</= 2.6
Subset 3	5639	0.0077	27	919	</= 1.3, ~2.3
Subset 4	5708	0.0078	19	227	No prevailing
Subset 5	3452	0.0047	11	559	No prevailing
Subset 6	1939	0.0027	10	306	No prevailing
Subset 7 (All)	98232	0.1348	351	20467	</= 1.6, ~7.2

ALFIANELLO (0496-1A)

TM1	**pixel (all, µm2)**	**(chromite grain # density) %**	**grain count:**	**Total # of chr grain pixels**	**Prevailing Grain Size**
Subset 1	11440	0.0278	69	3549	~8.1, ~9.3
Subset 2	15415	0.0374	37	4648	~6-8, ~13.5
Subset 3	8692	0.0211	36	2249	No prevailing
Subset 4	10594	0.0257	54	1948	</= 5.6, ~7.3
Subset 5 (All)	46141	0.112	196	12394	</= 8.5

TM2	**pixel (all, µm2)**	**(chromite grain # density) %**	**grain count:**	**Total # of chr grain pixels**	**Prevailing Grain Size**
Subset 1	4863	0.0074	61	1491	~1.9, ~2.4, ~3.2
Subset 2	2768	0.0042	32	559	~1.6
Subset 3	1448	0.0022	23	415	~1.2, ~1.8
Subset 4	9978	0.0152	151	3035	</= 1.9
Subset 5	26935	0.0409	368	7633	</= 2
Subset 6	14279	0.0217	215	3565	</= 1.5
Subset 7	6058	0.0092	80	1566	</= 1.8, ~2.8
Subset 8	8368	0.0127	110	2455	</= 2.3
Subset 9	40642	0.0618	578	11075	</= 2.2
Subset 10	7203	0.0109	99	1622	</= 1.1, ~2.1
Subset 11	3598	0.0055	47	928	</= 1.2, ~2.3
Subset 12	16045	0.0244	39	4580	</= 5.9
Subset 13	158343	0.2406	1753	42348	</= 2
Subset 14 (All)	178214	0.2708	2015	47431	</= 2

TM3	**pixel (all, µm2)**	**(chromite grain # density) %**	**grain count:**	**Total # of chr grain pixels**	**Prevailing Grain Size**

Subset 1	43823	0.1084	221	13291	</= 1.1, ~2.5
Subset 2*	2334	0.0058	6	314	No prevailing
Subset 3 (All)	46157	0.1141	227	13605	</= 1.8, ~2.6

TM4	**pixel (all, µm2)**	**(chromite grain # density) %**	**grain count:**	**Total # of chr grain pixels**	**Prevailing Grain Size**
Subset 1	2366	0.0059	13	278	~1.1, ~1.24, ~1.35
Subset 2	12916	0.0319	106	3107	</= 1.1, </= 1.5
Subset 3	10536	0.0261	75	3174	</= 1.3, ~3.2
Subset 4	15435	3.82	98	5929	</= 2.3, ~3.6, ~5
Subset 5	25849	0.0639	174	9419	</= 1.5, </= 2.3, ~3.6
Subset 6	4231	0.0105	10	1541	No prevailing
Subset 7	4668	0.0115	10	2945	No prevailing
Subset 8*	1743	0.0043	7	642	No prevailing
Subset 9	3693	0.0091	13	722	No prevailing
Subset 10 (All)	56411	0.1395	336	18761	</= 1.4, >/= 2.2

TM5	**pixel (all, µm2)**	**(chromite grain # density) %**	**grain count:**	**Total # of chr grain pixels**	**Prevailing Grain Size**
Subset 1	22296	0.0551	163	7505	</= 2, ~5.2
Subset 2	19580	0.0484	153	7125	</= 2.5, ~4.7
Subset 3	2473	0.0061	17	658	~1.1, ~1.8, ~2
Subset 4	17174	0.0425	140	5188	</= 1.8, ~4.7
Subset 5*	939	0.0023	3	287	No prevailing
Subset 6 (All)	65976	0.1631	528	25595	</= 1.2, ~4.5

TM6	**pixel (all, µm2)**	**(chromite grain # density) %**	**grain count:**	**Total # of chr grain pixels**	**Prevailing Grain Size**
Subset 1	12582	0.0311	63	3896	</= 2.6, ~6, ~7.1
Subset 2	10886	0.0269	70	3076	</= 2.8, ~4.2, ~5.8
Subset 3	12226	0.0302	94	2951	</= 2.7, ~3.3, ~3.8
Subset 4*	2821	0.007	0	--	No prevailing
Subset 5*	1559	0.0039	5	91	No prevailing
Subset 6*	1009	0.0025	4	358	No prevailing
Subset 7*	1567	0.0039	8	416	No prevailing

Subset 8 (All)	42573	0.1053	224	10788	</= 2, ~4.4

NWA 13533 (0995-1)

TM1	**pixel (all, µm2)**	**(chromite grain # density) %**	**grain count:**	**Total # of chr grain pixels**	**Prevailing Grain Size (µm)**
Subset 1	9681	0.0097	104	1144	<1.7
Subset 2	2868	0.0029	21	245	1.3-1.5, ~2.5
Subset 3	2092	0.0021	28	271	</=2, 2.8
Subset 4	9651	0.0097	94	1051	</= 1.7
Subset 5	2209	0.0022	28	281	</= 1.5, ~1.9
Subset 6*	1101	0.0011	8	61	No prevailing
Subset 7	1972	0.002	22	241	No prevailing
Subset 8	4872	0.0049	37	346	No prevailing
Subset 9	10948	0.011	117	1268	</=2
Subset 10	11448	0.0115	148	1794	<2.5
Subset 11	1940	0.0019	30	325	No prevailing
Subset 12	6632	0.0067	78	910	</=2.7
Subset 13	2005	0.002	26	252	</= 1.05, ~1.3, ~1.7
Subset 14*	1415	0.0014	9	79	No prevailing
Subset 15*	1261	0.0013	5	38	No prevailing
Subset 16	3334	0.0033	22	244	</= 1.2, </= 1.5, ~2.7
Subset 17	18472	0.0185	222	2754	</= 2.6
Subset 18	6240	0.0063	68	710	*</= 1.5, ~2.4, ~3*
Subset 19	1147	0.0012	13	97	*No prevailing*
Subset 20	1696	0.0017	12	112	No prevailing
Subset 21	3407	0.0034	41	451	</= 1.1, </= 1.4, </= 1.6
Subset 22	4226	0.0042	46	375	No prevailing
Subset 23	7901	0.0079	92	1092	</= 1.6, ~2.3
Subset 24 (All)	116518	0.1169	1271	14141	</= 2

TM4	**pixel (all, µm2)**	**(chromite grain # density) %**	**grain count:**	**Total # of chr grain pixels**	**Prevailing Grain Size**
Subset 1	10532	0.011	70	3184	</= 2.7
Subset 2	20482	0.0215	112	3827	</= 2.1
Subset 3	2971	0.0031	15	658	</= 1.7, ~3.1
Subset 4*	1973	0.0021	9	334	No prevailing
Subset 5	12872	0.0135	62	3114	~1.3, ~3.3, ~4.1
Subset 6	15469	0.0162	78	4430	</= 2.3, 2.7

Subset 7	21087	0.0221	96	4566	< 2, ~2.3, ~2.5
Subset 8	7998	0.0084	45	1850	</= 1.3, ~2.6, ~3.7
Subset 9	6805	0.0071	37	1143	~1.2, ~1.5, >/= 1.7
Subset 10	2270	0.0024	14	412	>/= 0.4, ~2.8
Subset 11	5114	0.0054	17	540	~1, ~1.4, ~1.9
Subset 12	6322	0.0066	24	480	</= 0.8, ~1.3, ~1.4
Subset 13	8817	0.0092	26	625	</= 1.3
Subset 14*	5111	0.0054	1	726	No prevailing
Subset 15*	5113	0.0054	0	--	No prevailing
Subset 16*	2018	0.0021	2	1306	~7.4
Subset 17*	6199	0.0065	4	2739	~10.5
Subset 18*	2710	0.0028	1	12	No prevailing
Subset 19	143713	0.1505	614	30068	</= 1,5
Subset 20 (All)	261262	0.2737	714	40867	</= 2

TM5	**pixel (all, µm2)**	**(chromite grain # density) %**	**grain count:**	**Total # of chr grain pixels**	**Prevailing Grain Size**
Subset 1	5699	0.0063	13	1524	No prevailing
Subset 2*	6664	0.0074	3	627	No prevailing
Subset 3	69690	0.0774	150	5969	</=2.5
Subset 4	186325	0.2071	373	15815	</=3.5
Subset 5 (All)	268378	0.2982	539	23935	</=3.5, ~5

TM6	**pixel (all, µm2)**	**(chromite grain # density) %**	**grain count:**	**Total # of chr grain pixels**	**Prevailing Grain Size**
Subset 1	2200166	0.4621	1771	887487	5-27
Subset 2	155225	0.0326	77	67469	9-29
Subset 3 (All)	2355391	0.4947	1848	954956	5-27